EFFECTS OF THERMO-MECHANICAL TREATMENT ON THE SHAPE MEMORY BEHAVIOR OF NiTi AND CoNiAl ALLOYS

A Thesis

by

HALUK ERSIN KARACA

Submitted to the Office of Graduate Studies of
Texas A&M University
in partial fulfillment of the requirements for the degree of

MASTER OF SCIENCE

December 2003

Major Subject: Mechanical Engineering

EFFECTS OF THERMO-MECHANICAL TREATMENT ON THE SHAPE MEMORY BEHAVIOR OF NiTi AND CoNiAl ALLOYS

A Thesis

by

HALUK ERSIN KARACA

Submitted to Texas A&M University
in partial fulfillment of the requirements
for the degree of

MASTER OF SCIENCE

Approved as to style and content by:

Ibrahim Karaman (Chair of Committee)	Dimitris C. Lagoudas (Member)
Mustafa Yavuz (Member)	Dennis L. O'Neal (Head of Department)

December 2003

Major Subject: Mechanical Engineering

ABSTRACT

Effects of Thermo-mechanical Treatment on the Shape Memory Behavior of NiTi and CoNiAl Alloys. (December 2003)

Haluk Ersin Karaca, B.S., Bogazici University, Turkey

Chair of Advisory Committee: Dr. Ibrahim Karaman

Nickel-Titanium (NiTi) shape memory alloys have been the focus of extensive research due to its unique characteristics such as high recoverable strain and ductility. However, solutionized samples of NiTi do not demonstrate good shape memory characteristics due to low strength for dislocation slip. Thermo-mechanical treatments are required to strengthen the matrix and improve the shape memory characteristics. Plastic deformation and the subsequent annealing is the common way to improve shape memory properties. In this case, deformation magnitude, temperature, rate, mechanism, and annealing temperature and time are all important parameters for the final shape memory properties. Equal channel angular extrusion (ECAE) is a well-known technique to severely deform materials by simple shear with no change in cross-section. In this study, Ti- 49.8 at% Ni samples are deformed by ECAE at three different temperatures near transformation temperatures. X-ray analysis, calorimetry, transmission electron microscopy and thermo-mechanical cycling techniques are utilized to investigate the effects of severe deformation and subsequent annealing treatment on shape memory properties. Martensite stabilization, formation of strain induced B2 phase, change in transformation temperatures, formation of new phases, recrystallization temperature, texture formation, and increase in strength and pseudoelastic strain are the main findings of this study.

Co-32.9 at% Ni-29.5 at% Al is a newly found ferromagnetic alloy. Its low density, high melting temperature and cheap constituents make the alloy advantageous among other shape memory alloys. Although some magnetic properties of this alloy are known, there is no report on basic shape memory characteristics of CoNiAl. In this study, effect of thermo-mechanical treatments on the microstructure and shape memory characteristics such as transformation behavior, pseudoelasticity, stages of transformation, temperature dependence of the pseudoelasticity, response to thermal and stress cycling is investigated. Formation of second phase along the grain boundaries and inside the grains, about 4% pseudoelastic and two-way shape memory strain, very narrow stress hysteresis, large pseudoelastic window (>150˚C), two-stage martensitic transformation, stable response to cyclic deformation, high strength for dislocation slip, slope of Clasius-Clapeyron curve, and twinning plane are determined for the first time in literature.

To My Parents

ACKNOWLEDGEMENTS

First of all, I would like to thank my advisor, Prof. Ibrahim Karaman, who gave life to this project, and without his endless encouragement and support this project would not have been completed. He has helped me in all aspects of this project and turned me into a researcher. He has been a model for me and influenced me in almost every aspect of my academic life.

I would like to thank my committee member, Prof. Mustafa Yavuz, for sharing his invaluable life experience with me and his guidance on how to be a good academician. I am also grateful to Prof. Dimitris Lagoudas for being a member of my committee and a role model.

I would like to express my appreciation to Prof. Yuriy Chumlyakov for his motivation in my research and sharing with me his deep knowledge on shape memory alloys. Our discussions were always a pleasure. Special thanks also goes to Dr. Hans Maier for his help in X-ray results and his kind, useful and complete answers that cover all aspects of my questions.

I am also thankful to Dr. Zhipping Luo, who helped me a lot on TEM and indexing the diffraction patterns. Also, Robert Barber is thanked for his assistance for extrusions and in any technical difficulties. I would like to thank Bill Merka from chemistry glass shop for his help in the preparation of glass tubes for heat treatments.

I would like to thank my officemates, Mohammed Haouaoui, Guney Yapici, Ajay Kulkarni, Joseph Mather, Bryan Bagley and Yang Cao for providing a good environment for research and their social relations. At this point, Mr. Guven Yapici is thanked especially not only as an officemate and classmate but also as a good friend coming from my native country. Ajay Kulkarni and Yang Cao taught me a lot about their cultures and gave me a chance to taste their delicious food.

I would also like to thank all my friends; Refik Sahin, Burak Basaran, Mert Atilhan, Resul Iskendarov, Mehmet Ayvaci, Fatih Mutlu, Renat Schaykutdinov and many others in College Station for helping me adopt a new life style and enjoy my life. Special thanks to my soccer teammates, with whom we won the 2002 Intramural Soccer Championship. It has always been a pleasure to play with that unbeatable team. I would also like to thank Mr. Osman Anderoglu, my old friend, for not letting me be alone in the graduate school and being such a good friend.

Finally, I would like to thank my parents who have supported and trusted me throughout my life. They bore and overcame lots of difficulties in order to provide me with a good educational environment. Also, my brother, Erdem Karaca, is thanked for always being one step ahead of me, facing difficulties and sharing his experience with me. His guidance and motivation helped me a lot in my research. It has been always very comfortable to know that I have somebody who can solve or guide me in solving any kind of problems.

TABLE OF CONTENTS

LIST OF FIGURES

LIST OF TABLES

Page

CHAPTER I

INTRODUCTION

1.1 Background

Shape memory alloys (SMAs) have unique properties, such as high recoverable strains, as a result of reversible martensitic transformation (MT). Diffusionless phase transformation can be triggered by temperature change, applied stress or magnetic field and high temperature phase called austenite or parent phase transforms to low temperature and lower symmetry phase called martensite and vice versa.

MT can be defined simply as a lattice deformation involving shearing deformation and resulting cooperative atomic movement. There is a 1-to-1 correspondence called "lattice correspondence" between the lattice points of parent and martensitic phases. Habit plane is a specific plane between the parent and martensitic phase along which the shear occurs during transformation. Since there is no strain and rotation in the habit plane through out the entire transformation, this type of shape deformation is called invariant shear strain. Martensites with different habit planes are called variants [1].

MT is a first order transformation which results in large transformation strain. In order to reduce the strain during nucleation and growth two types of lattice invariant shear (LIS) mechanisms could take place; dislocation slip or twinning [2]. These are called LIS because they do not change the structure of martensite. Generally twinning is the LIS for most of the SMAs . A schematic of twinning system is shown in Figure 1.1.1. K_1 and η_1 are called the shear plane and shear direction respectively. K_1 is an invariant plane and K_2 is another undistorted plane. The plane which is normal to K_1 and parallel to η_1 is called plane of shear, and η_2 is the intersection of K_2 and t he plane of

---

This thesis follows the style and format of *Materials Science and Engineering A.*

shear. If K_1 and η_2 are rational and K_2 and η_1 are irrational the twinning is called type I twinning, if K_1 and η_2 are irrational and K_2 and η_1 are rational the twinning is called type II twinning and if all of them are rational they are called compound twinning.

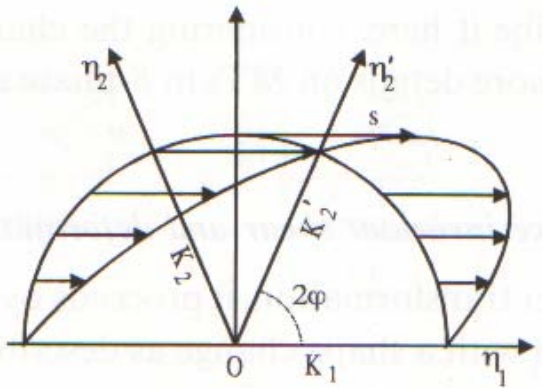

Figure 1.1.1. The deformation of a sphere into an ellipsoid and the definition of K_1, η_1, K_2 and η_2 [2].

The driving force for diffusionless phase transformation in shape memory alloys is the chemical free energy between the phases. When the difference in chemical free energies is enough to overcome the energy to nucleate the other phase, transformation will start and continue as the energy for growth is supplied by further increase in chemical energy difference. The transformation start and finish temperatures from austenite to martensite are called M_s and M_f respectively and transformation start and finish temperatures from martensite to austenite are called A_s and A_f where the former transformation is named as forward transformation and the latter one as back transformation.

When the MT starts during cooling in order to minimize the strain a second step of minimization strain takes place in addition to LIS which is self accommodation of martensite variants. The basic morphologies of self accommodation structures are shown in Figure 1.1.2 which are the called diamond and parallelogram morphology of self

accommodation. Different self accommodation morphologies could be formed as it will be shown later for NiTi alloys.

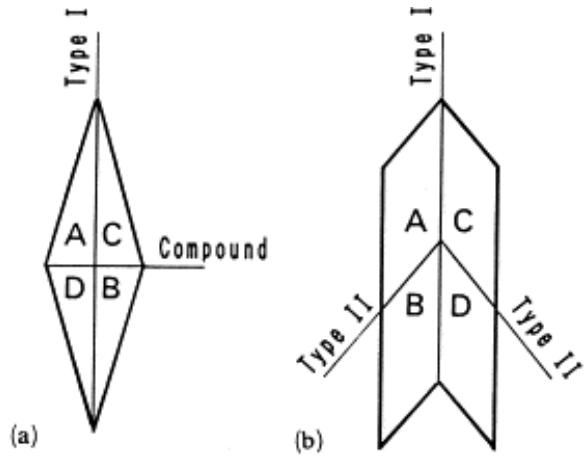

Figure 1.1.2. Basic self-accommodating morphologies [3].

MTs can be classified in two categories thermoelastic and nonthermoelastic. For thermoelastic MTs; the transformation temperature hysteresis is small, the interface between parent and martensite is mobile and the transformation is crystallogrophically reversible. For nonthermoelastic MTs, the transformation temperature hysteresis is large, the interface between the martensite and parent phase is immobile, and once the martensite grows to some critical size, the reverse transformation takes place by renucleation of parent phase. Figure 1.1.3 shows the difference in transformation temperature hysteresis between the thermoelastic and nonthermoelastic MTs. Most of the thermoelastic shape memory alloys are intermetallic alloys since they have ordered structure, which means that lattice sides are occupied by particular species of atoms. Since MT is a diffusionless process the product martensite is also ordered and the process is crystallographically reversible. Also ordering promotes a higher flow stress in the parent phase which prevents the damage of martensite/parent interphase during growth of martensite.

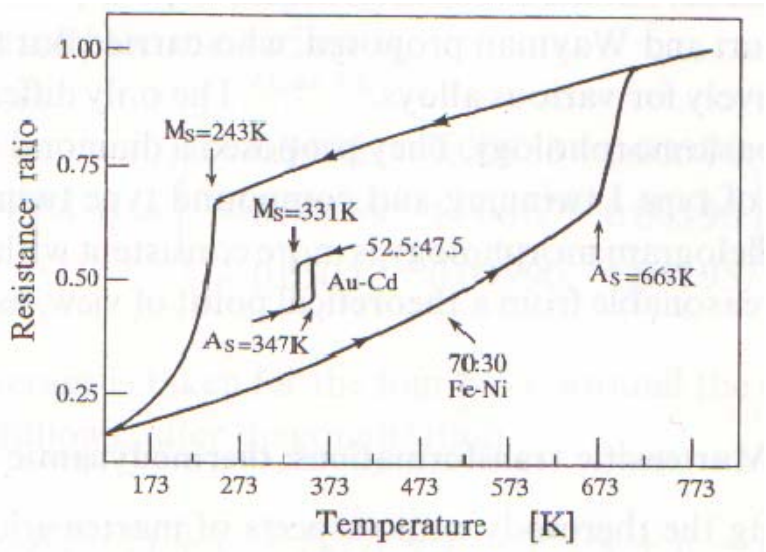

Figure 1.1.3. Electric resistance vs. temperature curves for thermoelastic and nonthermoelastic shape memory alloys [2].

There are two deformation types in shape memory alloys which lead to high recoverable strains; reorientation of martensite and stress induced martensite. When NiTi alloys cooled down under zero stress, parent phase transforms to martensite and 24 possible internally twinned martensite variants form self-accommodating structures to minimize the macroscopic volume change [1]. The applied stress biases the self accommodating structure and favors the growth of selected martensite variants among the others. When this biased structure is heated above A_f temperature, it recovers back to its original shape which is called shape memory effect (SME) and there will be no net transformation strain with following forward transformation under no applied stress. If self-accommodated structure is permanently biased (generally by forming dislocations, internal stresses or applying force during transformation), large macroscopic strain will be induced with forward and back transformations which is called two-way shape memory effect (TWSME) [4,5].

It is well known that deformation of austenite in the range of A_f to a certain temperature (Md) results in stress induced transformation (SIM). Favored martensite variants form and during unloading, these martensite variants transform back to austenite since they are not chemically stable at that temperature. This deformation behavior is called pseudoelasticity (PE) or superelasticity. Pseudoelasticity is a more generic term than superelasticity. It encompasses also rubber like behavior which is observed in some SMAs when the bars in martensite phase are bent and aged to recover its original shape. Shortly, pseudoelasticity can be used for both martensite and austenite phases where superelasticity is used for parent phase only. As the temperature increases the stress needed for transformation also increases exceeding the stress for dislocation slip which deteriorates the pseudoelastic response. Deformations at temperatures higher than Md do not lead to stress induced transformation because dislocation slip is the only deformation mechanism.

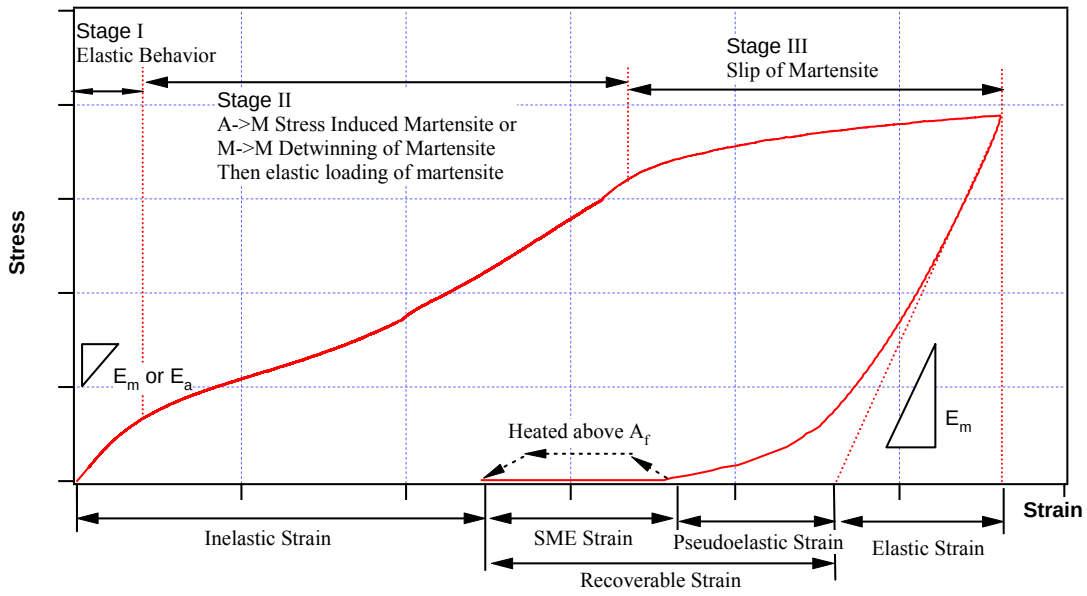

Figure 1.1.4 A schematic of stress-strain behavior of shape memory alloys.

A schematic deformation plot is shown in Figure 1.1.4. There are three possible deformation cases. Case I: If the material is initially in austenitic phase, then at Stage I; elastic deformation of austenite and at Stage II; stress induced martensite and at Stage III; slip deformation of martensite will occur. Case II: If the initial material is in martensitic state, then at Stage I; elastic deformation of martensite and at Stage II; detwinning of martensite which means that some favored variants will grow in expense of others and at Stage III; slip deformation of martensite will occur. Case III: If the initial material is a mixture of austenite and martensite phases, mixture of the previous deformation types will take place. Upon unloading martensitic structure will unload elastically in all cases which would be followed by pseudoelastic strain (back transformation from martensite to austenite) in Cases I and III. Further strain can be recovered if the deformed samples are heated above A_f temperature which is known as shape memory effect (SME). The remaining permanent strain is inelastic strain and mainly due to the dislocations formed during loading. The end of first plateau region is not the end of transformation. The recoverable strain decreases with increased plastic deformation which corresponds to the second plateau region in NiTi. This is because of the fact that slip formation inhibits reverse transformation [6].

1.2 Brief History of SMAs

First shape memory effect was discovered by a Swedish physicist, Arne Olender, in gold-cadminum alloy in 1932. The alloy was plastically deformed when it was cooled and returned to its original shape when it was heated. Later in 1938, the same effect was also observed in CuZn and CuAl [7]. In 1951, Chang and Read observed shape memory effect in AuCd alloy [8]. In 1961, Muldaver and Feder used an AuAgCd alloy in a thermally actuated electrical switch and took the first patent for a shape memory alloy [9]. But the turning point is the discovery of SME in equiatomic NiTi by Buehler and his co-workers at the U.S Naval Ordinance Laboratory (NOL) in 1962 [7]. An extensive study has began on to reveal the shape memory characteristics of NiTi and the first application was Cryofit shrink-to-fit pipe couplers, which were used to join hydraulic

lines of airplanes in 1970 and in 1975 NiTi braces were used [9]. After the confirmation of biocompatibility of NiTi, the application field of NiTi has been tremendously enlarged. Application of shape memory alloys are summarized well by [1,7,10,11] and will not be discussed here.

1.3 Phase Diagrams

In order to understand the martensitic transformations and control the microstructure the phase diagrams are essential. Hence the physical properties of materials are strongly correlated with compositions and phases. Figure 1.3.1 shows the phase diagram of NiTi. The central part of the Figure1.3.1 where NiTi transforms to B19' martensitic phase is important. On the nickel rich side Ti_3Ni_4, Ti_2Ni_3 and $TiNi_3$ precipitation formation has been reported and resulted in confusion for a while, whether there is a eutectoid reaction or not. But it is understood that the Ti_3Ni_4 and Ti_2Ni_3 phases are intermediate phases and they transform to equilibrium $TiNi_3$ phase with longer aging time [12]. For Ti rich side the equilibrium phase is Ti_2Ni but Ti is so active that it easily combines with oxygen and carbon at high temperatures. The order-disorder transition temperature is at 1090˚C as indicated by dotted line on the phase diagram [13].

As it can be deduced from the phase diagram, the composition range for ordered B2 phase NiTi is from 49 to 57 at% Ni at 1090˚C. The composition range should be kept close to equiatomic composition since precipitations do not demonstrate shape memory behavior. The phase diagram of NiTi has been used to improve the shape memory characteristics by formation of precipitates. As it will be discussed later, precipitates change the transformation temperatures (TTs), strength and PE substantially.

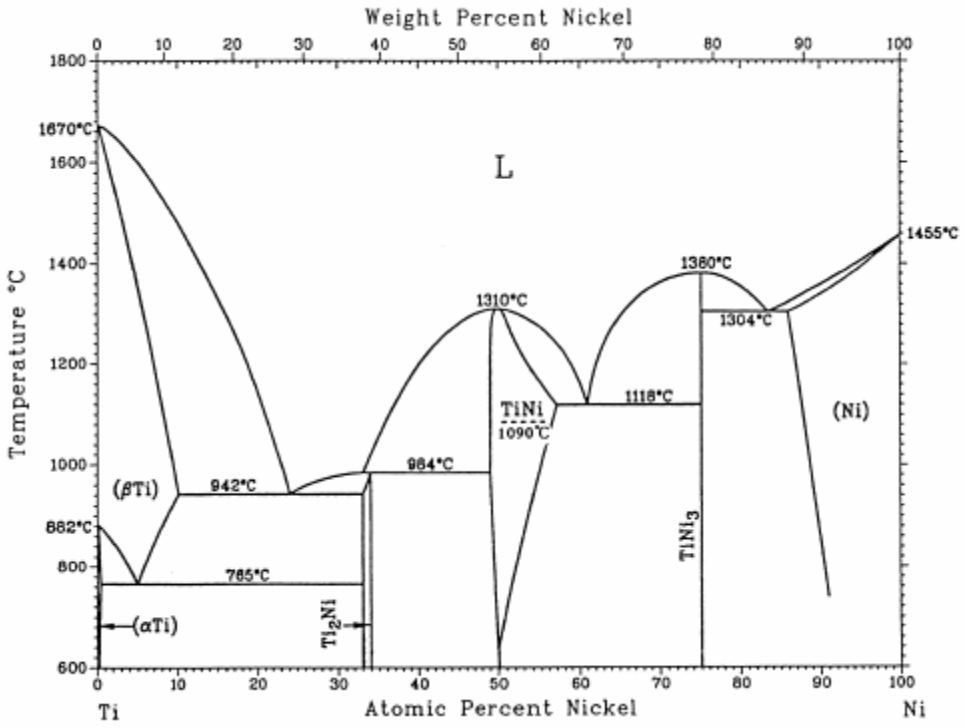

Figure 1.3.1 Phase diagram of NiTi [13].

1.4 Crystal Structures

It is very important to know the crystal structures of phases in order to understand their physical properties. The parent phase of NiTi has BCC B2 crystal structure which is ordered like CsCl type with lattice constants of about a=0.301nm [1].

So far three martensitic phases are determined for NiTi and NiTiX alloy systems. B19' is most common phase observed in NiTi and its alloys. Its space group is $P2_1/m$ and has a monoclinic crystal structure with lattice parameters of a=0.2898 nm, b=0.4108 nm and c=0.4646 nm and β=97.78˚ for Ti-49.2 at% Ni [14]. The lattice parameters are composition dependent. The other phase, so called "premartensitic phase" is triclinic R-phase which belongs to the space group of P3 with lattice parameters of about a_R=0.732nm and c_R=0.532nm [15]. The R-phase is elongated 0.94% along the parent

$[111]_{B2}$ orientation which is one order smaller than B19' [2]. B19 is an orthorhombic phase with lattice constants of a_o=0.29nm, b_o=0.425nm and c_o=0.45nm [16]. Structural relationships of parent phase and two martensitic phases are shown in Figure 1.4.1 [17].

Aging, cold working and annealing, thermal cycling, increasing Ni content and alloying of NiTi (eg. NiTiFe and NiTiAl) could promote R-phase transformation by suppressing M_s temperature [2,18]. B2 to R-phase transformation results in only small shape change (~0.8%) which results in very small temperature hysteresis. Also this small transformation strain is responsible for the stability of TTs after thermo-mechanical treatments. B19 is observed in ternary alloys of NiTi. For NiTiCu alloys, the transformation behavior is changing from one stage B2-B19' to B2-B19-B19' and than to B2-B19 with increasing Cu content [16,19]. The amount of transformation strain of B19 is between the R and B19' phases. Stability of mechanical and thermal properties under thermo-mechanical treatments, lower hysteresis due to small transformation strain and lower cost due to Cu addition make NiTiCu suitable for industrial applications.

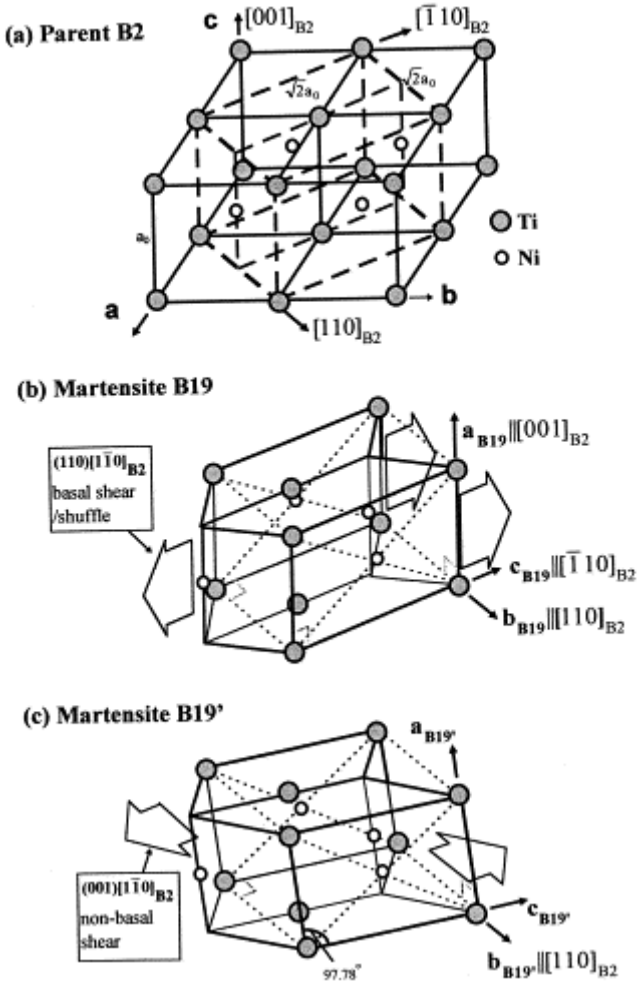

Figure 1.4.1. Structural relationship among cubic parent phase (B2) and two kinds of martensites B19 and B19'. (a) the parent phase B2, (b) orthorhombic martensite B19, (c) monoclinic B19' martensite of NiTi [17].

1.5 Self Accommodation

As explained before in order to minimize the overall strain energy martensite variants forms self-accommodated structures. For NiTi each martensitic phase has a different self accommodating morphology as described below.

There are 12 lattice correspondence between the parent B2 and martensite B19' phase resulting in 24 martensite variants. They form a triangular self accommodating morphology as shown in Figure1.5.1. The interphase between each two of three variants is a twin plane. There are 16 groupings which forms a triangular self accommodating morphology around each of the $[001]_{B2}$ poles, resulting in 48 possible combination of variants for such triangles [18].

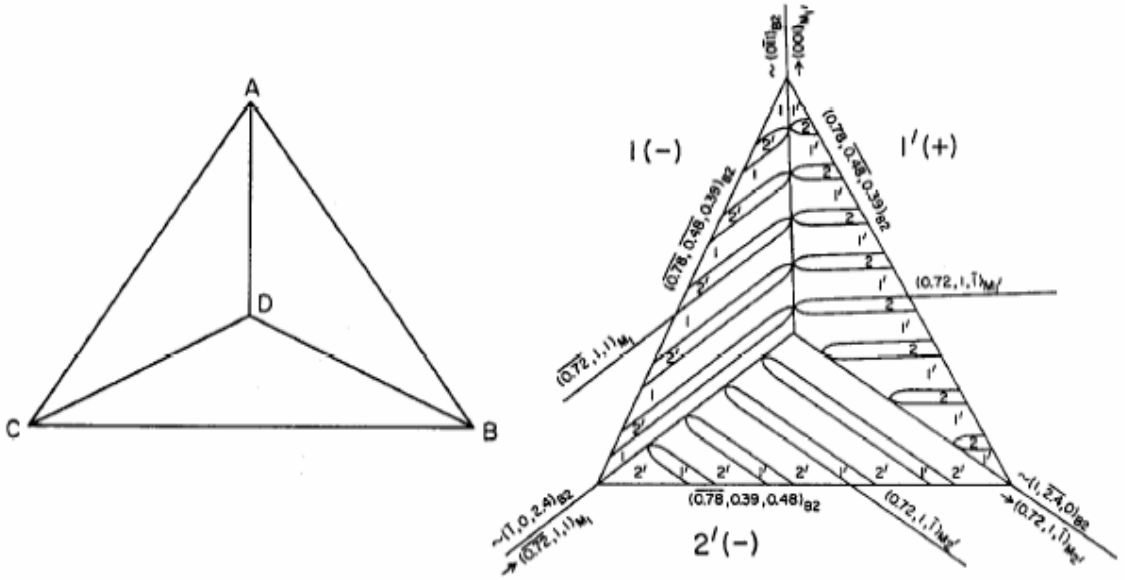

(a) (b)

Figure 1.5.1. Self accommodating morphology of B19'[20].

There are 4 equivalent lattice correspondences between the B2 and R phases. Figure 1.5.2 shows the typical example of self accommodating structure. There are two types of morphology, one is straight band morphology corresponds to the view from $[100]_{B2}$ and $[010]_{B2}$ and the other one is herring-bone (saw-tooth) morphology corresponds to the view from $[001]_{B2}$ of Figure1.5.2 [2].

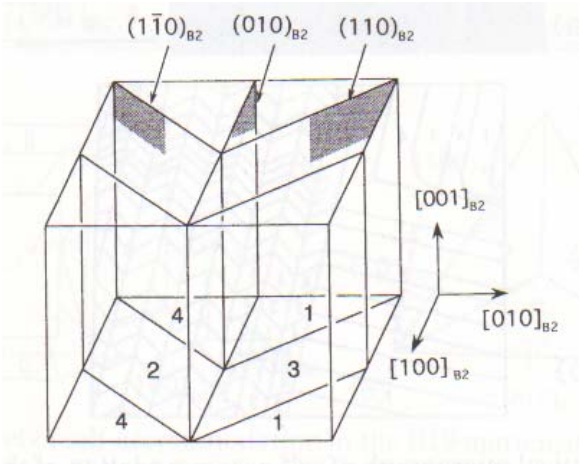

Figure 1.5.2 Self accommodating morphology of R phase [2].

For orthorhombic B19 phase there are 6 equivalent lattice correspondences between the parent and martensitic phases. Again a triangular morphology could be observed in the $[111]_{B2}$ orientation as shown in Figure1.5.3 [2].

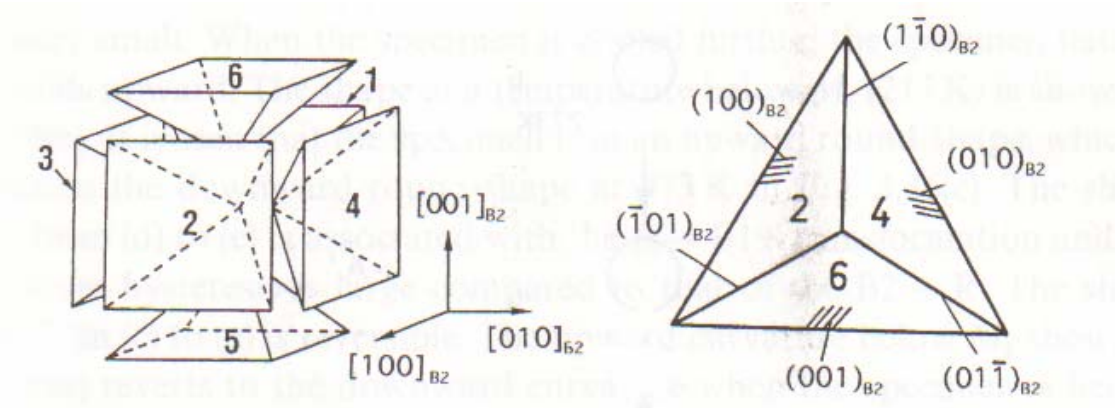

Figure 1.5.3 Self accommodating morphology of B19 phase [2].

In all self accommodating structures martensite variants have twin relations with each other and when an external force is applied the most favorable variant grows at the expense of others, resulting in net shape change.

1.6 Ductility of NiTi

Although most of the intermetallics are brittle, NiTi has a very peculiar ductile nature. The main reasons of this ductility are the low anisotropy factor, small grain size, low strength for slip near M_s and availability of twinning modes in martensitic phase. Anisotropy factor of NiTi is ~2 and grain size is ~30μm where for the other intermetallic alloys they are around 15 and ~1-5mm respectively. High anisotropy factor results in grain boundary fracture in most intermetallics. Also the low elastic constant c_{44} leads to low stress for the activation of {110}<001> slip system in NiTi which enhances ductility.

1.7 Determination of Transformation Temperatures

Resistivity is the oldest method to characterize TTs but it is difficult to distinguish the peaks and determine the TTs for untrained researcher. Also this method is very sensitive to thermal cycling that changes the resistivity curves.

Constraint cycling is another method that can be used to determine the TTs by applying a very small stress and then thermally cycling under this stress and recording the strain response. This method would result in slightly shifted TTs as a result of applied stress but this method is very useful to characterize TTs under different stress levels and formation of Clausius-Clapeyron curves.

Differential Scanning Calorimetry (DSC) is the most common method to determine the TTs. Because of the fact that forward transformation is exothermic and reverse transformation is endothermic the TTs can be determined by the change in heat loss curve during cooling and heating. A schematic of a DSC curve and determination of

TTs by intersecting slopes method is shown in Figure1.7.1. Advantages of DSC are: ease of determining TTs, small sample size (10mg) needed, ease to operate and fast response.

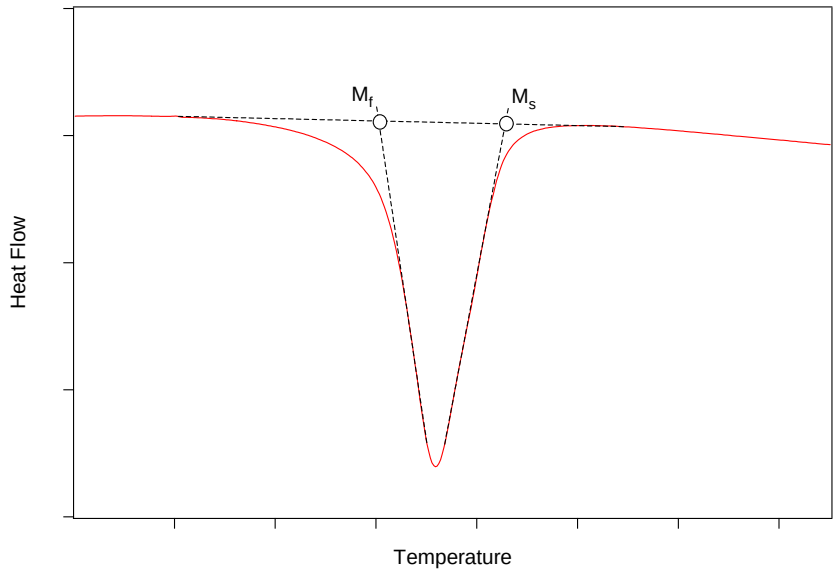

Figure 1.7.1. Schematic of intersecting slope method for finding transformation temperatures from DSC response.

Magnetic susceptibility or magnetization curves under constant applied magnetic field lower than saturation values are also very effective to determine the TTs. Especially if at least one of the phases is ferromagnetic a strong magnetization response can be obtained under a constant applied magnetic field and its change with temperature can be used to determine the TTs.

Acoustic emission and in-situ observation techniques are the other methods to determine the TTs. The former technique determines the acoustic bursts occur during interphase movement where the latter uses optical or electron microscopy techniques to observe the changes on the surface of specimens during thermal cycling.

1.8 Effect of Thermo-mechanical Treatments on Shape Memory

Thermo-mechanical treatments have drastic effects on shape memory characteristics of materials. Ausforming, deformation in austenitic phase and marforming, deformation in martensitic phase introduce defects to the structure. These defects can raise the critical stress for dislocation slip which can improve SME, TWSME and PE. Also, these defects are possible nucleation sites for martensitic transformations which can lead to a change in TTs. On the other hand, complex dislocation structures and other internal defects can behave like barriers to martensitic transformations as well. As a result, plastic deformation in SMAs can strengthen the matrix which can result in higher stress for SIM transformation, longer fatigue life by suppressing irreversible dislocation slip and alter TTs [21]. Heat treatment is another effective method to change shape memory characteristics. Coherent or incoherent precipitates form with different heat treatment temperatures and time in appropriate compositions. Coherent precipitates form an internal stress field around them and this can help or oppose the martensitic transformation depending on the applied stress direction. If there is no applied stress, they increase the M_s temperature due to the internal stress field around them. Another effect of precipitates is that they change the composition of matrix because precipitates are either Ni-rich or Ti-rich depending on the initial composition. Composition effect is dominant for overaged precipitates where the sizes of precipitates are larger than the peakaged precipitates [22]. When the annealing temperature is higher than the recrystallization temperature, formation of new grains, and grain growth will take place. Heat treatments after deformation can be performed to utilize the mechanical characteristics by rearrangement of dislocation structures, formation of precipitates and grains as will be shown in this study.

In the studies to date on marforming, low to moderate strain levels (up to 70 % area reduction) are usually applied in subsequent rolling or simple compression steps [21,23-29]. In marforming, these strain levels lead to martensite stabilization [21]. Martensite stabilization is attributed to the high dislocation density stored in martensite

plates especially at the prior internal twin boundaries and to the dislocation debris present after recovery annealing. This leads to strengthening by suppressing further slip.

The main focus of these previous studies was mostly the effect of different deformation levels on transformation temperatures [21,26]. However, there are not many studies in which the aforementioned goals of ausforming and marforming are clearly demonstrated to be achieved and if not, the possible reasons for failure are clearly identified [24]. There is not an extensive study that focuses on treating a NiTi alloy with fixed composition in both austenitic and martensitic phases separately and on comparing the resulting microstructures and properties. Such a study would be valuable in understanding how defects affect austenite to martensite and martensite to austenite transformation. Moreover, it is intuitive to look into how marforming through other stress-states such as simple shear would change the shape memory behavior of NiTi.

1.9 Effect of Deformation on Microstructure

It is known that the dominant twinning system in solutionized NiTi is <011> type II twinning [30]. Depending on the deformation mode and amount, different mechanisms take place to accommodate the resulting shape change. For Ti-49.8 %at Ni, the composition used in this study, Zheng et al. [30] studied the effect of cold rolling and revealed that up to 12% area reduction (AR), coalescence of martensite variants is the mechanism for accommodation of the shape change. The dominant twinning mode is still type II twinning but some type I twinning is also observed. The intervariant boundaries became curved, distorted and blurred eventually. After 16% AR, the deformation took place mainly inside the variants; formation and rearrangement of structural bands and formation of new twins would occur. Type I and compound twinnings operate and consume type II twinning. The substructural bands partially arranged their orientations along the deformation direction and the formation of new subplates will diverse the orientation.

<001> compound twinning can be considered as the deformation twinning in martensite [31]. One of the slip systems of NiTi is [100](001) (the other one is [100](110)) and it is proposed that <100> compound twin is created by the slip of a/2 on the (001) plane because of the presence of a partial pseudo-mirror [14,31]. It is also reported that <100> compound twinning is sensitive to internal stress fields and can relieve the elastic interaction inside the martensite variant effectively [30-32]. These facts explain why <100> compound twinning is observed in deformed NiTi.

Deformation of NiTi on martensite will result in martensite stabilization as mentioned before. One of the reasons is the release of elastic energy stored during forward transformation. Elastic energy resists the forward transformation where it helps the reverse transformation [13]. Furthermore, it has been reported that half of the chemical energy difference between the parent and martensite is stored as elastic energy in thermoelastic equilibrium condition [13,33]. This stored elastic energy lowers the A_s temperature from its original value and if this energy could be released A_s would rise to higher temperatures toward its original value. After first heating, during the forward transformation the elastic energy will be stored again and A_s temperature will decrease to its initial value.

1.10 Two-Way Shape Memory Effect

Thermo-mechanical treatments are also required in obtaining pseudoelastic response and developing a TWSME in near equiatomic NiTi alloys. Otherwise martensite variants form upon cooling in a self accommodating manner [2] and there is no mechanism to bias stress or thermally induced martensite variant formation for pseudoelasticity or TWSME. The common procedures of thermo-mechanical treatments for obtaining pseudoelasticity are:

1) Shape memory training: repeated cycles of deformation of the alloy by martensite reorientation and recovery of the deformation by a reverse transformation induced by heating under no stress [1,34].

2) Pseudoelastic training: mechanical cycling process of deformation above A_f through the stress-induced martensitic transformation and the reverse transformation upon unloading [1,35].

3) Thermal cycling: subjecting the alloy to repeated thermal transformation cycles under the influence of an external bias stress [1,36].

4) Deformation of martensite or austenite beyond the elastic limits [1].

The main idea for training procedures is to bias the microstructure by formation of dislocations or residual martensite that would lead the formation of oriented martensite variants instead of self-accommodating martensite variants. Among these training procedures constant-stress thermal cycling has appeared to be the most effective method in introducing pseudoelasticity [36]. The plastic deformation of parent or martensite phases would be easier as compared to the other methods as it does not require a cyclic treatment. In the present study, the understanding of how severe simple shear deformation in different phases alters SME and PE in Ti rich NiTi alloys will be improved.

1.11 Cyclic Deformation

1.11.1 Thermal Cycling

It has been shown in solutionized materials that dislocations will be introduced by thermal cycling and their density will increase with the number of cycling. This will result in decrease in M_s temperature. The decrease of M_s could be prevented by increasing the strength of the material by cold working or precipitation hardening to prevent the formation of dislocations during repeated phase transformation [18].

1.11.2 Stress Cycling

Generally, with increased number of cycles the residual strain will increase, critical stress to induce martensite (σ_{SIM}) and stress hysteresis will decrease [18, 37]. The

increase of residual strain is due to the formation of dislocations during phase transformation and deformation of matrix. Sometimes, dislocations can also prevent the reverse transformation of martensite. Internal stress fields around the dislocations or residual martensites will assist the formation of stress-induced martensites, which means hysteresis. After certain number of cycling the steady state condition is obtained. This is due to the fact that work hardening suppresses the formation of new dislocations.

1.12 Effects of Texture

It is shown on single crystals and rolled polycrystals that mechanical response of the material is highly orientation dependent [6,38]. Critical resolved shear stress, the stress required to trigger the martensitic transformation, is orientation and deformation mode dependent (compression vs tension). In some orientations more than one martensite variants could be activated. Activation of multiple variants results in rapid hardening in the stress-strain response, and limits the overall transformation because the stress for transformation exceeds the stress for slip. The max recoverable strain levels and stress levels for martensite formation and slip as a function of orientation are reported in the literature [6,39,40].

The strong tension-compression asymmetry in single crystals is because of the unidirectional nature of shear strain across the martensite habit planes [39]. The asymmetry in single crystal level is responsible for the tension-compression asymmetry in polycrystals.

1.13 Effects of Grain Size

It is proposed that small grain size is effective to improve PE since grain boundaries would support the needed back stress for back transformation and act as nucleation sites. Figure 1.13.1 shows the effect of grain size to PE [2] for Ti- 50.5 at% Ni. It is clear that reduction in grain size is effective for improving the pseudoelasticity.

It is reported that the decrease in grain size increases M_s which is attributed to increase in elastic energy due to the interaction of martensite plates and grain boundaries in microcrystalline materials For nanocrystalline materials the increase in Ms is attributed to the homogeneous nucleation of martensite phase caused by internal stress arising from greater anisotropy of nanoscale grain size [41,42].

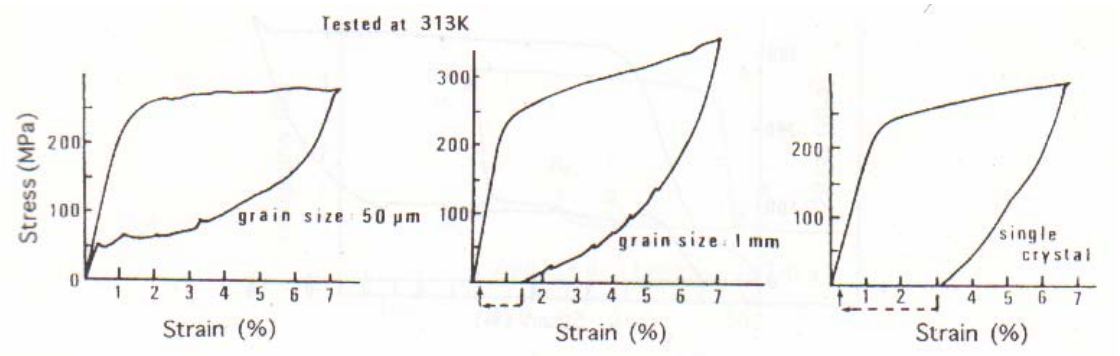

Figure 1.13.1. Effect of grain size on pseudoelastic behavior [43].

1.14 Effects on Transformation Temperatures

Addition of ternary element decreases the M_s temperature. Transition elements with different valance electrons are used as ternary alloys and all resulted in decrease in M_s and in some cases formation of intermediate phases [1]. Addition of Cu is important from industrial view since copper is a cheap substitution. It also changes the transformation sequence as B2-B19 or B2-B19-B19' depending upon composition. TTs do not change much and they are more stable to thermo-mechanical treatments than NiTi and temperature hysteresis A_f-M_f decreases with addition of Cu [1].

Contaminating impurity C forms TiC carbides and decreases M_s of about 15˚C but do not affect mechanical behaviors [1].

Oxygen contamination lowers the M_s due to formation of Ti_4Ni_2O precipitates which results in increase in the Ni content of matrix. Also the degradation of mechanical properties is observed and the material becomes more brittle [1].

Aging of Ni rich NiTi has drastic effects on TTs. Aging below the recrystallization temperature for a short time will form very small precipitates and strengthen the matrix enormously. This will prevent the shear deformation needed for martensitic transformation resulting in low M_s temperature. As the time of aging is increased, the particles will grow and form internal stress fields around them that could help nucleation of martensite or oppose them depending on the applied stress direction. After some point they will lost their coherency with the matrix and their only effect is the change the composition of the matrix which will alter the TTs. Generally, precipitates do not undergo phase transformation, decreasing the overall strain due to transformation.

1.15 Equal Channel Angular Extrusion

The severe plastic deformation methods are usually used to obtain nanostructured, sometimes even amorphous, bulk materials that have received increasing attention because of their unique properties such as high strength and superplasticity [44].

Generally in order to induce large deformation in materials a large reduction in cross-sectional area is required. This reduction often results in stress-strain non-uniformity. In order to prevent this, ECAE method is developed. Figure1.15.1 is a schematic representation of the ECAE process. Load is applied from the top of the vertical channel and well lubricated billet is deformed in the shear zone and extruded from the horizontal channel. Under these conditions the billet is moved inside the channels as a rigid body, and the deformation is achieved by simple shear in the shear zone which is the intersecting region of the two channels. By this method the entire billet could be deformed uniformly except small end sections and a minor surface area.

Because the shape of the billet is almost the same after extrusion, it could be extruded again by ECAE. The flexibility of changing the billet orientation between the passes through ECAE allows the development of different microstructures and texture [45,46]. The angle between the two channels (2φ) is 90° in the present case. Multiple channels, movable channel walls, round or sharp corners, extrusion speed and temperature are other parameters that affect the final product [45].

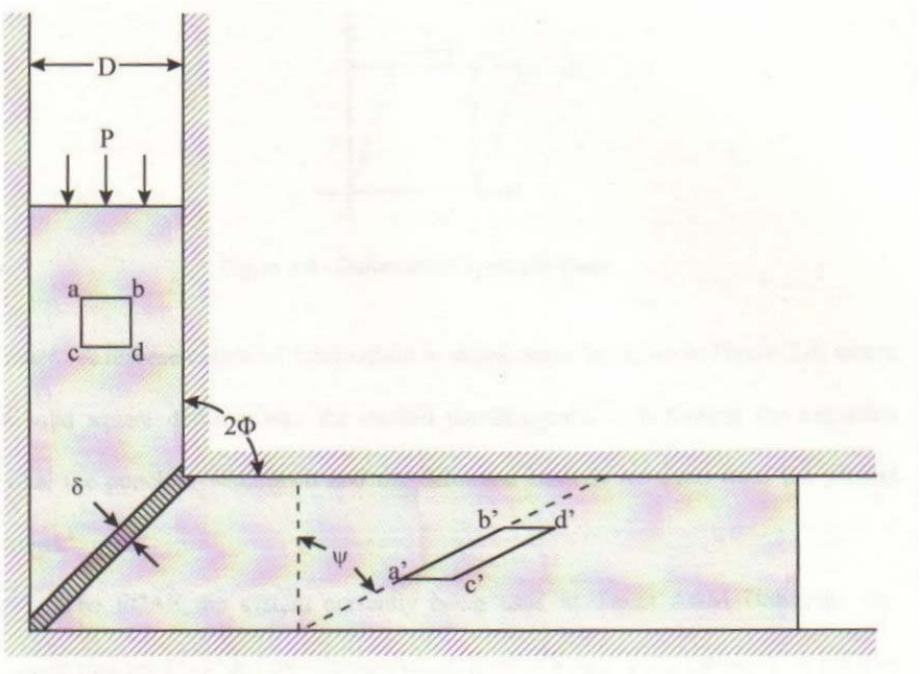

Figure 1.15.1 Schematic view of ECAE procedure. Illustrating angle of deformation (ψ), angle of intersecting channels (2φ), and width of shear zone (δ) [47].

High pressure torsion, ECAE, ball milling, mechanical alloying by cold working, cold rolling, shot peening, and particle irradiation are known techniques to obtain amorphous or nanostructured materials [48]. ECAE is superior to the other techniques in permitting the application of a large amount of strain without a significant change in

sample cross section, the formation of uniform microstructures, control over the development of grain morphology and ease of process [46,49].

In literature amorphization after severe deformation is reported [29,50,51]. The origin of amorphization is attributed to either the high dislocation energy formed especially in shear bands where the shear instability (decreased shear modulus as a result of volume change) helps this process [51] or formation of nanocrystalline structures. Formation of amorphous phase and nanocrystals are attributed to immobile and mobile dislocation respectively [50]. Formation of macroscopic shear bands are observed in 40% cold worked NiTi. Formation of shear bands raises the local strain in the order of 10. So the formation of the amorphous phase would be attributed to the formation of shear bands because of high dislocation density and localized shear deformation [27, 52]. For nanocrystalline materials, amorphization could be attributed to high grain boundary energy rather than dislocation energy [53].

1.16 Ferromagnetic CoNiAl Shape Memory Alloy

In recent years, ferromagnetic shape memory alloys (FSMAs) have attracted increasing interest since Ullakko et al. [54] observed a large magnetic field induced strain (MFIS) in NiMnGa. Later Murray et al. [55] and Tickle and James [56] reported 6% and 4.3% MFIS respectively. Recently, Sozinov reported the highest value of 9.5% MFIS in NiMnGa alloy in the literature obtained by martensite variant conversion [57]. Other FSMAs reported to date are FePd [58,59], FePt [60] and NiFeGa [61,62]. However, these materials are expensive and in most cases brittle for practical applications. Main requirements to obtain large MFIS [62,63] are: 1) low twin boundary energy [62], 2) high strength matrix (to prevent dislocation slip) and 3) high magnetocrystalline anisotropy energy [63] with thermoelastic martensite.

The mechanism for MFIS can be described as follows: when an external magnetic field is applied there will be a competition between rotating magnetization direction from easy axis to the applied direction and rearranging the martensite variants

such that their easy axis aligned with the applied magnetization direction [55,56]. As far as the energy needed to move the twin boundaries is lower than the energy needed to rotate the direction of magnetization, anisotropy energy, MFIS would be obtained when sufficient magnetic field applied.

More recently, the potential of Co based alloys such as CoNiGa [64,65] and CoNiAl [65-68] as FSMAs have been revealed. CoNiAl alloys seem promising for FSMA applications because of the possibility for obtaining sufficient ductility through thermal treatments [23,69,70], relatively cheap constituents and the ability to control transformation temperatures and Curie temperature (T_c) independently over a large composition range [66]. Upon cooling from the high temperature cubic phase, CoNiAl alloys exhibit paramagnetic to ferromagnetic transition followed by thermoelastic martensitic transformation or vice versa, depending on their composition [66]. Although the required magnetic characteristic of CoNiAl alloys to be a potential FSMA has been principally shown [65-68], the mechanical requirements have not been quantitatively investigated (first two parameters above). Moreover, pseudoelastic behavior has not been revealed to date, if any. SMAs with β parent phase such as CuNiAl and NiMnGa are known to have multiple martensite phases and intermartensitic transformations [71-75]. However, there has been no report on whether CoNiAl alloys exhibit multiple martensite phases. Another interesting question that has not been addressed is the effect of different martensitic phase structures on MFIS. It is believed that thorough knowledge of martensitic transformation, transformation stress vs. strain behavior and transformation stress-temperature phase diagram of CoNiAl alloys will enhance the further development of these materials as FSMAs as well as establishing a basis for conventional shape memory applications of these alloys.

CoNiAl intermetallic alloy could be considered as addition of Co to NiAl system or Ni to CoAl system. NiAl is a well-known intermetallic alloy with low density, high melting temperature, good corrosion and oxidation resistance at high temperatures that resulted in wide usage in high temperature applications [69]. NiAl transforms from cubic

β-phase (B2) parent to tetragonal β'($L1_0$) martensitic phase in the composition range of 61.5 to 69 at% Ni [75]. New CoNiAl undergoes β to β' martensitic transformation similar to NiAl [66]. Although the martensitic transformation in CoNiAl alloys has been discovered a long time ago [23], it did not receive much attention since the primary aim was to solve the biggest problem of intermetallic alloys: the brittleness of the beta phase of NiAl by addition of ternary alloys. It was explained in Section 1.6 why NiTi does not have this problem. It was shown that formation of second phases γ(A1) and γ'$(Ni,Co)_3Al$ in the matrix can increase the ductility of CoNiAl [69,75]. Secondary phases can be precipitated or dissolved with appropriate heat treatments provide the ability to deform the material and then gain the desired characteristics with simple heat treatments.

CHAPTER II

EXPERIMENTAL TECHNIQUES

Ti-49.8 at% Ni alloy was obtained from Special Metals Corporation in cold drawn condition. The as-received materials were coated with Y_2O_3, solution treated at 850 °C for 1 hour and water quenched. The transformation temperatures of the solution treated material were determined by a Perkin-Elmer Pyris-I differential scanning calorimeter with a heating rate of 10ºC/min. The ECAE extrusions were conducted at room temperature (RT) (in the fully martensitic state), 50ºC (also in the martensitic state but very close to A_s) and 150ºC (in the austenitic state) with a die angle of 90º. For ECAE, the samples were canned in nickel to minimize tool wear during extrusion. The extrusion could be performed without canning the samples. However, since the strain hardening and failure behavior at such high strain levels and under simple shear deformation was not known for NiTi, the cans were used for these first tests. The dimensions of the cans are 1”x1”x5” and the bars were 3” in length in order to have uniform deformation. The cans were heated up to the deformation temperatures in the furnace before they were put into the pre-heated die. Only one pass (equivalent strain ~ 1.16) was applied as extensive macro shear localization and failure in shear bands did not allow the second passes. The extrusion rate was kept extremely small (Table 2.1.1) to minimize deformation heating. The deformation between shear bands were uniform as demonstrated by several hardness measurements in which maximum variation was 6% at the most. Table 2.1.1 summarizes the extrusion conditions; extrusion temperature, rate of extrusion, max force applied by punch and diameter of the NiTi bars inside the cans.

Table 2.1.1 Summary of extrusion conditions

Extrusion Temperature	Extrusion Rate	Max. Load	Diameter
˚C	mm/sec	kN	mm
RT	0.127	1089	12
50	0.025	934	16
150	0.025	760	8

A CoNiAl alloy has also been obtained from Special Metals Corporation. It was cast to a nominal composition of Co-32.9Ni-29.5 Al in atomic %. Specimens were homogenized at 1350 ˚C for 24 hours in sealed quartz tubes and quenched in water. The resulting grain size was in the range of 1-10 mm with no discernable grain boundary precipitates.

The phases present after deformation of NiTi were determined using a Bruker-AXS D8 diffractometer with Cu Kα radiation. Samples were polished before the X-ray analyses unless they were used for fracture surface analyses.

Thermal cycling was performed by heating samples in the DSC to determine the transformation temperatures. Also DSC is used to investigate the stability of the microstructure and the effect of recovery and recrystallization (if any) on transformation temperatures for NiTi.

The microstructures of the selected samples were investigated utilizing transmission electron microscopy (TEM) and optical microscopy (OM). The TEM foils were prepared from the samples by mechanical thinning of slices down to 100 μm, punching 3 mm disks, and afterwards twin-jet electropolishing with a 20 volume % H_2SO_4 in a methanol solution at -15 °C for both NiTi and CoNiAl alloys. A JEOL 2010 microscope operated at a nominal accelerating voltage of 200 kV was utilized for investigation. Some of the CoNiAl alloy samples were electropolished using a solution consisted of 5% perchloric acid in ethanol and the resulting thin foils were examined in a PHILIPS CM 200 electron microscope operated at 200kV. The OM specimens of CoNiAl were etched in 75ml HCl, 75ml ethanol, 15g $CuSO_4$ and 10ml distilled water solution after mechanical polishing

The thermo-mechanical cycles and mechanical experiments were conducted using square, 4 mm wide and 8 mm long specimens. In the experiments, the loads were measured with a load cell and strains were measured with a miniature MTS (Materials Test Systems) extensometer with 3 mm gage length. Rubber bands or springs (for

temperatures higher than 120 °C) were used to attach the extensometer to the specimens. The use of the miniature extensometer circumvents the end effects associated with stroke measurements. The test temperature of the samples was achieved by conduction through compression plates. Copper tubes were wrapped tightly around the grips and heating bands around them. Liquid nitrogen was passed through the tubes in order to cool the specimen and heating bands are used to heat the specimen by conduction. Temperature was measured using thermocouples spot-welded on the sample. TWSME tests were done by thermal cycling of compression samples on the MTS test machine under constant loads. The compression tests are done by displacement control during loading and force control during unloading unless it is stated differently. The displacement rate was $4x10^{-4}$ $mm.s^{-1}$ which corresponds to the strain rate of $5x10^{-4}$ s^{-1} to minimize rate effects and temperature rise during the experiments

Hardness tests were done by using Buehler Micromet II digital microhardness test machine. The working principle of microhardness testing is forcing a diamond indenter of specific geometry to into the pre-polished surface of the samples. The Vickers hardness number (Hv) is determined by measuring the length of the diagonals of the indentation and applied load. The geometry of the indenter is square based pyramidal diamond with face angles of 136˚ in our case. 500gf load is applied for 13 seconds and average of at least 8 measurements was used after removing the highest and lowest values to determine the hardness of the specimens.

Solutionizing of samples was done by using quartz tubes. In order to reduce the oxidation by the air inside, quartz tubes were sealed under argon gas atmosphere or vacuum. Stainless steel or inconel wires were used to prevent the bars from interacting with quartz at high temperatures.

CHAPTER III

NiTi ALLOY

3.1 DSC Results

3.1.1 DSC Response of ECAEd Samples

The DSC tests are conducted on samples in the range of 10 to 40 mg which were cut by using a low speed Buehler Isomet diamond saw. Figure 3.1.1 shows the DSC result of the as-received material which is solutionized at 850 °C for 1 hour and water quenched.

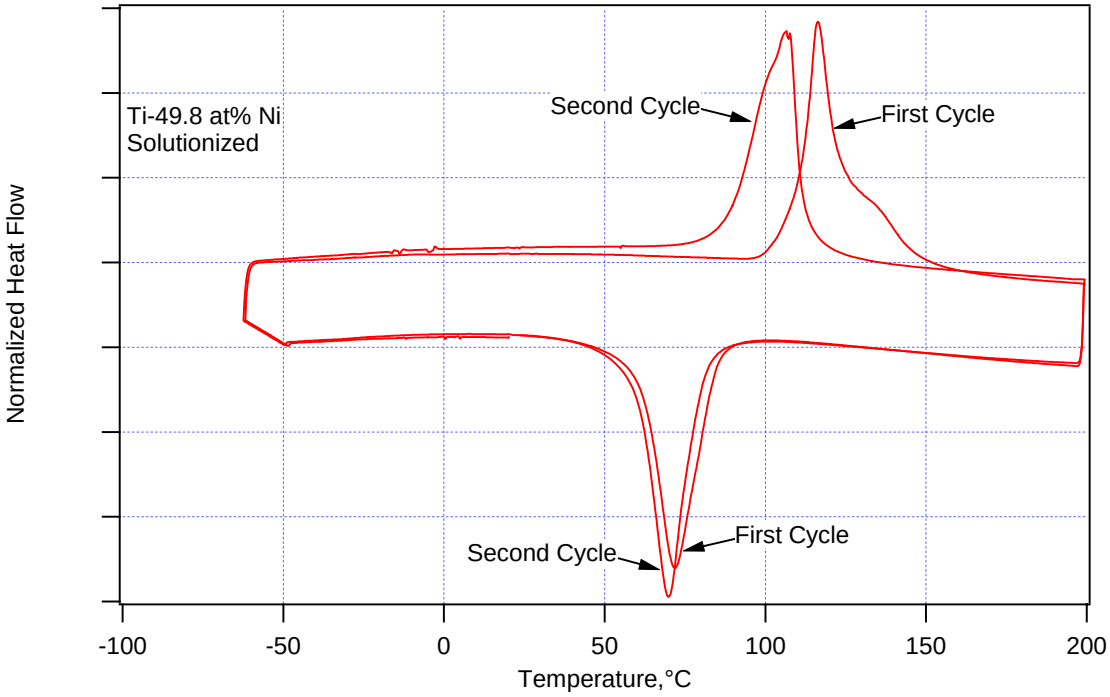

Figure 3.1.1. DSC response of the solutionized material.

In order to differentiate the TTs at different DSC cycles, the number of cycles is added as subscript to TTs. For example, M_{s1} means the martensite start temperature for the first cycle. TTs for the solutionized sample are shown in Table 3.1.1. The DSC curve in Figure 3.1.1 demonstrates that the transformation temperatures for the first cycle are higher than the second cycle. This phenomenon is called martensite stabilization as explained before. This behavior is not expected since the material is solutionized after cold drawing. The stabilization in the first cycle is attributed to the internal stress field formed during water quenching which vanishes after the first cycle.

TTs after ECAE deformation were also determined by DSC. In order to investigate the effect of annealing after deformation several DSC tests were performed. The samples were heated to the desired annealing temperature, held there for one minute and cooled down to -60ºC and heated to RT with a heating rate of 10ºC/min. In order to determine the effect of first cycle this process was repeated or in some cases the second cycle was between -60ºC and 200ºC. Figures 3.1.2 and 3.1.3 show the effects of deformation by ECAE at RT, 50ºC and 150ºC followed by subsequent annealing on the TTs. All the TTs were obtained by intersecting line methods as described in Section 1.7 and shown in Table 3.1.1. In the table, R_s and R_f correspond to the R-phase start and finish temperatures during cooling. First column of Table 3.1.1 indicates the temperature ECAE conducted, second column stands for the maximum temperature of the DSC cycle which will be called annealing temperature. Temperature hysteresis is defined as the temperature difference between the phase transformation start and finish temperature, such as ΔM means M_f-M_s.

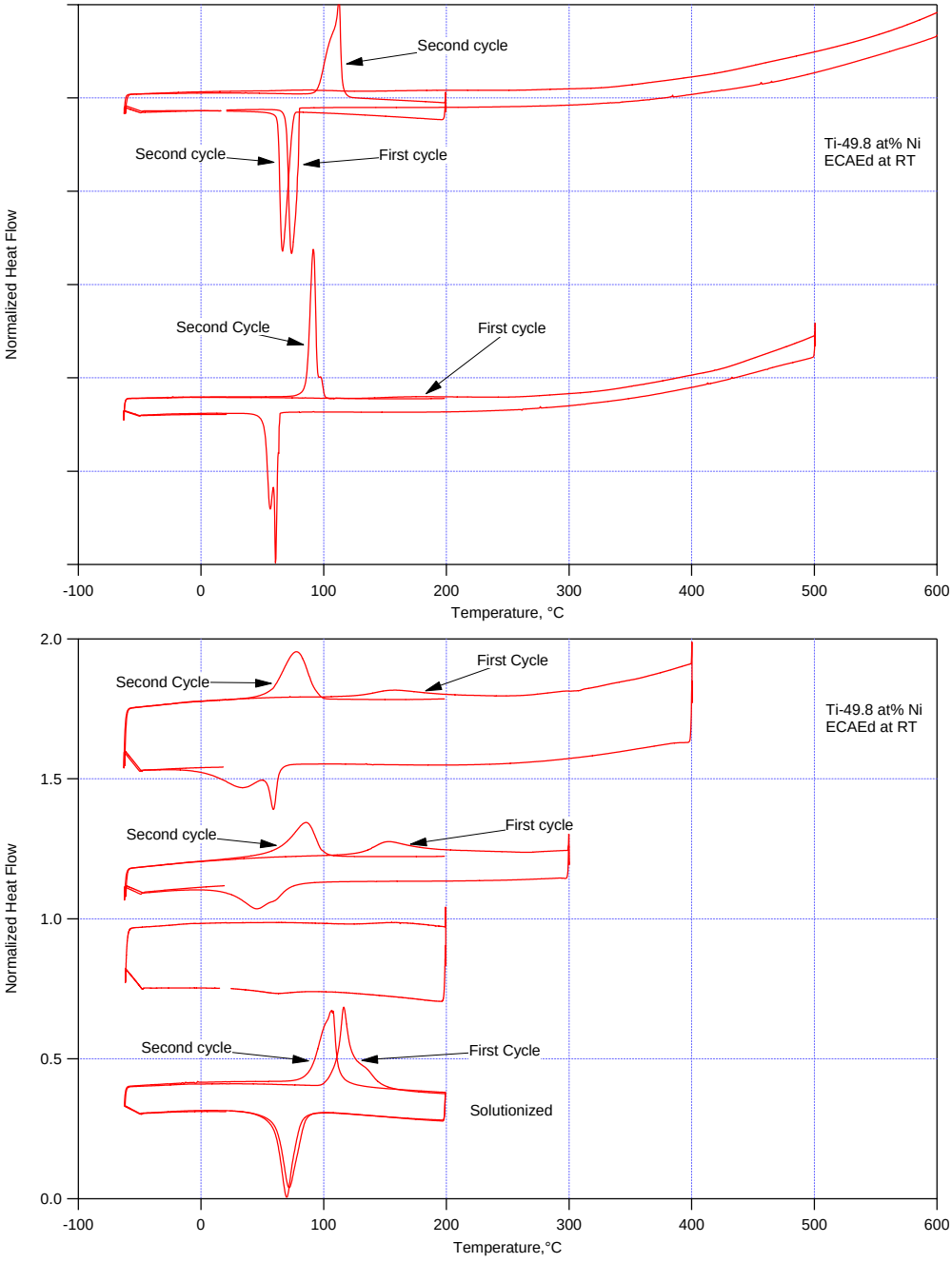

Figure 3.1.2. DSC response of the samples ECAEd at room temperature followed by annealing at 200ºC up to 600ºC. DSC curve of the solutionized material is also included for comparison.

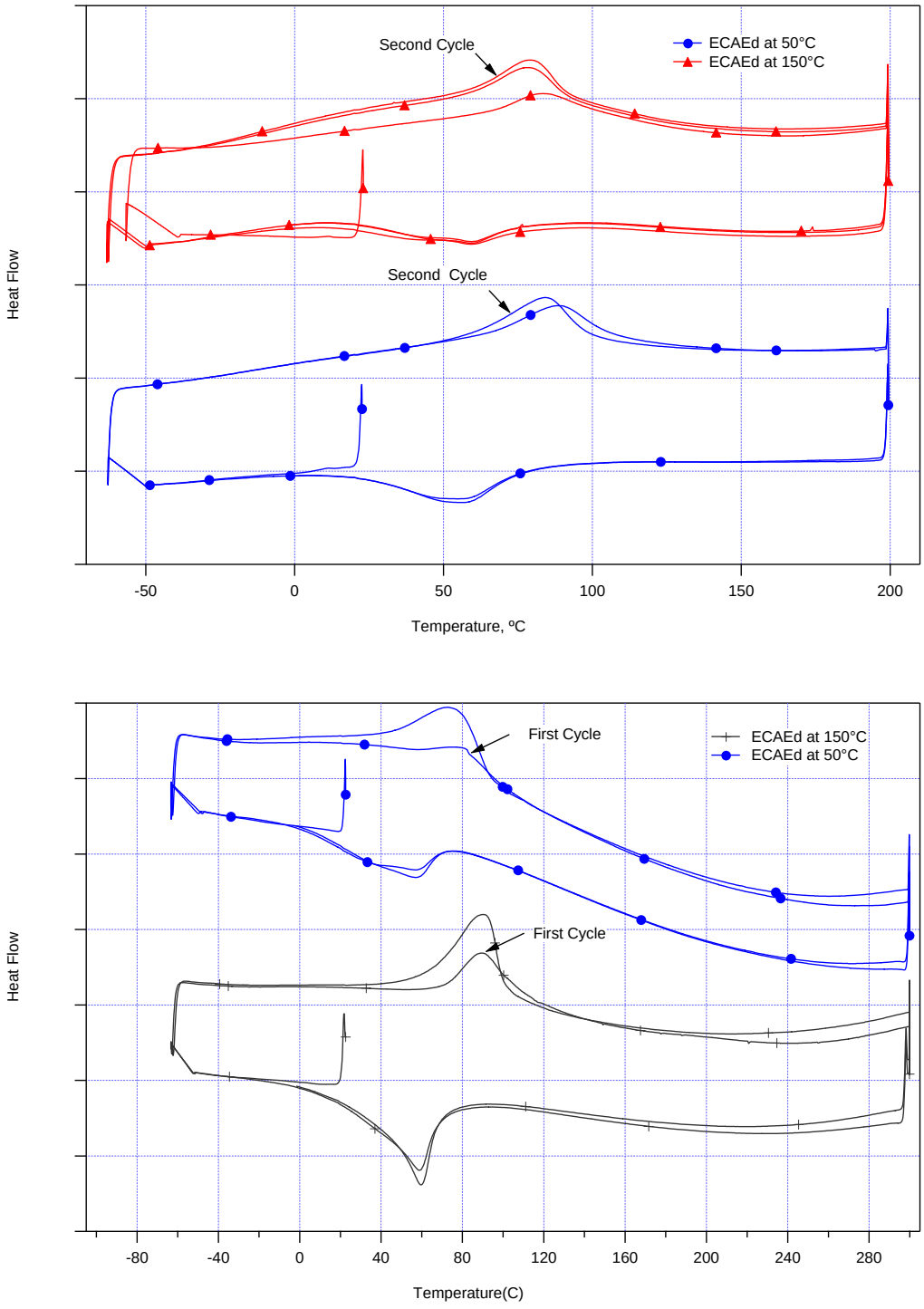

Figure 3.1.3. DSC response of the samples ECAEd at 50ºC and 150ºC followed by annealing at 200ºC and 300ºC.

Table 3.1.1. Transformation temperatures for samples ECAEd at room temperature.

		M_s		M_f		M_p		R_s		R_f		R_p	
ECAE Temp	**HT**	**1**	**2**	**1**	**2**	**1**	**2**	**1**	**2**	**1**	**2**	**1**	**2**
	solutionized	86	80	60	59	70	69						
RT	200	84	84	33	33	62	62						
RT	300	74	74	19	19	45	45						
RT	400	72	72	0	0	34	34	63		51		59	
RT	500	64	64	52	52	56	56	63		58		61	
RT	600	80	75	70	63	74	67						
50	200	77	77	22	22	59	59						
50	300	70	70	5	5	57	57						
50	400			15	15	42	42	66	66	53	53	60	60
150	200	80	80	13	13	52	52						
150	300	72	72	9	9	60	60						
		A_s		A_f		A_p		M_s-M_f	A_f-A_s	A_f-A_s			
		1	**2**	**1**	**2**	**1**	**2**	**1**	**1**	**2**			
	solutionized	108	92	148	112	116	106	26	40	20			
RT	200	130	46	200	120	160	80	51	70	74			
RT	300	124	60	211	99	151	85	55	87	39			
RT	400	124	53	211	95	158	77	72	87	42			
RT	500	121	86	230	101	175	91	12	109	15			
RT	600	130	90	240	115	190	112	10	110	25			
50	200	62	56	112	102	83	78	55	50	46			
50	300	55	42	106	95	79	75	65	51	53			
50	400	64	55	108	101	94	80		44	46			
150	200	65	61	115	98	88	84	67	50	37			
150	300	75	65	123	92	90	90	63	48	27			

The stability of TTs after the first cycle has been demonstrated by performing a cyclic DSC test on a sample deformed at RT at different test times as shown in Figure 3.1.4. The nonlinearity of the upper DSC curve is due to experimental error.

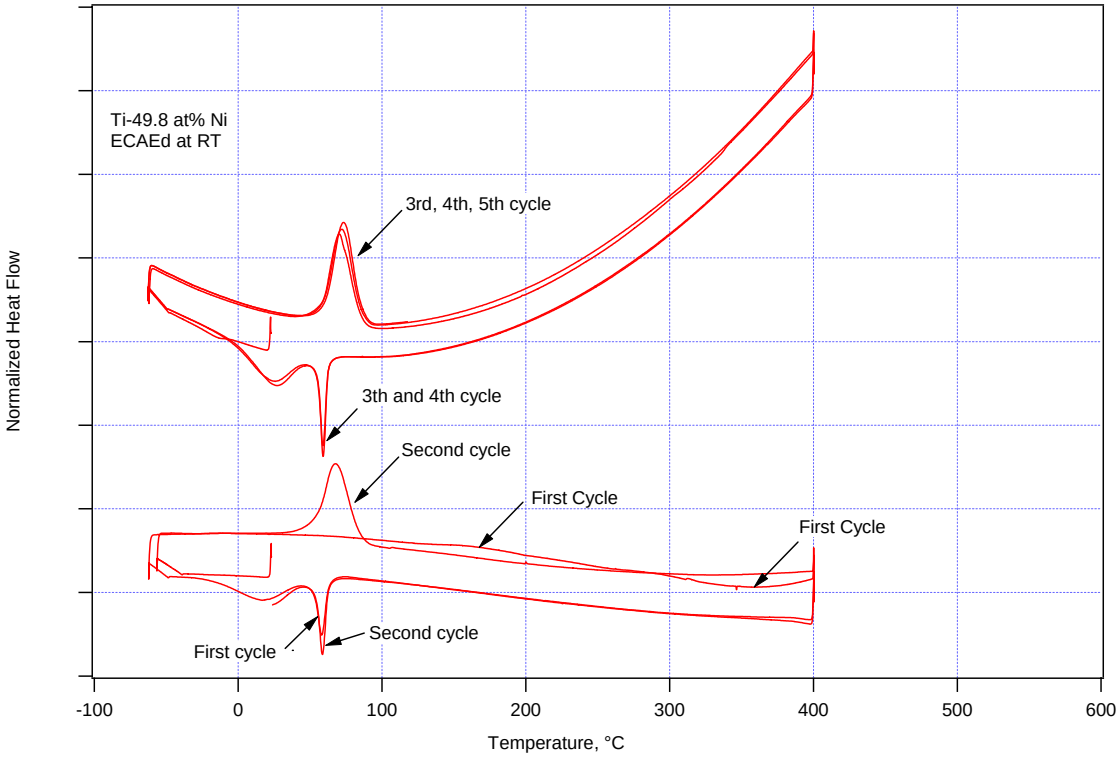

Figure 3.1.4. Cyclic DSC response of the samples ECAEd at room temperature demonstrating the stability of TTs after second cycle.

In order to visualize and to better understand the change in TTs after deformation, TTs for the first and second cycles were plotted in Figure 3.1.5.

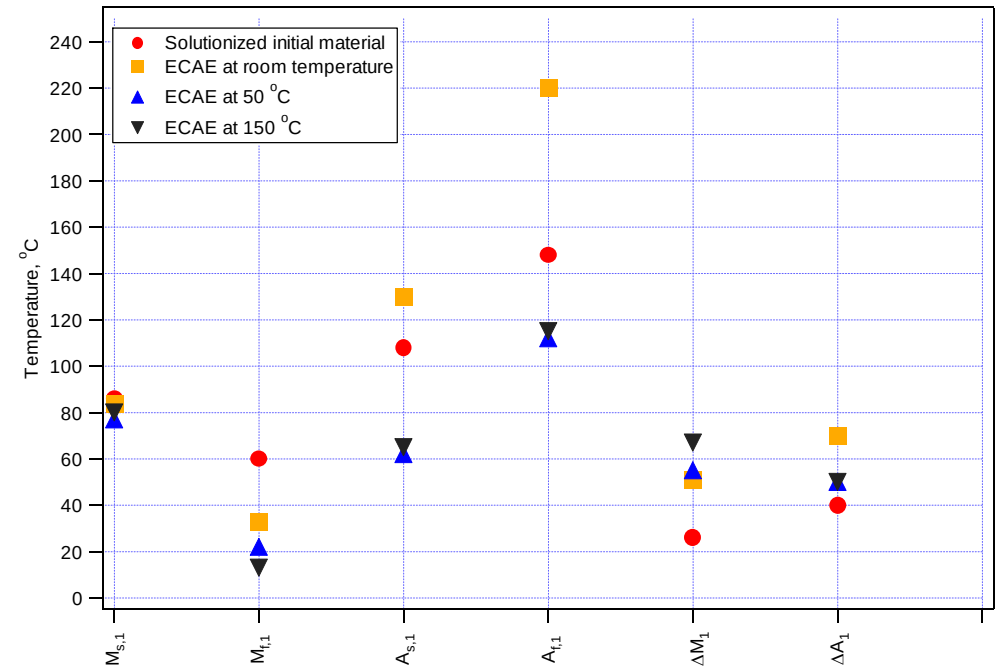

(a)

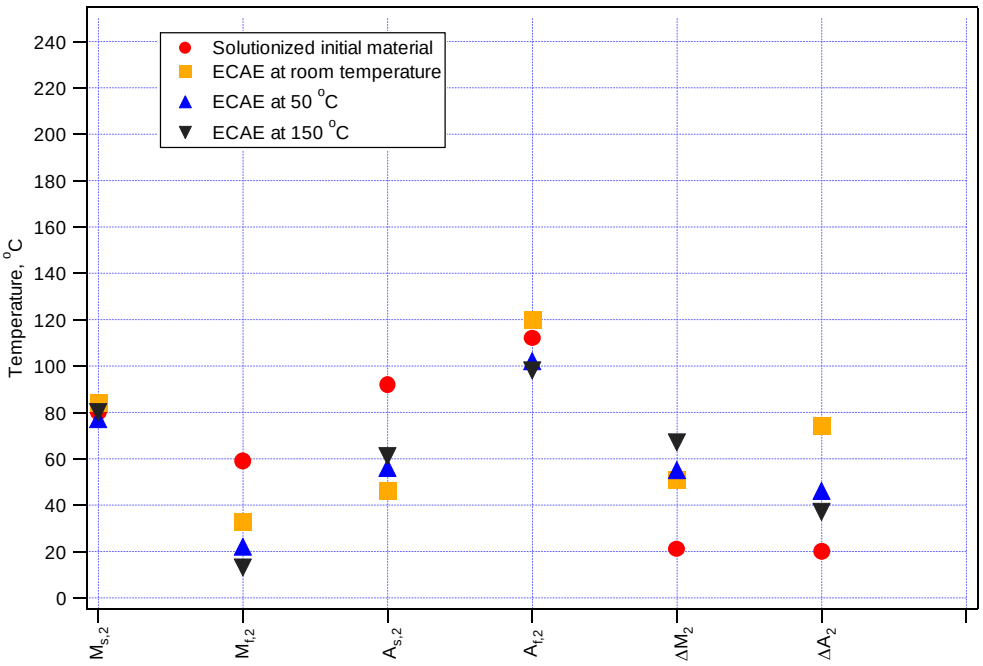

(b)

Figure 3.1.5. The effect of severe deformation temperature on characteristic transformation temperatures and transformation intervals. (a) first reverse and forward transformations and (b) second reverse and forward transformations.

Before reaching to conclusions from DSC results, it is important to keep in mind that there are some minor differences from sample to sample. These are all in the range of experimental error and the main reason is the fact that samples were obtained from different places of the specimens. Although ECAE provides a uniform deformation the formation of macroscopic shear bands may result in different behaviors.

The first reverse transformation temperatures (A_{s1} and A_{f1}) increase significantly in the sample deformed at room temperature while the situation is opposite in the samples deformed at 50°C and 150°C. Surprisingly, M_{s1} has not changed much in all cases while M_{f1} decreases with increasing deformation temperature. Both transformation intervals (ΔM_1 and ΔA_1) increase after deformation, however, they exhibit an opposite deformation temperature dependence, e.g., ΔM_1 slightly increases with increasing deformation temperature while ΔA_1 slightly decreases.

In the second and successive thermal cycles, M_s and M_f do not differ significantly from the ones in the first thermal cycle. However, A_s and A_f temperatures considerably drop. The drop (80 – 100 °C) is substantial in the sample deformed at room temperature while it is only about 15°C in the samples deformed at 50°C and 150°C.

When the sample is deformed at room temperature, it is deformed in the martensitic state. A very high dislocation density is stored especially in martensite plates and internal twin boundaries [30,76,77]. Phase boundaries are hindered for reverse transformation due to high dislocation density [21,78]. Thus, there is a significant increase in A_s and A_f temperatures in the first reverse transformation of the samples deformed at room temperature (Figure 3.1.5.a). The ΔA_1 is large probably because of the non-uniform distribution of internal stress field leading to local reverse transformation at different temperatures.

The stable M_s temperature after deformation and first heating is attributed to the dislocation substructure formed during martensite deformation and the anisotropic

internal stress field. The anisotropic internal stress field helps biased A→M transformation and therefore, no change is evident in M_s. A similar concept is observed in heavy austenite deformation [24,79-81] after which the A_s temperature does not change while the M_s temperature drops (austenite stabilization). The effect of an anisotropic internal stress field on M_s can be thought as similar to the effect of applied stress in which the applied stress favors the nucleation of certain martensite variants and increases the M_s temperature [6].

Once the internal stress assisted martensite variants form upon cooling after first heating, it is easier to transform them into austenite in the second cycle than transforming all multiple martensite variants into austenite in the first cycle. This is because of the effect of unrelaxed stored elastic strain energy that is available once the internal stress field assisted martensite variant forms. As an analogy to the anisotropic internal stress hypothesis, in recent studies on precipitation hardened single crystalline NiTi, it is observed that the higher the applied stress is, the lower the thermal hysteresis (A_s-M_s) becomes [6]. At certain applied stress levels, A_s is lower than M_s. The coherent precipitates in these materials which provide anisotropic internal stress field magnify the effect of an applied stress field.

In the samples deformed at 50°C and at 150°C, the lower A_s and A_f temperatures during the first heating is attributed to the effect of the initial deforming phase and the deformation mechanism. In the 50°C case, the deformed sample consists of both deformed martensite phase and strain induced B2 phase as it will be shown in Section 3.2. When it is cooled to room temperature and the DSC analysis is started at room temperature, some of the B2 phase has already transformed back into martensite. Therefore, the conditions for either stabilization of austenite or martensite might have been relieved. Due to the anisotropic internal stress field developed and the stored elastic strain energy due to the newly formed martensite upon cooling, the first heating does not demonstrate any martensite or austenite stabilization. On the contrary, the drop in A_{s1} and A_{f1} temperatures is similar to what is observed in the second heating of the sample

deformed at room temperature. The same mechanism holds for the sample deformed at 150°C.

The effect of annealing temperatures on the characteristic transformation temperatures of the sample deformed at room temperature is illustrated in 3.1.6. Figures 3.1.6a and 3.1.6b present the temperatures for the first and second thermal cycles, respectively. The M_{s1} and M_{f1} temperatures slightly decrease and the ΔM_1 increases with increasing annealing temperature up to 500°C. At 500°C and above, M_{f1} significantly increases leading to decrease in ΔM_1 to values lower than the one in the solutionized material (Figure 3.1.5). In the second thermal cycle, the A_{s2} and A_{f2} temperatures are significantly lower than A_{s1} and A_{f1} temperatures such that increasing annealing temperatures only lead to a slight decrease in the former up to 500°C and an increase above 500 °C. ΔA_2 does not change much with annealing. The M_{s2} and M_{f2} temperatures follow the same trend with the M_{s1} and M_{f1} temperatures.

The main conclusions that can be drawn considering the effects of deformation are:

- Martensite stabilization in the samples ECAEd at RT
- No salient first cycle effect after ECAE at 50°C and 150°C
- Similarity of DSC curves between the samples ECAEd at 50°C and 150°C
- Stability of TTs after first cycle
- Stability of M_s in all cases
- Decrease in A_s and A_f for ECAE at 50°C and 150°C
- Increase in ΔA and ΔM in all cases

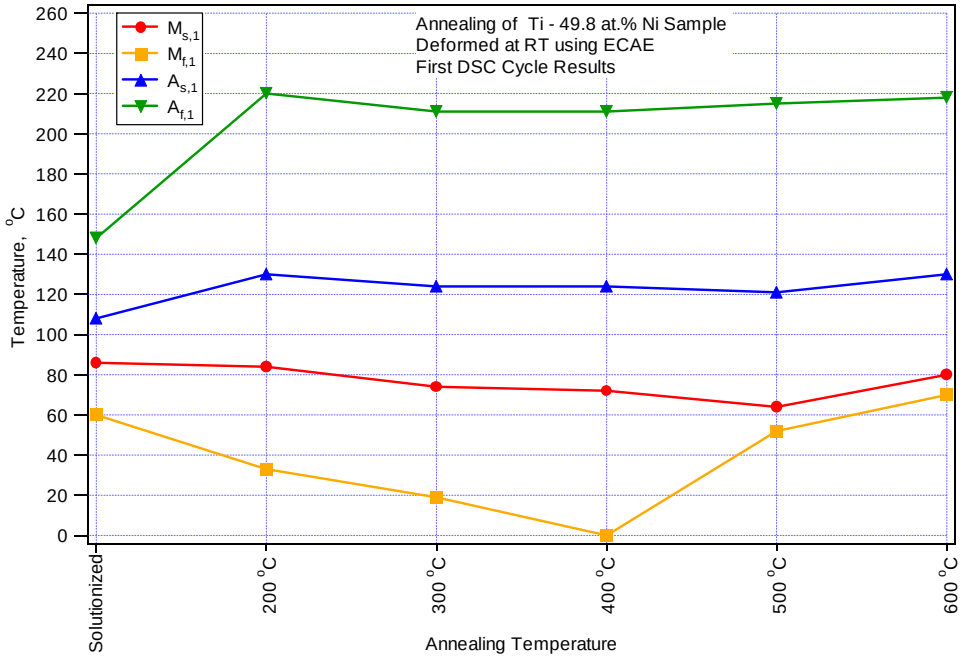

(a)

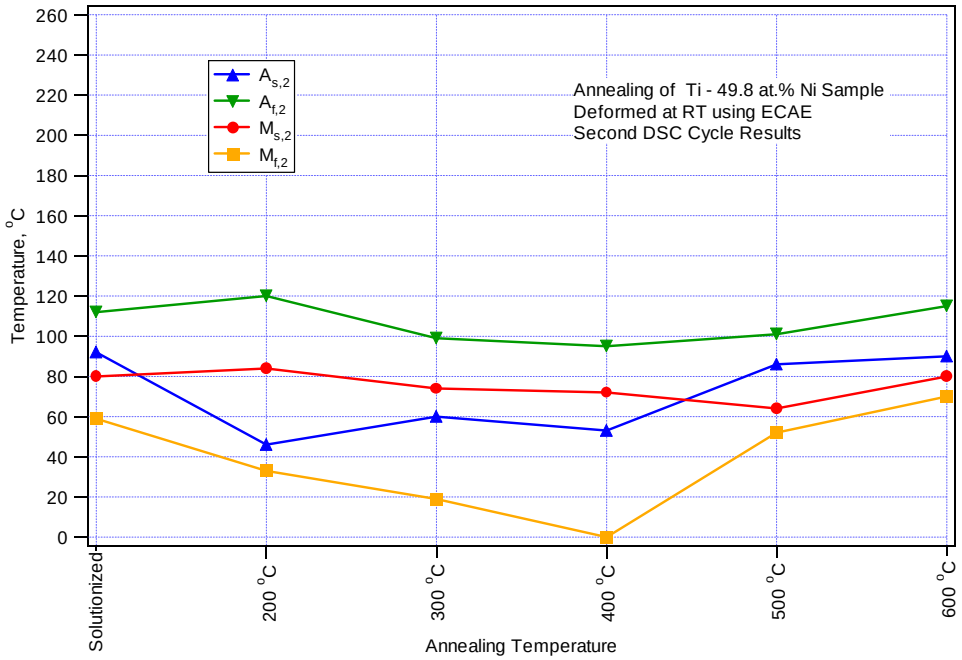

(b)

Figure 3.1.6. The change of transformation temperatures upon annealing of the sample deformed at room temperature in the martensitic state using ECAE, (a) upon first heating and first cooling and (b) upon second and successive heating and cooling. The data points were extracted from the DSC scans.

The effects of annealing after deformation at RT can be summarized as;

- M_{f1} and M_{f2} decrease after annealing up to 400°C and increase after annealing above 400°C
- M_{s1} and M_{s2} decrease slightly after annealing up to 500°C and return back to original value after annealing above 600°C
- A_{s2} is lower than A_{s1} and constant for annealing up to 400°C and returns back to original value after annealing at 500°C or 600°C
- A_{f2} slightly decrease up to 400°C and increase after that.
- Recrystallization starts around 500°C and completed at 600°C
- Up to 400°C only recovery takes place
- Increasing the number of thermal cycles does not change the TTs but increases amount the material undergoes phase transformation slightly.

In summary, the present results and the previous studies on the cold rolling of austenitic NiTi [24,77,79,82] proves that the deformation in the fully martensitic state leads to martensite stabilization while austenite stabilization is demonstrated to be the result of deformation in the austenite. If the TTs of the undeformed material are close to each other (low thermal hysteresis), then deformation near M_s in the austenitic state and deformation near A_s in the martensitic state can cause formation of stress-induced martensite and strain-induced austenite (parent phase), respectively. When this is the case, the above generalization for the martensite and austenite stabilizations do not hold. The consideration of an anisotropic internal stress field and the stored elastic strain energy of newly formed martensite variants is helpful in understanding the change in TTs after deformation under different conditions (cold rolling, tension, shear, simple shear) and at different deformation levels, in an analogy with the effect of applied stress on TTs.

These observations demonstrate that up to 500 °C the samples deformed at room temperature experience restoration and above 500 °C recrystallization starts. Although

A_{s1} and A_{f1} temperatures are observed upon first heating, the transformation enthalpies are low and thus, it is likely that the reverse transformation ($M \rightarrow A$) continues to occur simultaneously with restoration. This is also evident when comparing the martensite transformation peaks upon first cooling. The higher the annealing temperature, the higher the $A \rightarrow M$ transformation enthalpy and sharper the peaks, indicating that there is more austenite to be transformed into martensite. The sudden decrease in ΔM upon annealing above 500 °C to values which are lower than the one for solutionized material is probably because of recrystallization and preferred martensite variant formation. Another possibility is the effect of grain size on the martensite transformation temperatures. Khelfaoui and his colleagues [82] observed in their study on deformed and recrystallized near equiatomic NiTi that the transformation interval decreases with decreasing recrystallized grain size. Therefore, since the annealing treatment in the present study is just for short times, it is likely that the recrystallized grain size is lower than in the initial solutionized material, and thus the transformation interval is smaller.

3.1.2 DSC Analysis for Peak Identification

As explained in Chapter 1, R-phase formation could be observed in materials by several ways and thermo-mechanical treatment is one of them. The TTs obtained from DSC curves are complicated because of the broad nature of peaks. It is not clear whether the shoulders on the main peaks or in some cases formation of two peaks are due to the R- phase transformation or not. In order to clarify this point, interrupted DSC tests were conducted on the samples deformed at RT and annealed at 400°C and 500°C. For the former case there are two distinguishable peaks during cooling but there is only one peak during heating as shown in Figure 3.1.2. For the latter one, there are two peaks which are very close to each other and the valley between them is not well-defined.

DSC responses of two different samples annealed up to 400°C are shown in Figures 3.1.2 and 3.1.4. In both cases there are two transformation peaks during cooling and one during heating. The small hysteresis of transformation start and finish temperatures implies that the first peak could be attributed to the R-phase but there is no peak for reverse transformation of this R-phase. The sample used to obtain the DSC curve in Figure 3.1.2 is used again for this analysis and results are shown in Figure 3.1.7. During first heating, a broad peak with a shoulder on left is obtained and the cooling process is interrupted after the first peak. During second heating a new peak at 60°C is formed which is not seen before. Also a small peak at 84°C is formed. The new peak at 60°C is the back transformation from R-phase to austenite. Small hysteresis between forward and back transformations is the salient feature of R-phase transformations. During cooling, again two peaks are observed and the following heating resulted in disappearance of the peak at 60°C and a smooth curve as in the initial DSC curve. The thermal hysteresis of R-phase during is determined to be only 4°C.

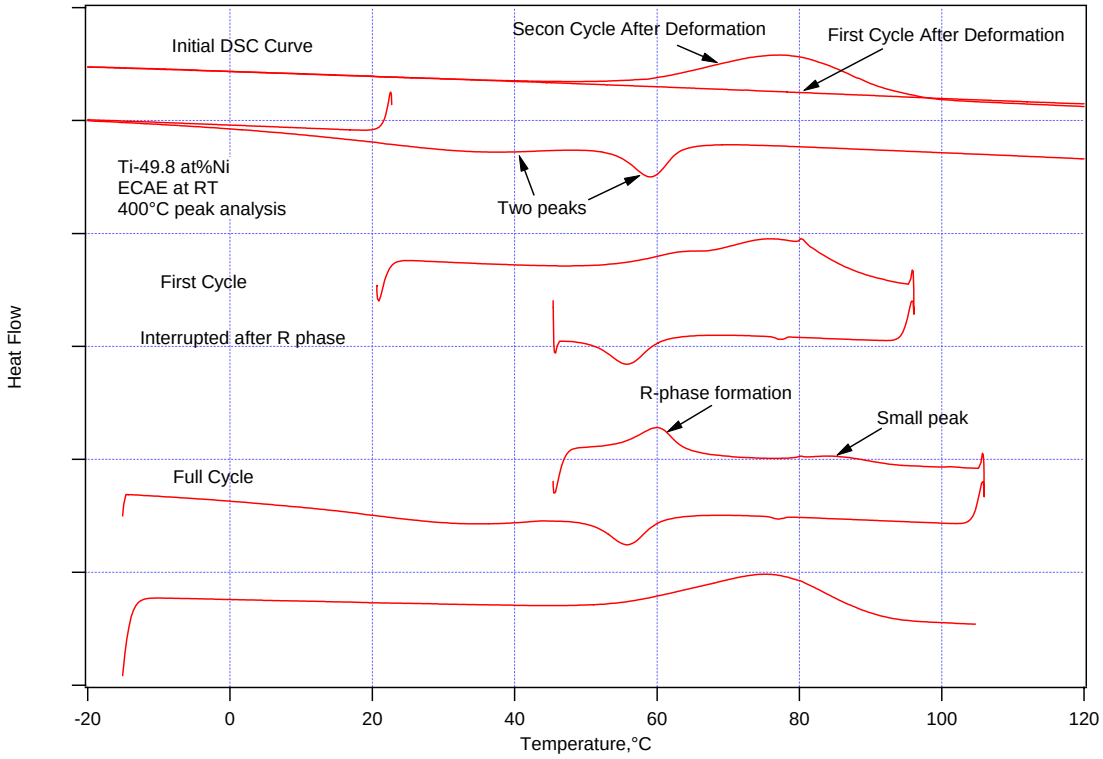

Figure 3.1.7. DSC response of sample ECAEd at room temperature and annealed at 400˚C for transformation peak analysis.

DSC analysis for peak identification after annealing at 500°C is conducted on the sample shown in Figure 3.1.2. The initial DSC curves are added to the bottom of the sets as shown by Figure 3.1.8. After first heating of the sample, the cooling process is interrupted after the first peak (R-peak). In the following heating, a new peak (R'-peak) at 64°C is formed and instead of a large peak at 89°C two small peaks observed. The second small peak (S-peak) corresponds to the shoulder of the initial curve and the first small peak (A-peak) is attributed to the transformation from B19' to austenite since the interruption temperature slightly exceeded the valley temperature and some of the R-phase is transformed to B19'. The R-peak is formed during second cooling and the process is interrupted at M-peak temperature. The formation of R-phase during heating is suppressed since the height of new R'-peak is smaller. Height of the A-peak is

increased which reveals that this peak is related to back transformation of the transformation products at the second peak (M-peak) during cooling which is R to M transformation and S-peak is still remained.

In order to make sure that the A-peak is related with the M-peak, the cooling process is interrupted at R-peak temperature. During heating R' and S peaks are observed and A- peak is disappeared. So it is very clear that the first peak during cooling is A to R phase transformation and the second one is R to M transformation and during heating formation of martensite suppress the R phase transformation and transforms directly to austenite. However the formation of shoulder or if there is no R to M phase transformation formation of S-peak at the shoulder temperature is not clear. In order to clarify this, heating process is interrupted before the formation of shoulder and during cooling there is no change in R-peak but M-peak is shifted about 1°C to the left. On the subsequent temperature cycles, the shoulder has disappeared.

In literature, at most three transformation peaks were reported on DSC curves during cooling and two peaks during heating [83-85]. The three peaks were identified as R-phase transformation and two B19' phase formation in precipitated and non-precipitated areas [83]. The precipitation effect could be neglected in our material since the composition is Ti-rich and very close to equiatomic composition. However, due to severe deformation, nanograins could be formed by annealing at temperatures close to recrystallization temperature. TEM results confirmed the formation of nanograins after severe deformation. It is also revealed that the newly formed nanograins have stress contrast [86]. Required transformation energy for reverse transformation could be higher for newly formed nanograins than the rest of the material since the grain boundaries could act as extra energy barriers. This idea is supported by the observation that if the grain size is less than 15 nm only R-phase (small transformation strain) transformation could occur in the grains.

In this study, S-peak is still formed after interruption at R-peak which means that S-peak is related with back transformation of R-phase. The formation of S-peak is attributed to the back transformation of nanograins formed by annealing up to 500˚C after ECAE at room temperature. When the reverse transformation of these nanograins is suppressed, their transformation ability ceases. Two explanations are proposed for disappearance of S-peak. 1) The nanograins could also be considered as precipitates in the matrix. During forward transformation they suppress the martensitic transformation and stress fields formed around them prevents their back transformation. 2) During R-phase transformation the elastic energy is stored in nanograins and this elastic energy is released during the forward transformation of the surrounding matrix. This phenomenon is same with martensite stabilization and higher temperatures would be needed for back transformation of nanograins.

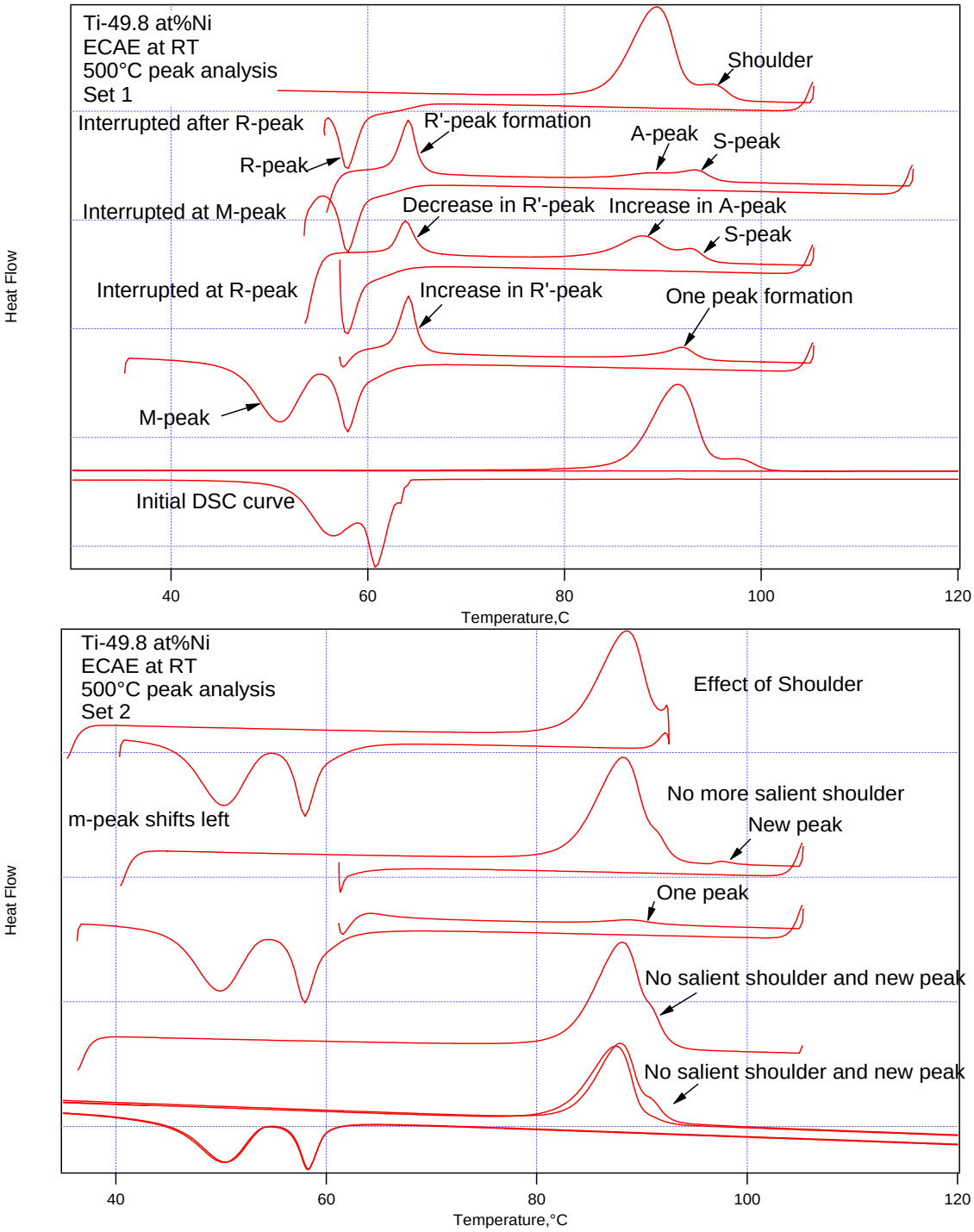

Figure 3.1.8. DSC response of sample ECAEd at room temperature and annealed at 500˚C for transformation peak analysis.

3.2 X-ray Diffraction Results

DSC results give us the information about transformation of the phases but not detailed information about microstructure and the phase structure. In order to determine the phases present after deformation, X-ray diffraction (XRD) patterns obtained from the samples severely deformed at different temperatures and from the initial material are presented in Figure 3.2.1.

The solutionized material is identified as monoclinic B19' martensite by using. As seen in Figure 3.2.1, the broad central set of peaks may have contributions from all three possible phases, i.e. B2 austenite, B19 orthorhombic martensite and B19' monoclinic martensite. The corresponding 2θ angles of the crystallographic planes of three phases are very close to each other between 35 and 45 degrees. Monoclinic martensite is, however, easily identified from the (001) reflection at around 2θ = 19 ° and the whole spectrum obtained on the solutionized material could be fitted based on B19' only. The experimental spectrum also displays strong $(001)_{B19'}$, $(002)_{B19'}$ and $(-111)_{B19'}$ reflections but a rather weak $(012)_{B19'}$ reflection, whereas the latter should be more pronounced in randomly oriented polycrystals. This demonstrates that a significant texture is present in this material. Severe simple shear deformation using ECAE causes a drastic change in texture as it is evident from the change in relative peak intensity of the $(002)_{B19'}$ reflection upon deformation at room temperature. Substantial peak broadening is apparent upon deformation. However, given the substantial overlap of the prominent peaks, no attempt was made to extract more quantitative information on dislocation density and the relative volume fraction of the phases from the experimentally obtained spectra.

The spectrum obtained on the sample deformed at room temperature indicates the presence of orthorhombic B19 phase, as shown by an arrow in Fig. 3.2.2. A good fit to the whole experimental spectrum was only obtained when orthorhombic martensite was included. Normally monoclinic and orthorhombic martensites are not observed at the

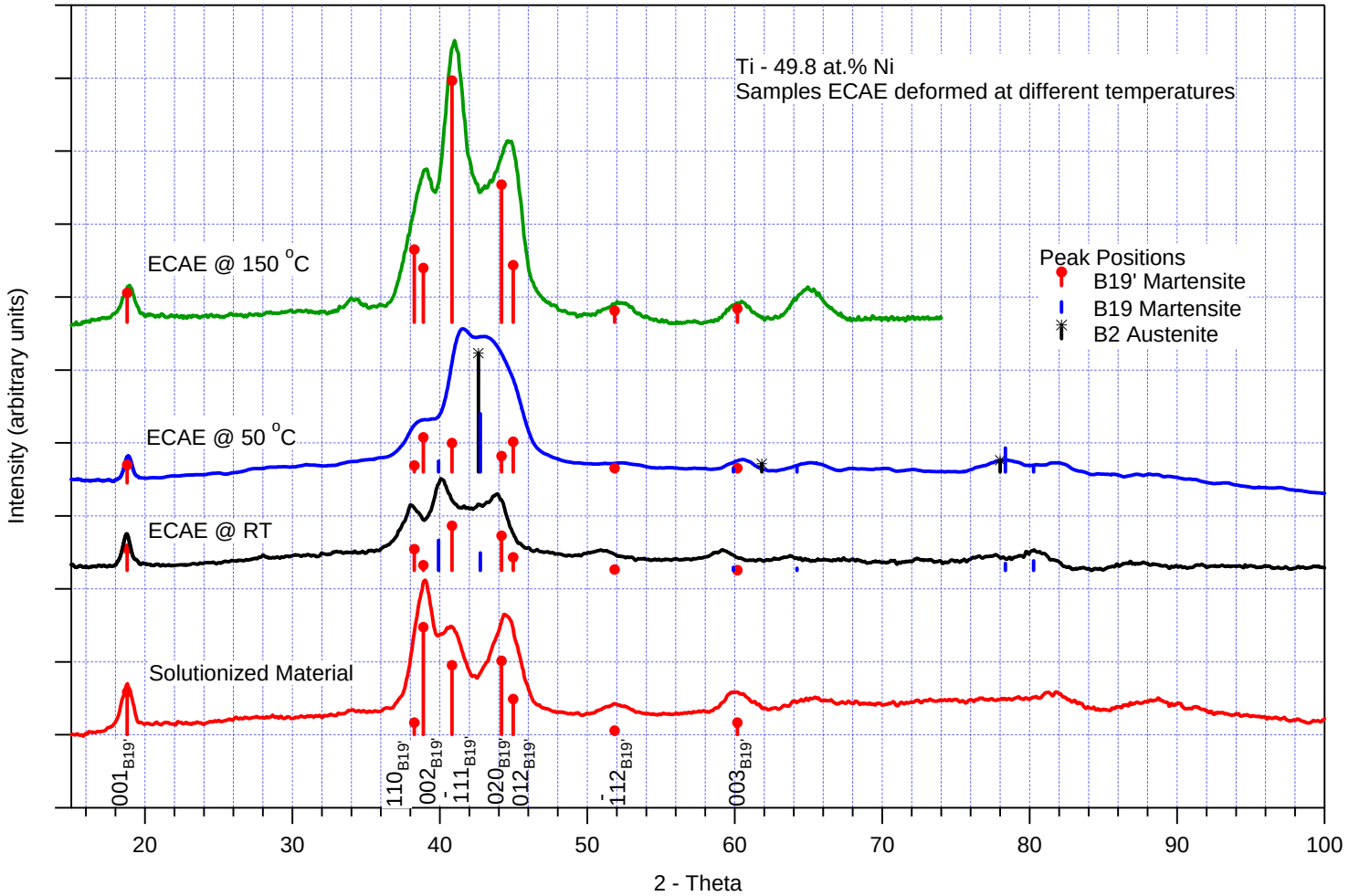

Figure 3.2.1. Comparison of XRD patterns from the samples deformed with ECAE at different temperatures and the initial material. The experimental spectra were fitted considering three possible phases B2, B19' and B19. Vertical lines demonstrate these fitting results.

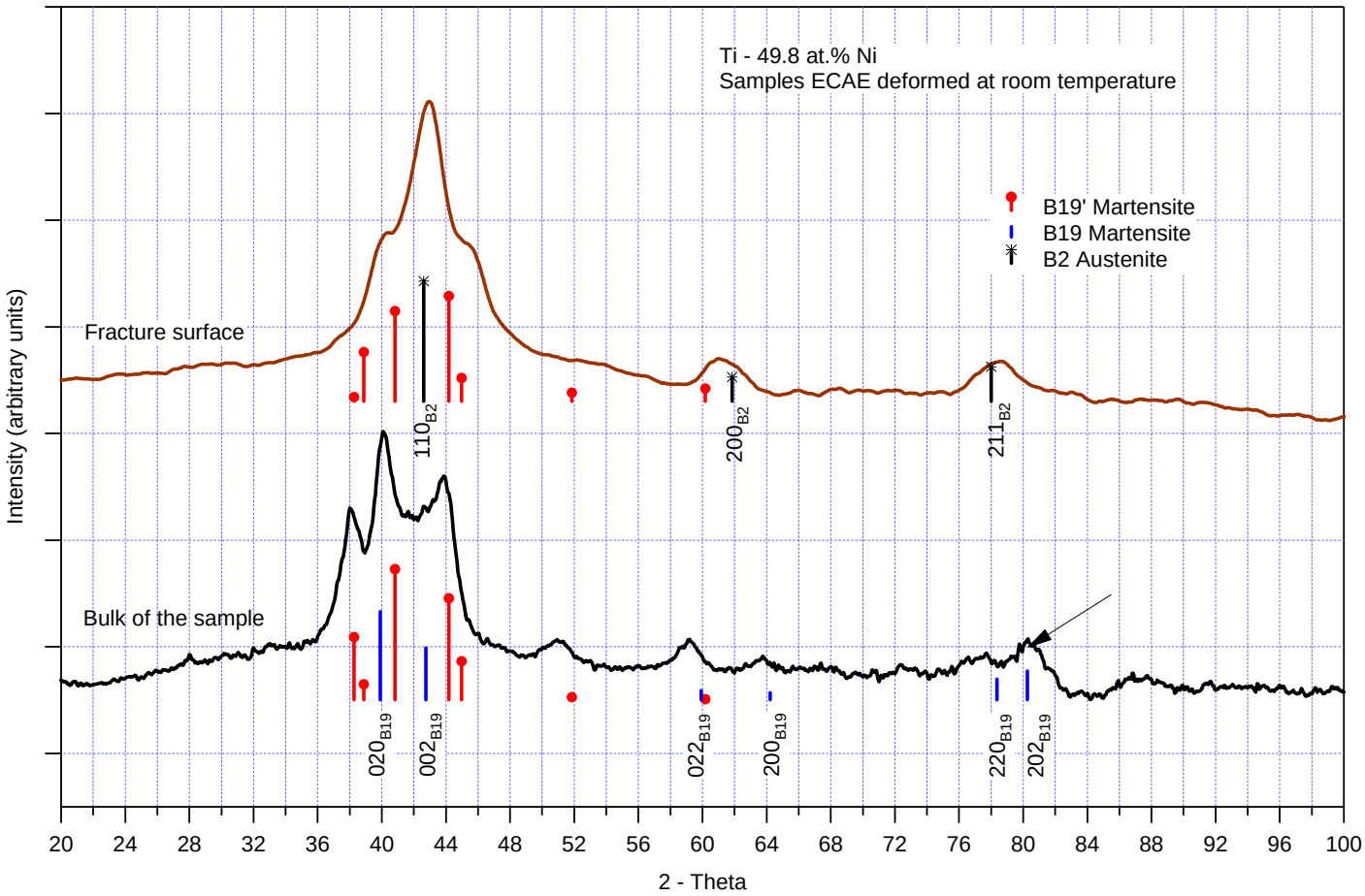

Figure 3.2.2. Comparison of XRD patterns from the fracture surface and the bulk of the sample deformed at room temperature. The experimental spectra were fitted considering three possible phases B2, B19' and B19. Vertical lines demonstrates these fitting results.

same time in near equiatomic NiTi. It is assumed that orthorhombic martensite could form because of the unique deformation conditions present during ECAE.

It is important to emphasize one of the major drawbacks of XRD analysis such that it only provides information about phases near the surface. In order to prove the existence of B19 phase in bulk, bulk diffraction methods such as neutron scattering should be utilized [87]. Moreover, as will be discussed later TEM investigations and corresponding electron diffraction patterns did not reveal any B19 phase in the sample deformed at room temperature supporting the necessity of bulk diffraction analysis.

The XRD patterns from samples deformed at 50°C and 150°C appear significantly different (Figure 3.2.1). For the samples deformed in the austenitic phase at 150°C, XRD patterns are indicative of mostly monoclinic B19' martensite and strong texture is evident. $(110)_{B19'}$, $(020)_{B19'}$ and $(-111)_{B19'}$ peaks are dominant. On the other hand, a good fit to the spectrum obtained on the sample deformed at 50°C was only obtained when all three phases, i.e. B2, B19 and B19' were assumed to be present. For the following discussion it is important to note that any significant B2 peaks were not observed after deformation at room temperature in the bulk of the samples.

To prove that B2 phase is evident in the sample deformed at 50°C, a detailed TEM diffraction analysis was conducted. Figure 3.2.3 demonstrates the bright field images from this sample with the corresponding diffraction patterns. As it can be seen from the images, martensite is very thin (about 100 nm thick) and the boundaries can still be seen although the deformation level was quite high (Fig 3.2.3b). The diffraction patterns demonstrate that B2, B19' with internal twins and B19' without internal twins are present in the microstructure. B2 and B19′ phases are along $[-110]_{B19'}$ and $[-1-11]_A$ directionsas shown in Figure 3.2.3b. Note that $[-1-11]_A$ //$[-110]_{B19'}$ while $(101)_A$ deviates about 3° away from $(001)_{B19'}$, which is close to the orientation relationship observed before [16,24]. As a result, TEM observation supports the X-ray analysis fit as shown for B2 and B19' phases. It is also noteworthy that the martensite plates can be ditinguished

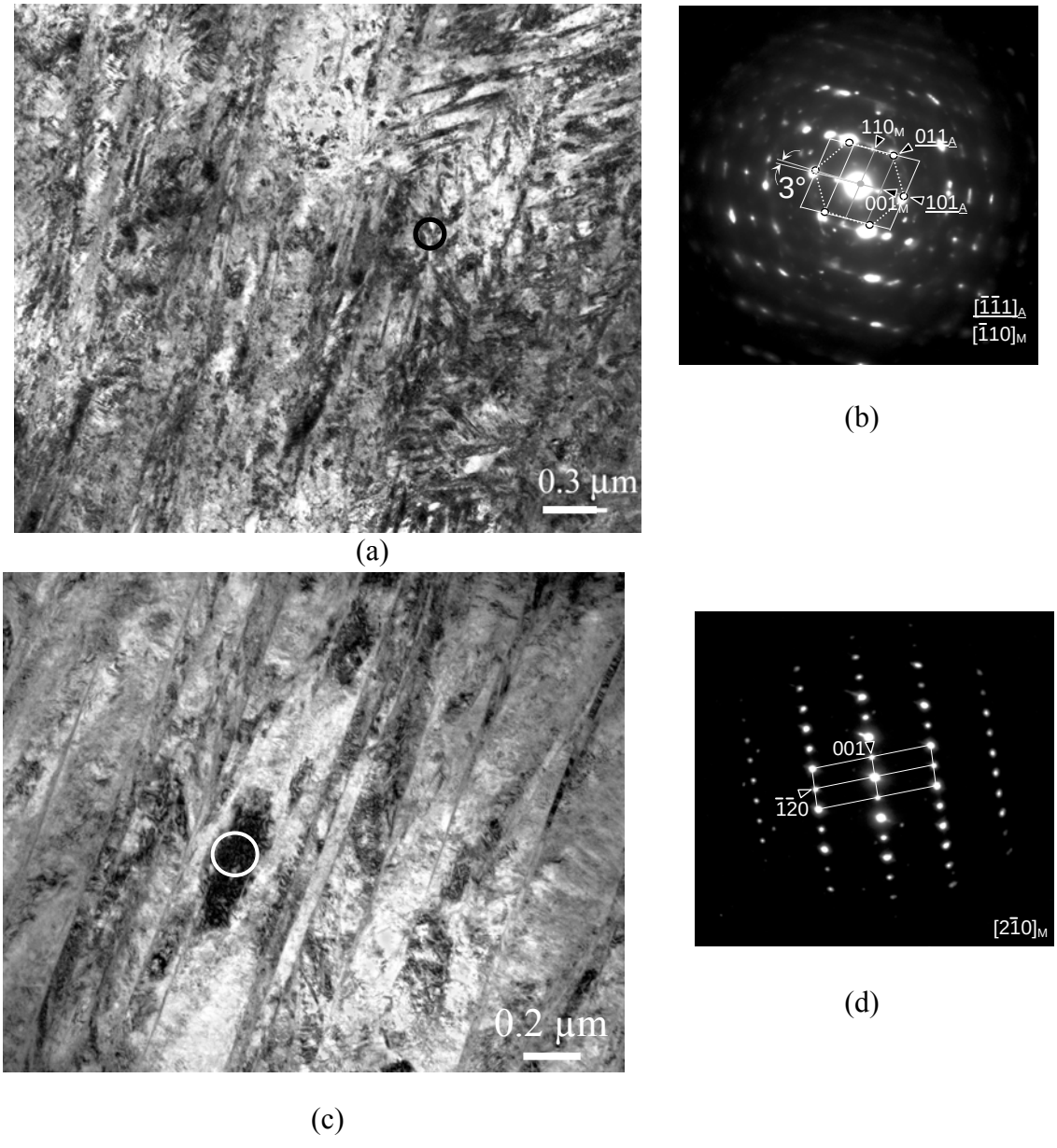

Figure 3.2.3. a) Bright field TEM images of the sample ECAE processed at 50°C initially having B19′ structure. The deformed material has both B2 and B19′ phases present as shown in the electron diffraction pattern along $[\bar{1}10]_{B19'}$ and $[\bar{1}\,\bar{1}\,1]_A$ in (b), c) shows twinned martensitic microstructure and the corresponding diffraction pattern in (d). The diffraction patterns were taken from the circled areas in (a) and (c).

easier in Figure 3.2.3b than Figure 3.2.3a representing less deformed structure than the microstructure shown in Figure 3.2.3b. The rationale of this diference will be discussed later.

XRD patterns from the fracture surfaces were also investigated to reveal the possible reasons of failure and whether there is any relation between failure and existing phases near cracks. A representative pattern is shown in Figure 3.2.2 and compared with the spectra obtained on the bulk material. In comparison with the bulk of the material deformed at room temperature, a significant amount of B2 phase reflections are evident. Moreover, the relative peak intensities obtained for the B2 phase are in good accordance with those on pure B2 phase reported in literature, indicating that there is not a strong texture in the B2 phase.

A few other studies [26,88,89] reported similar experimental findings that after deformation of the martensitic phase, the materials had B2 phase. This observation is either attributed to the strain-induced B2 phase formation [89] near crack tip or non-uniform distribution of martensite and austenite phases in the initial material [26]. The present study demonstrates that the former is a more plausible explanation as the fracture surfaces mostly involve austenite. It is likely that a significant portion of the work of deformation is converted into heat as a result of the interaction of several martensite and internal twin interfaces. This can be quite significant as it has been demonstrated that very high dislocation densities are accumulated at these boundaries [76]. Consequently, the material can locally reach the A_s temperature and transform into B2. Since the thermal conduction is poor in these alloys, the transformation remains local. The stress fields around the strain-induced B2 phase would cause it to remain in this structure even if martensite is more stable at a particular temperature. That's probably why the sample deformed at 50°C has an austenite component. Some of the strain-induced austenite should transform back into martensite through stress-induced martensitic transformation especially at crack tips or by stress relaxation at crack surfaces or upon cooling to room temperature [89]. The nucleation of new phases on crack tips has been reported in the

literature for various materials [90]. Therefore, the fracture surfaces in the present deformed samples consist of both martensite and austenite phases.

The observation of the strong martensite reflections is peculiar for the specimens deformed at 150°C which are expected to be in the austenitic state. Even though the specimen is cooled down to room temperature, if the sample is deformed plastically in the austenitic state to high strain levels, one would expect austenite stabilization and significant drop in M_s and M_f such that at room temperature the material would be in the austenitic state. However, the specimen probably experiences stress induced martensitic transformation at the beginning of deformation before any significant slip activity occurs. Then, the martensite goes through the same deformation mechanisms similar to the one in the samples deformed in the martensitic state.

Figure 3.2.3b shows the oriented martensite plates and Figure 3.2.3a shows the area with multiple variants in the sample ECAEd a 50°C. In the high dislocation zones, strain induced parent phase would form as a result of adiabatic heating. For the sample ECAEd at 150˚C, there is no martensite variant reorientation so the stress induced martensite could form throughout the material

The remaining question is why there is no B2 phase in the samples ECAEd at RT. The main differences between the deformation at RT and 50°C are the deformation temperature, extrusion rate and the diameter of the NiTi bars. The temperature increase at RT would not be enough to induce B2 phase since the high extrusion rate used for RT extrusion would not let the conduction of the localized temperature increase to the bulk of the specimen. This explanation is supported by the presence of B2 phase in the fracture surfaces only for the specimen deformed at RT while B2 phase is present also in the bulk of the sample ECAEd at 50°C.

3.3 Hardness

The material resistance to localized plastic deformation is a material property and can be measured by hardness test. Hardness is simple, inexpensive and nondestructive. Also the strength of the materials could be estimated or compared by using the hardness measurements of the materials. Vickers microhardness test is utilized for the hardness measurements in this study. The results for the solutionized and deformed samples are shown in Figure 3.3.1.

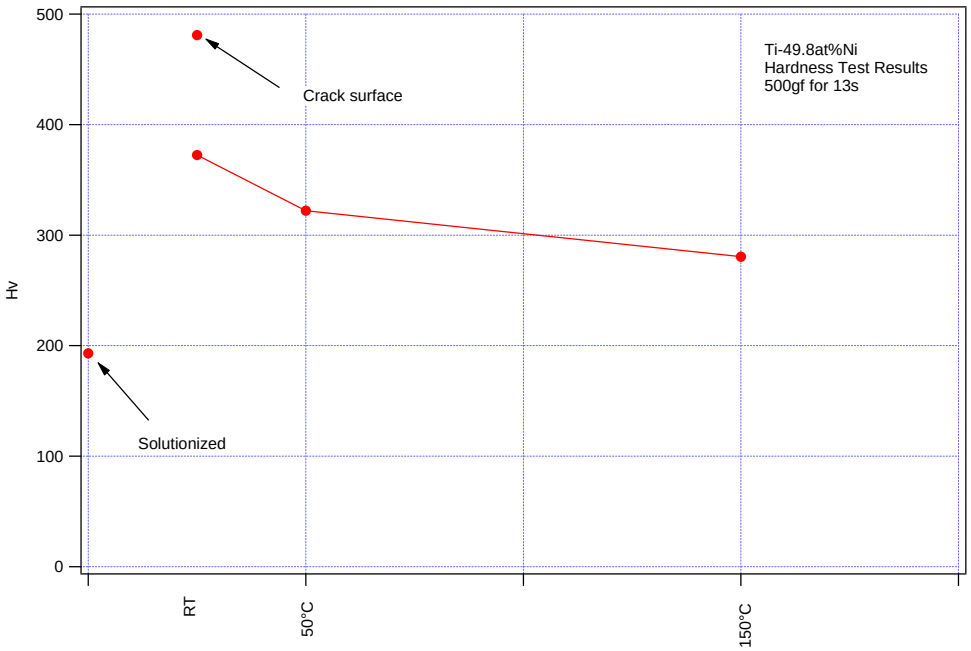

Figure 3.3.1 Vickers microhardness results of the solutionized and as-deformed samples.

The sample deformed at room temperature has the highest strength as its hardness value is increased 93% after deformation where Hv value is increased 67% and 45% for the deformations at 50˚C and 150˚C respectively. The increase in hardness is attributed to the high dislocation density which resists to the deformation by indenter.

The hardness of the fracture surface is also measured and added to the graph. The Hv value of 380 corresponds to the 35% cold rolling according to the hardness graph reported by Lin and Wu [21]. The corresponding cold rolling amount of fracture surface could be estimated by 40% by using the same graph. Furthermore Nakayama et al. [27] reports a hardness graph for different deformation amounts and stated that after some amount of cold rolling the hardness value (450 Hv) does not change with increased cold rolling and macroscopic shear band formation starts. These are in good agreement with the results shown in Figure 3.3.1. All the hardness values in the bulk samples are below the 450 Hv and the hardness of the surface which is 481 Hv is above it due to the formation of macroscopic shear band.

3.4 TEM Results

In order to investigate the effects of severe deformation and the test temperature on the microstructure TEM studies were conducted. Samples from solutionized and ECAEd at RT, 50˚C and 150˚C were cut and prepared as explained in the experimental techniques section. Samples from ECAEd at RT were heated up to 300˚C and 400˚C with a rate of 10˚C/min (same rate was used in DSC analysis) and air cooled to RT. The aim of these heat treatments was to investigate the effects of annealing on the samples.

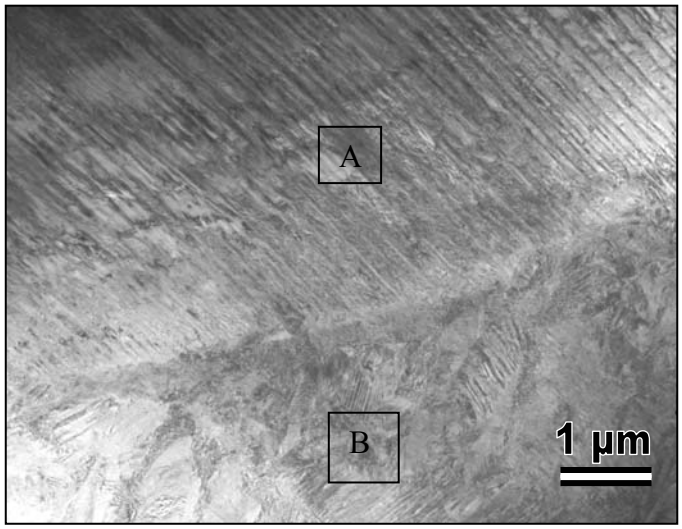

(a)

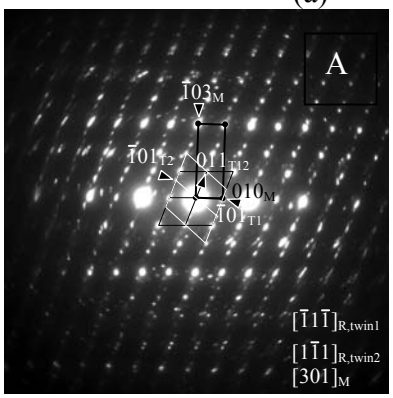

(b)

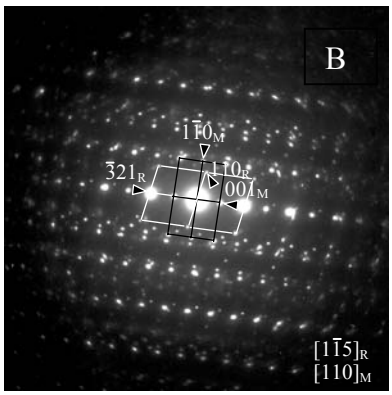

(c)

Figure 3.4.1 a) TEM image and the corresponding diffraction patterns of the solutionized Ti-49.8 at% Ni taken from area b) A and c) B shown in (a).

Figure 3.4.1 shows the TEM images of the solutionized sample. The internally twinned structure of B19' phase could be easily identified. However the corresponding diffraction patterns reveal that the matrix is a mixture of B19' and R-phase. Diffraction pattern was indexed and the crystallographic orientations between B19' and R-phase were revealed as:

$$[301]_{B19'} // [-1\ 1\ -1]_{R1} // [1\ -1\ 1]_{R2} \text{ and } (-1\ 1\ 3)_{B19'} // (011)_{R1} // (011)_{R2}$$

Two linear lines which are on the right and left hand side of the central spot are slightly shifted with respect to each other which are the characteristic of monoclinic structures.

TEM images of the samples ECAEd at RT are shown in Figure 3.4.2. The structure is highly deformed. The diffraction pattern reveals that B19' is the present phase. The martensite variants are oriented along one direction.

TEM images of the samples annealed up to 300˚C and 400˚C are shown in Figures 3.4.3 and 3.4.4, respectively. There isn't any significant microstructural changes observed when compared to the as deformed structures. However, the annealing of some dislocations is evident from bright filed images. Also formation of new spots in diffraction patterns indicates the formation of new grains or annealing of dislocations in highly deformed grains.

When a detailed investigation was conducted, very interesting findings could be revealed. Figure 3.4.5 shows the TEM image of the ECAEd at RT. The formation of nanostructures in the martensite plates is evident as could be seen in the enlarged picture. The diffraction pattern has a ring structure which reveals that these nanostructures are individual grains. The formation of nanograins is attributed to the formation of shear bands and the high dislocation density formed in these bands.

As explained in Section 3.2 the presence of B2 and B19' after deformation is supported both by the X-ray data and TEM images. Figure 3.4.6 shows the additional images and indexed diffraction patterns. The electron diffraction pattern from B2 and B19' phases are indexed as $[-1\ -1\ 1]_A$ and $[-3\ 2\ 0]_M$ zone axes respectively as shown in Figure 3.6.4b. The $(101)_A$ is 4° away from $(001)_M$. As compared to the orientation relation observed on the left side, $[-1\ -1\ 1]_A$ is not parallel to $[-1\ 1\ 0]_M$ but $[-3\ 2\ 0]_M$. However, note that $[-3\ 2\ 0]_M$ is only 11.4º away from $[-1\ 1\ 0]_M$, implies that they are the same type of orientation relation, only the $[320]_M$ is rotated towards the $[111]_A$ under the deformation. In fact, the $[-3\ 2\ 0]_M$ is not along the exact Bragg reflection orientation, as evidenced by the fact that the intensities of the spots in the upper-right row is weaker than the lower-left row.

Figure 3.4.6c shows another area of the samples ECAEd at 50˚C and corresponding indexed diffraction pattern. Electron diffraction pattern reveals the twined B19'phase along [010] and [0 –1 0] directions respectively. The twining mode is (001) compound twinning which is introduced as deformation twinning in the introduction section. As it could be easily determined from the images, there are two types of microstructures one is the lathe type martensite variants elongated in one direction and the other one the martensite variants with very high dislocation density. B2 phase is present in more severely deformed area.

Generally speaking, the material was precipitate-free but in some samples, small amount of overaged Ti_2Ni and TiC precipitates were found. Figure 3.4.7 shows the microstructure with precipitates and the corresponding diffraction pattern of the samples ECAEd at RT and heat treated at 400˚C sample. The precipitates are about 500 nm in diameter in this particular case and precipitates with diameter of 1μm are also observed in other samples. There isn't any stress field around the precipitates since they are not coherent with the matrix.

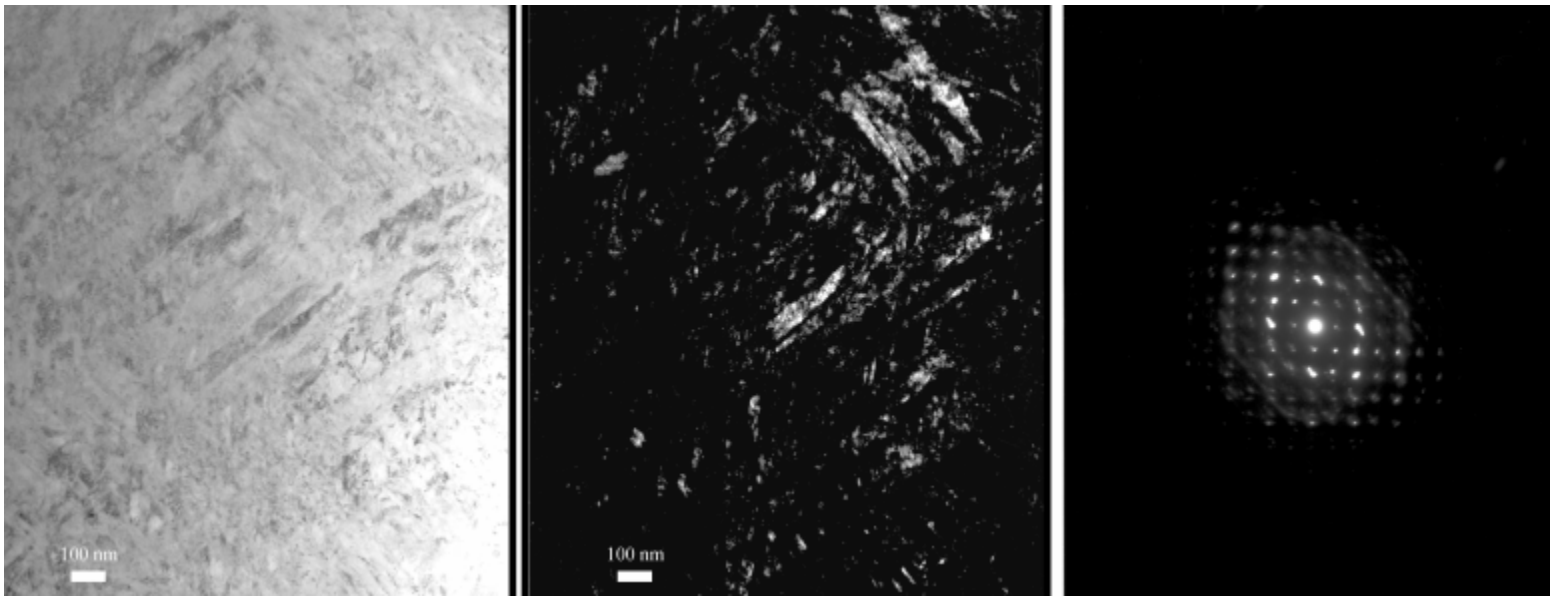

(a) (b) (c)

Figure 3.4.2. TEM images of the sample ECAEd at RT (a) bright field image , b) dark field image, and c) corresponding diffraction pattern.

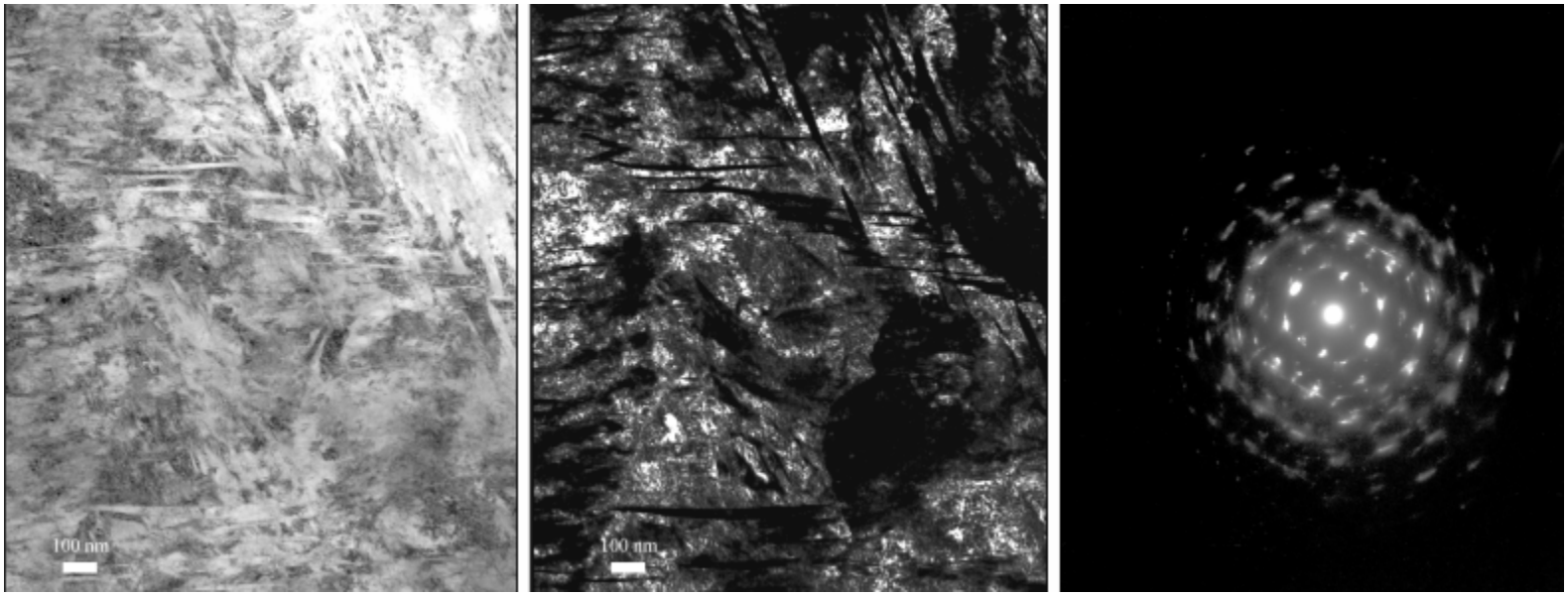

(a) (b) (c)

Figure 3.4.3. TEM images of the sample ECAEd at RT and annealed up to 300˚C, (a) bright field image, b) dark field image, and c) corresponding diffraction pattern.

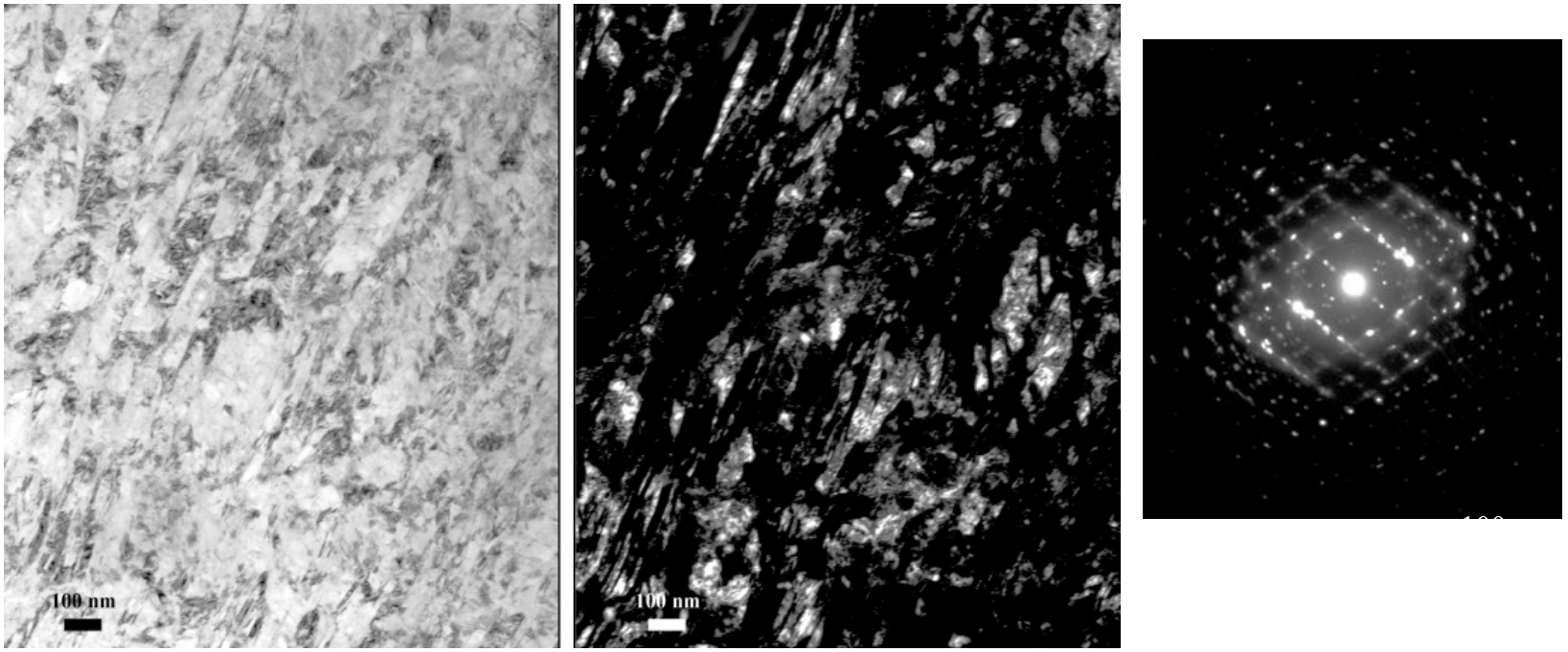

(a) (b) (c)

Figure 3.4.4. TEM images of the sample ECAEd at RT and annealed up to 400˚C, (a) bright field image, b) dark field image, and c) corresponding diffraction pattern.

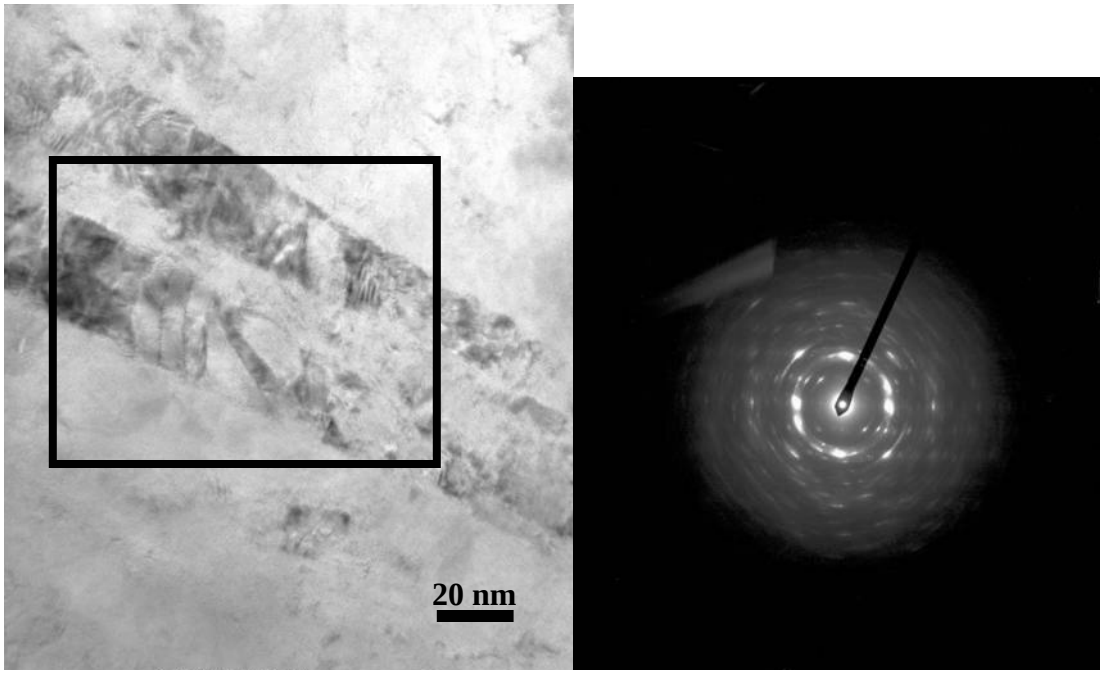

(a) (b)

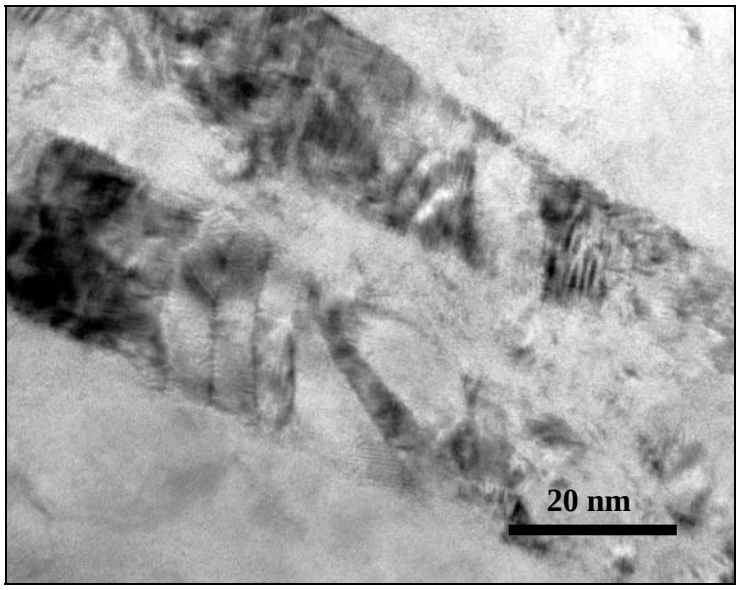

(c)

Figure 3.4.5 TEM images of the sample ECAEd at RT, (a) bright field image, b) corresponding diffraction pattern, and c) enlarged view of the area shown by the box in (a).

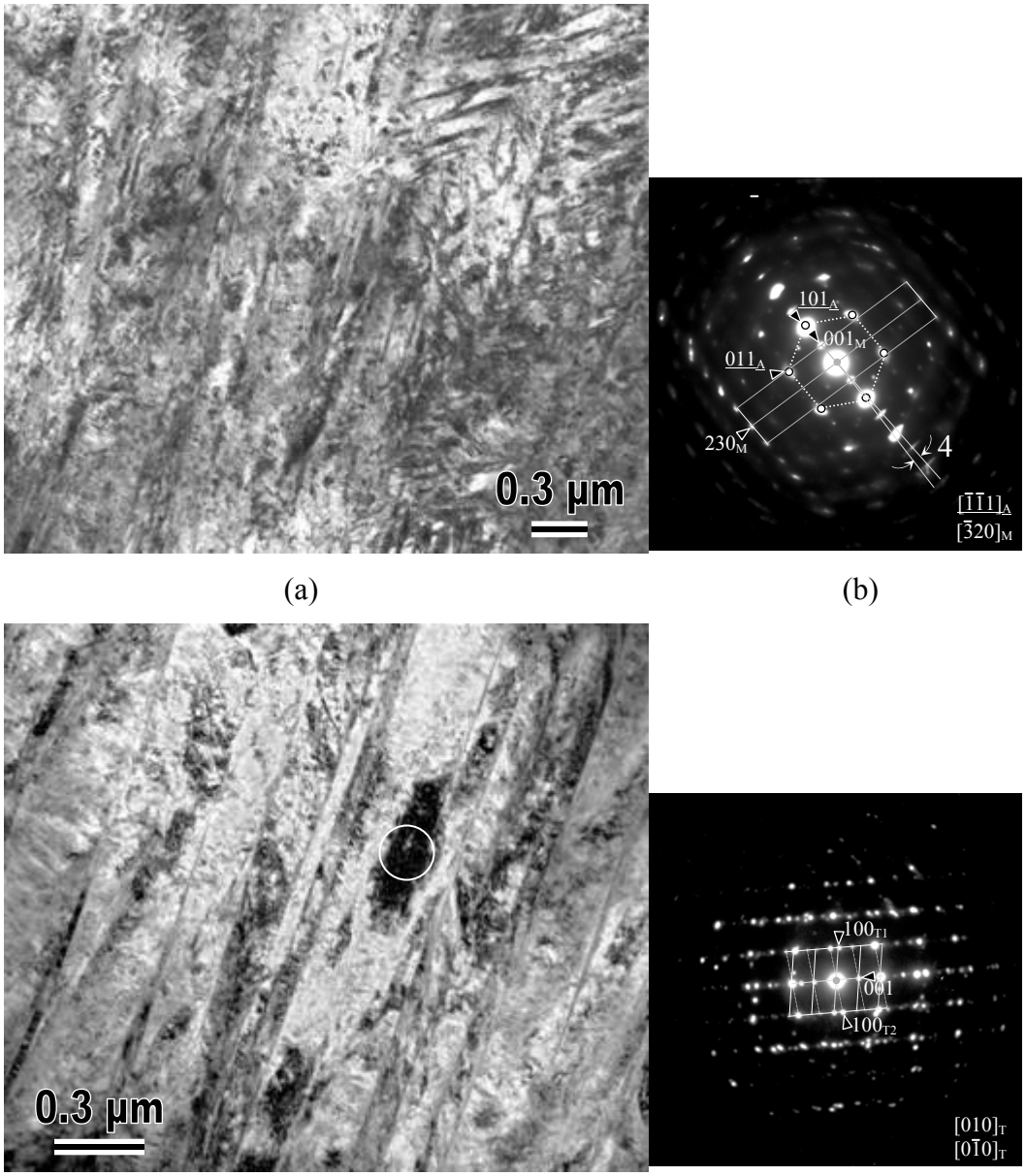

(a) (b)

(c) (d)

Figure 3.4.6. TEM images and corresponding diffraction patterns of the sample ECAEd at 50˚C, a) the mixture of B2 and B19’ phases b) the corresponding diffraction pattern of (a), c) the lathe type textured B19’ phase and d) its corresponding diffraction pattern.

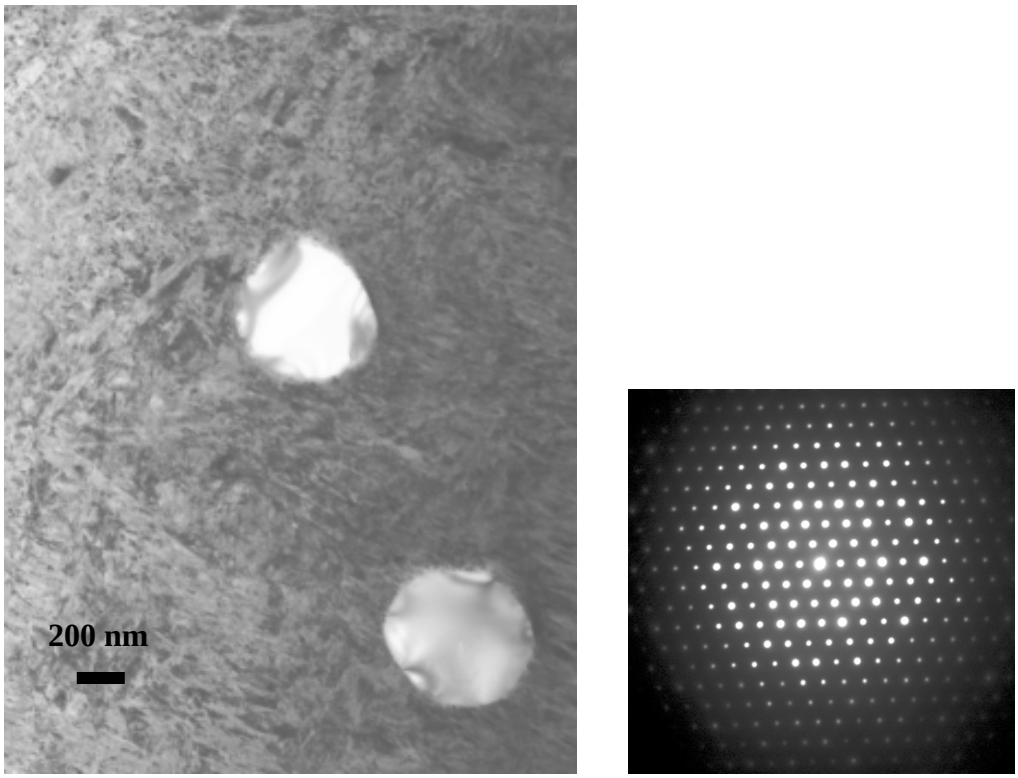

(a) (b)

Figure 3.4.7. a) TEM image of Ti_2Ni precipitates and b) corresponding diffraction pattern with [011] fcc zone axis.

3.5 Effect of Deformation on Strength, Shape Memory and Pseudoelasticity

As mentioned earlier the near equiatomic NiTi with less than 50.5at% Ni are insensitive to the low temperature heat treatments (300°C-500°C). And the solutonized samples demonstrate only no or partial pseudoelasticity [2]. This is attributed to the formation of dislocation due to weak matrix. However, pseudoelasticity could be improved by strengthening the alloy against slip deformation by thermo-mechanical treatments [1, 2].

Figure 3.5.1 demonstrates the compressive stress strain response of the as-received material at room temperature in the martensitic state (Figure 3.5.1a) and at 110 °C in the austenitic state after first heating (Figure 3.5.1b) which is 18°C above A_{s2} (see Figure 3.1.1). In the martensitic state, the initial inelastic deformation is due to the martensitic reorientation up to a strain level of about 4%. Then, detwinning and elastic deformation of the reoriented martensite is followed by plastic deformation of martensite at about 1100 MPa. After unloading, the sample was heated above A_f and 6.0% strain was recovered out of the 6.3% unrecovered strain.

In the austenitic phase (Figure 3.5.1b), the initial inelastic deformation is due to stress induced martensitic (SIM) transformation and probably slip in the austenite. It is hard to distinguish where SIM is completed and when elastic deformation of martensite becomes the governing mechanism. This is usually the case when multiple SIM variants form and there is hardening because of the interaction of different variants instead of non-hardening behavior observed in single variant SIM [6,40] formation. Strain hardening behavior is the indication of a certain texture in NiTi alloys which is the [111] austenite texture that usually develops during the cold drawing process [92]. Moreover, the material tested in the austenitic state did not exhibit significant pseudoelasticity. Also the test temperature was slightly below A_f that martensite is chemically stable at the test temperature.

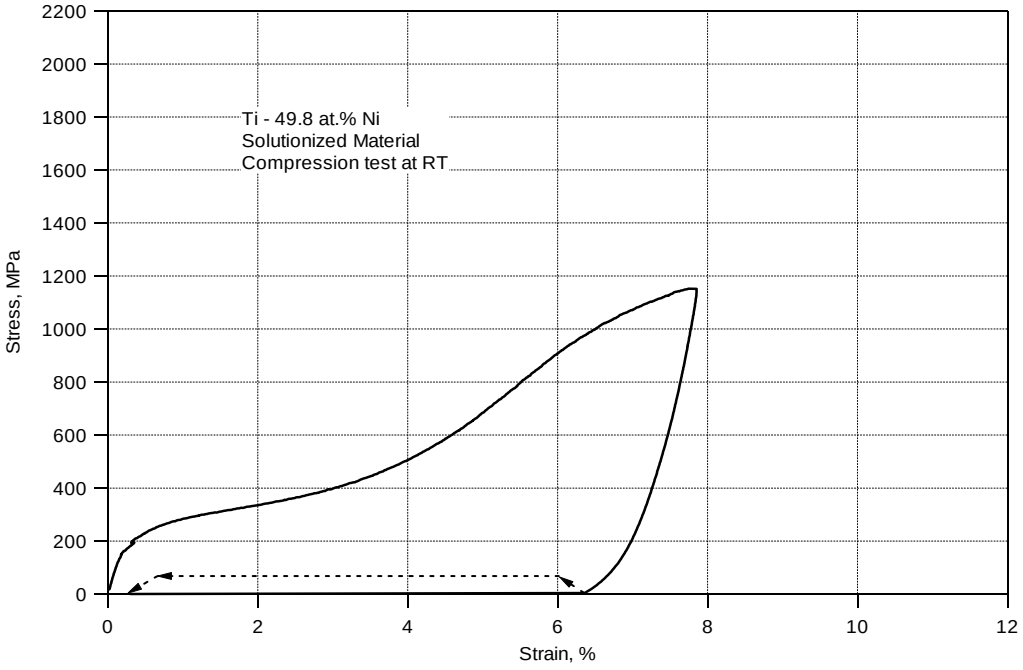

(a)

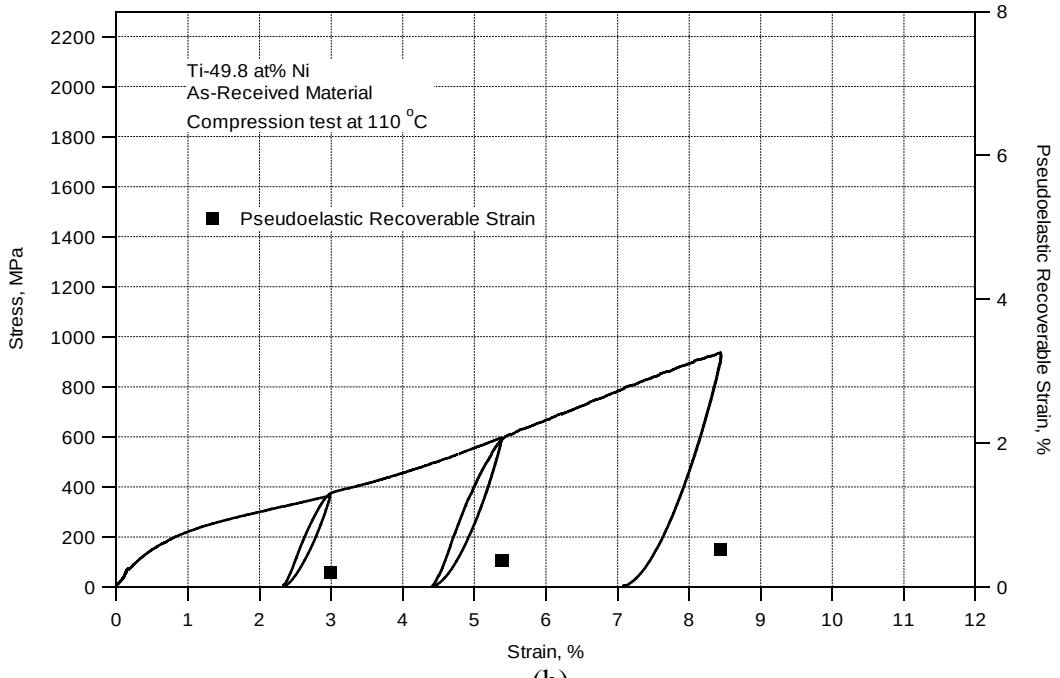

(b)

Figure 3.5.1. The compressive stress-strain response of the solutionized Ti – 49.8% Ni alloy (a) at room temperature (below M_f) and (b) at 110 °C (above A_s). (b) also demonstrates the very small pseudoelastic recoverable strain.

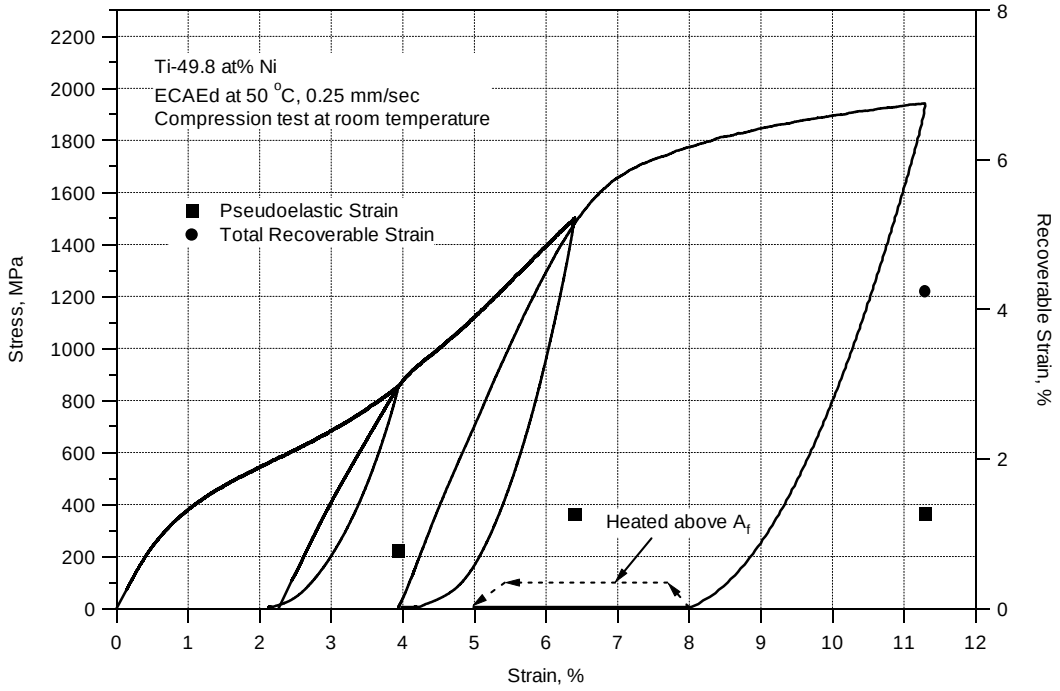

(a)

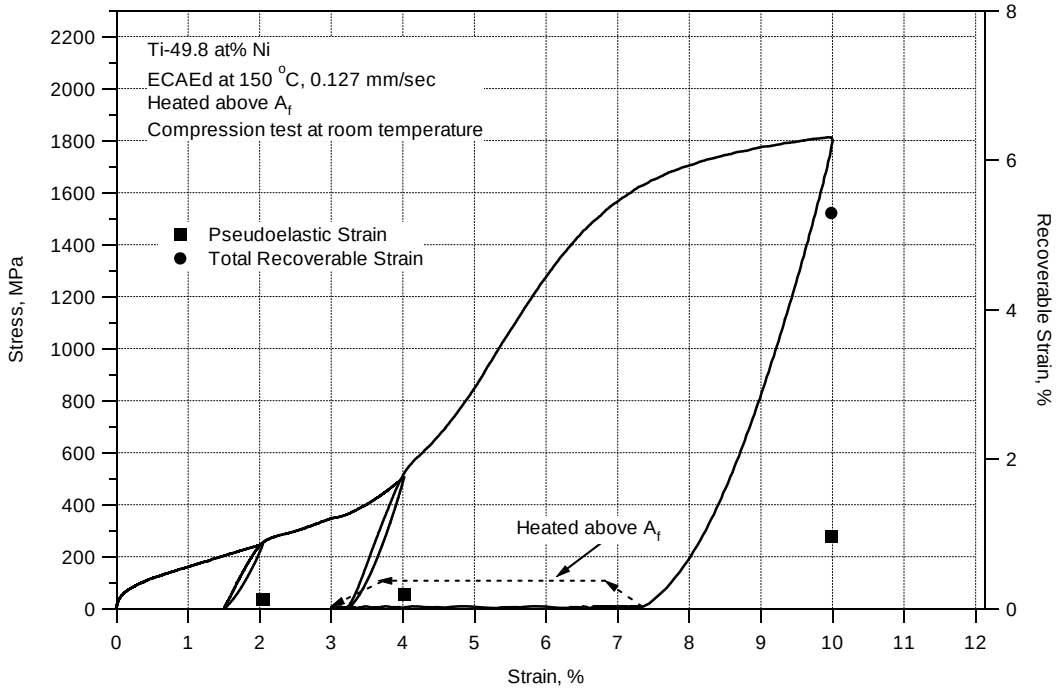

(b)

Figure 3.5.2. The room temperature compressive stress-strain and recoverable strain response of the samples that were (a) ECAEd at 50°C (below A_s), (b) ECAEd at 150°C (above A_f) and low temperature annealed to 400°C and (c) ECAEd at room temperature (below M_f) and low temperature annealed to 400°C.

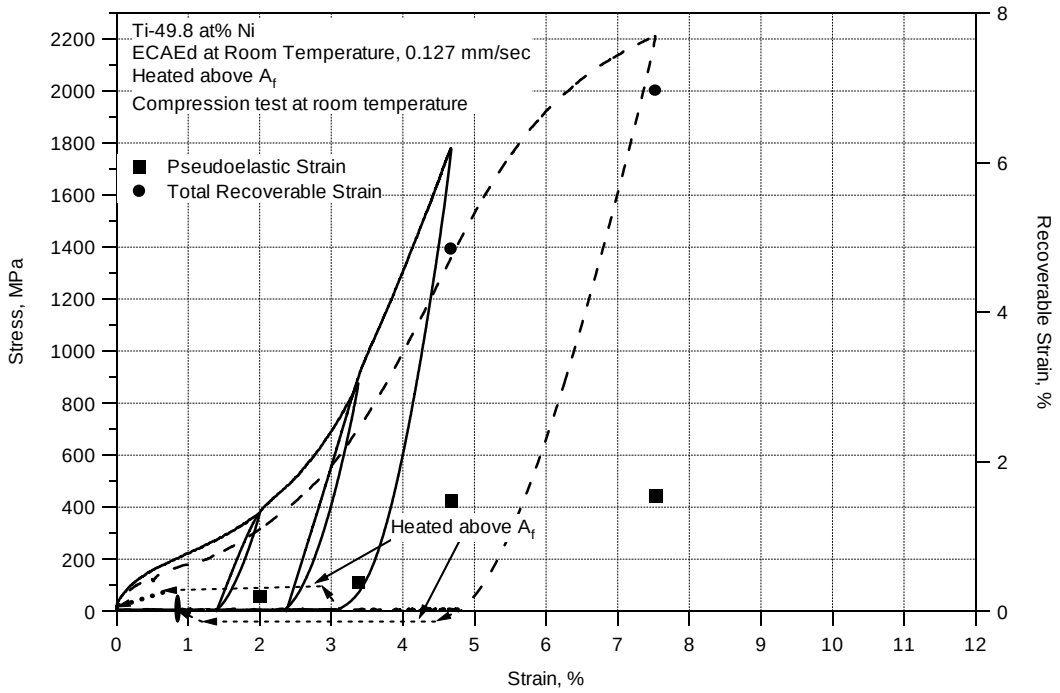

(c)

Figure 3.5.2. Continued

The room temperature (martensitic state) stress-strain and recoverable strain vs. applied strain responses of the materials ECAE processed at different temperatures are presented in Figure 3.5.2. Figure 3.5.2.a exhibits the response of the material ECAEd at 50°C. Although the microstructure is heavily deformed, martensite reorientation and probably SIM of the existing B2 phase is still evident as the initial inelastic deformation mode. However, the critical stress for the start of martensite reorientation increased 60% and the hardening rate increased considerably as compared to the solutionized material. When compared to the solutionized material, the strength level increased from 1100 MPa to 1900 MPa, while the recoverable strain level decreased from 6.7% to 4.2%.

To eliminate the first heating effects discussed before and to improve the recoverable strain level, the samples ECAE processed at 150°C in the austenitic state and at RT in the martensitic state were heated above $A_{f,1}$ temperature to 400°C (Figure 3.1.5a) and cooled down to room temperature. Figures 3.5.2b and 3.5.2c demonstrate the stress-strain response of these samples, respectively. This low temperature annealing (LTA) decreases the critical stress for martensite reorientation in the samples ECAEd at 150 °C and RT to levels lower than both the samples ECAEd at 50°C and the solutionized material. This difference can be attributed to the formation of different martensite variants upon cooling after first back transformation that are more favorable than the previous ones for martensite reorientation. On the other hand, the martensite yield stress did not change considerably by LTA of the sample ECAEd at 150°C as compared to the martensite yield stress in the sample ECAEd at 50°C. LTA improved the recoverable strain levels. In the sample ECAEd at 150°C, the recoverable strain is decreased to 5.3% but the strength level is increased to 1800 MPa as compared to the solutionized material. The sample ECAEd at RT demonstrated an increase in both the strength level and the recoverable strain. The martensite yield strength increased to 2000 MPa which corresponds to 82% increase while the recoverable strain level decreased to 4.8% as compared to the solutionized material. This is attributed to the strengthening of the martensite matrix more than in the other cases (solutionized, 50 °C and 150 °C samples) because of the lower deformation temperature and higher deformation level in the sample ECAEd at RT.

To study the effect of severe marforming on pseudoelasticity, the samples were also tested under compression above A_f and the results are presented in Figure 3.5.3. As compared to the solutionized material (Figure 3.5.2b), the sample ECAEd at 50°C exhibits very high stress level for SIM (~700 MPa), higher strain-hardening and higher pseudoelasticity strain. The deformed microstructure apparently provides some back stress upon the formation of SIM variants and thus, larger pseudoelasticity than the as-received material. Still the hysteresis is large as compared to what is usually observed in

pseudoelastic response of higher Ni content NiTi alloys and of equiatomic NiTi after lower marforming levels. The LTA of the sample ECAEd at 150 °C resulted in lower strain hardening during SIM. A clear distinction between SIM, elastic deformation of martensite and martensite yield is evident (Fig. 3.5.3.b). Two unexpected results obtained upon LTA in the sample ECAEd at 150°C are that only a small decrease in the critical stress for SIM was observed upon LTA and the pseudoelasticity strain did not increase as compared to the ones in the sample ECAEd at 50°C although a clear low strain hardening SIM regime was evident. A plausible explanation can be reached when the elastic moduli of the two samples are compared which indicate the presence of different textures in the samples. The elastic modulus of the sample ECAEd at 50°C is significantly lower than the sample ECAEd at 150°C and LTAd. This can be attributed to the fact that the former has a texture close to a [100] fiber texture and the latter has a texture close to a [111] fiber texture as the [100] orientation has the lowest elastic modulus while the [111] has the highest in the austenitic state [6,40]. It was also reported that the [100] orientation under compression is more favorable for pseudoelasticity than the [111] orientation[40]. This is because the austenite slip is more difficult in the [100] orientation as the austenite slip system is <100>{110} in NiTi alloys. The lower plastic yield stress level observed in the sample ECAEd at 150 °C and LTAd is an indication for easier slip in this case. The rationale behind the different texture evolution during deformation at different temperatures is not clear at this point. However, it is believed that it is related to the different deformation mechanisms at different deformation temperatures.

The LTA of the sample ECAEd at RT demonstrated improvement in the pseudoelasticity strain as shown in Figure 3.5.3.c (3.26% strain out of 5.38% inelastic strain at 1900 MPa). The higher pseudoelastic strain in this sample in spite of a similar elastic modulus value with the sample ECAEd at 150 °C and LTAd (which can be the indication of a similar texture) can again be attributed to the more efficient strengthening

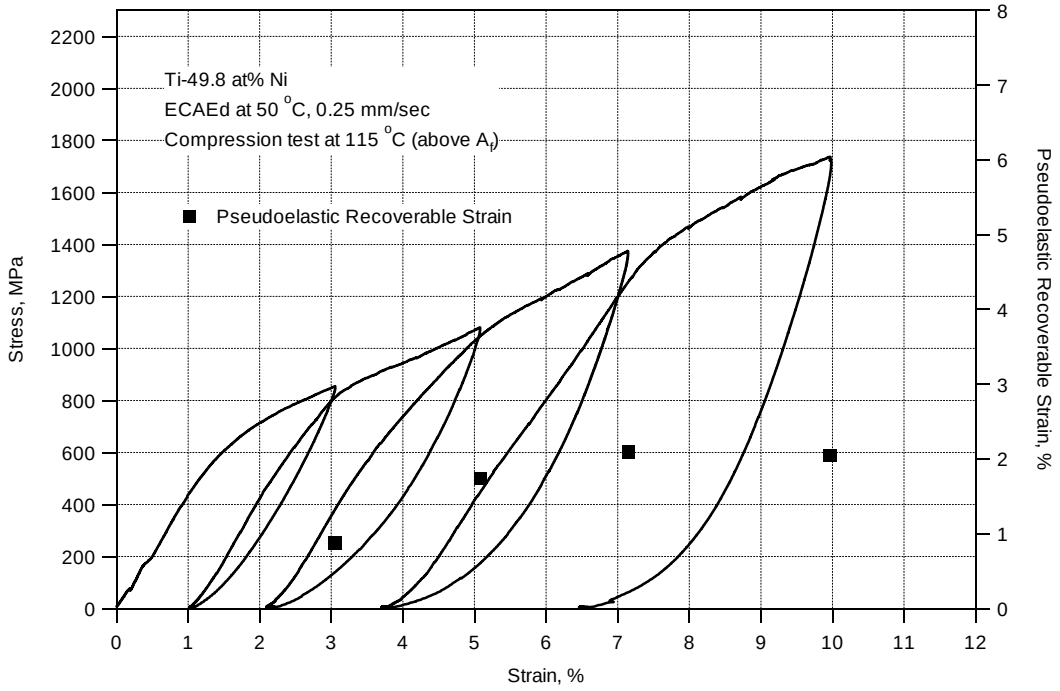

(a)

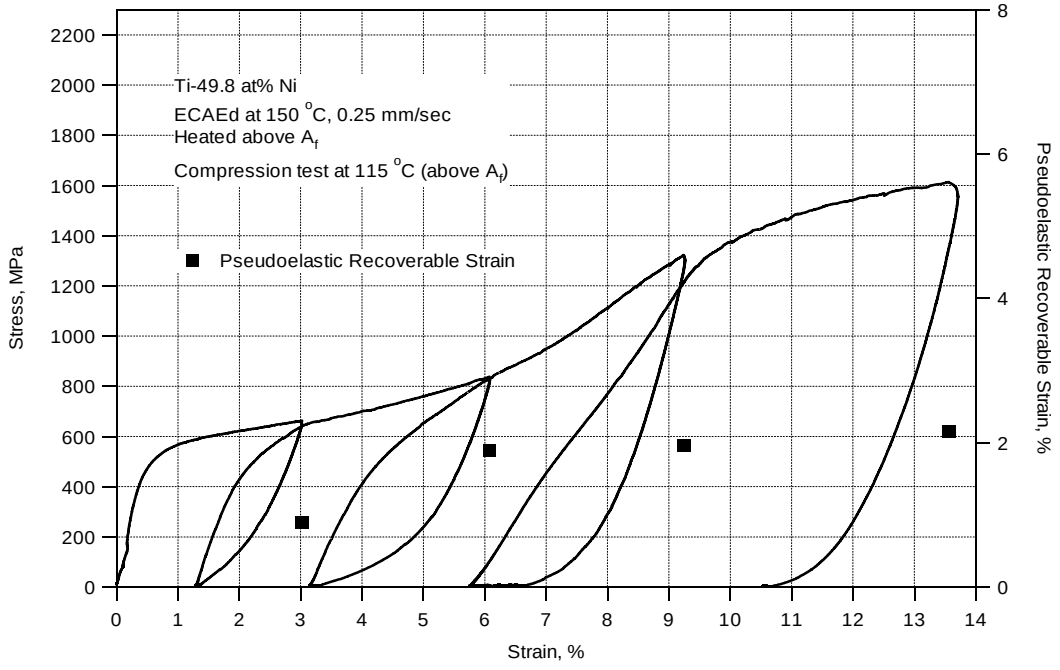

(b)

Figure 3.5.3. The compressive stress-strain and recoverable strain response of the samples that are (a) ECAEd at 50°C, (b) ECAEd at 150°C and low temperature annealed to 400°C and (c) ECAEd at room temperature and low temperature annealed to 400°C. Compression experiments were conducted above the A_f temperature at 115°C.

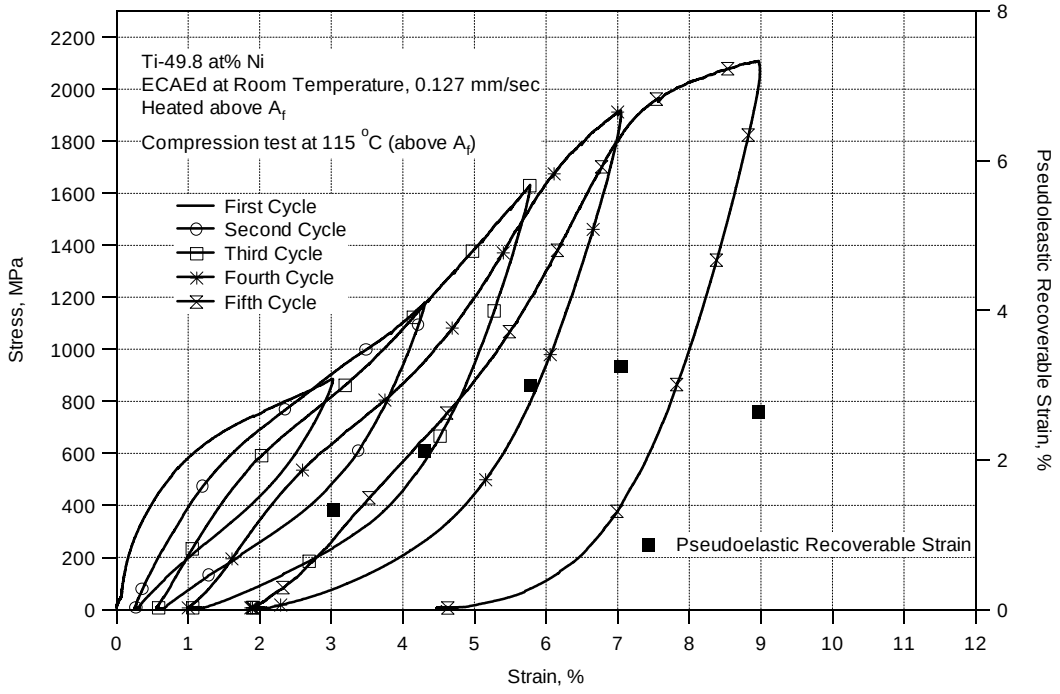

(c)

Figure 3.5.3. Continued.

of the austenite matrix against slip deformation in the former case. This can be better seen when the critical stress values for the start of the second plateaus are compared.

Table 3.5.1 summarizes the critical stress levels for martensite reorientation and stress induced martensitic phase transformation, the yield strength of martensite for plastic deformation and the recoverable strain levels of the all the samples tested in this study. One of the most important results in this table is the increase in the difference between the stresses for the start of dislocation slip and martensite reorientation (or stress-induced martensitic transformation) after the present processing conditions. These results are highlighted in Table 3.5.1. The increase is significant for applications as dislocation slip is detrimental for the fatigue life of the shape memory devices. Thus, the marforming using ECAE followed by low temperature annealing is a promising route for achieving high fatigue life in NiTi alloys

Table 3.5.1. Summary of the compressive test results conducted on the samples processed in the present study. The critical stress represents the stress level at which martensite reorientation or stress induced martensitic transformation starts depending on the initial deforming phase.

Processing condition	**Compression test temperature**	**Stress (MPa)**			**Recoverable Strain (%)**		
		Critical	**Yield**	**$\Delta\sigma$ (Yield-Critical)**	**Pseudoelastic**	**SME**	**Total**
As-received	RT	250	1000	750	0.7	6	6.7
ECAE @ 50 °C		400	1700	1300	1.27	3	4.27
ECAE @ 150 °C and LTA		100	1600	1500	0.96	4.4	5.34
ECAE @ RT and LTA		150	**2000**	**1850**	0.77	4	4.77
As-received	110 °C	200	> 900	> 700	0.5		0.5
ECAE @ 50 °C	115 °C	650	1700	1050	2		2
ECAE @ 150 °C and LTA		550	1400	850	2.15		2.15
ECAE @ RT and LTA		600	**1900**	1300	**3.25**		3.25

LTA: Low Temperature Annealing.

CHAPTER IV

CoNiAl ALLOY

4.1 Optical Microscopy and TEM Results

Optical microscopy analysis is the one of the basic microstructure characterization methods. Since there is a difference in the hardness values of martensite and austenite phases the surface relief will not be same during polishing which would allow the optical microscopy analysis. The OM image of the as-cast material is shown in Figure 4.1.1. Formation of second phases along the grain boundaries and inside the grains is evident. Second phases in CoNiAl could be γ (A1) and γ' ($(Ni,Co)_3Al$) phases. The formation of the second phases along the grain boundary is essential for increasing the ductility of CoNiAl and NiAl alloys. Active slip system of B2 NiAl is <100>[110], providing only three independent slip systems where five slip systems are required by the Von Mises criterion for uniform, arbitrary and volume conserving plastic flow. The formation of γ' along grain boundaries would provide additional <110>[111] slip systems that enable grain-to-grain compatibility and prevent grain boundary fracture [93,94].

In order to obtain B2 phase in CoNiAl, as-cast material homogenized for 24 hours at 1350˚C in an argon filled quartz tube. The quartz tube was evacuated and filled with argon gas and same procedure was repeated several times in order to obtain as pure argon atmosphere in the quartz tube as possible. Then, by using an arc-torch the quartz tube was sealed. After homogenization the samples were quenched in water and the quartz tube was broken. A representative optical image is shown in Figure 4.1.2a. The matrix is B2 phase with no second phase. In regions close to the edges, martensitic transformation observed after quenching. This is attributed to the shape and cooling rate effect which is also observed in other intermetallic shape memory alloys. Figure 4.1.2b shows the stress induced martensitic transformation from B2 to $L1_0$ as a result of hardness indentation. The twins or martensite plates are very thin compared to thermally

induced ones. In order to prove that the transformation is thermoelastic, an in-situ cooling heating experiment was conducted. Figure 4.1.3 shows the OM of homogenized CoNiAl during cooling. The temperatures were not recorded since the aim was only to prove the thermoelastic transformation. Initially the microstructure was B2 phase(Figure 4.1.3a), during cooling martensite plates were nucleated especially at the grain boundaries (Figure 4.1.3b). With further cooling they grew all the way to the other end of the grain (Figure 4.1.3c and 4.1.3d). When the sample was heated the initial microstructure was recovered.

The importance of the presence of the second phases was explained before. In order to investigate the formation of second phases, the samples homogenized at 1350˚C for 24 hours were heat treated at different temperatures. The optical images of heat treated samples are shown in Figure 4.1.4. The formation of second phase particles along the grain boundaries and inside the grains is confirmed. Heat treatment at 1100˚C for 20 hours produced excessive amount of second phase which must be avoided since the martensite transformation characteristics can be suppressed by these particles. A more detailed analysis will be done on the shape memory characteristics of CoNiAl alloys with the presence of second phase on the matrix.

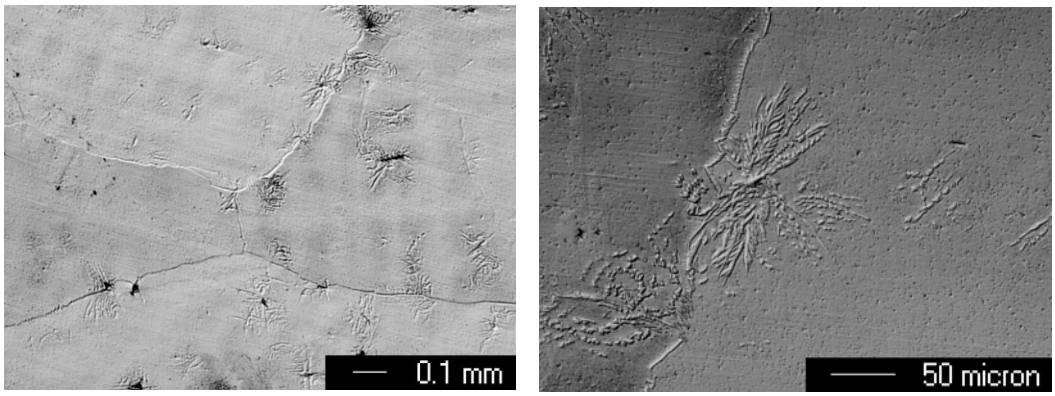

(a) (b)

Figure 4.1.1 Optical images of as-cast material. Second phase formation along the grain boundaries and inside the grains is evident.

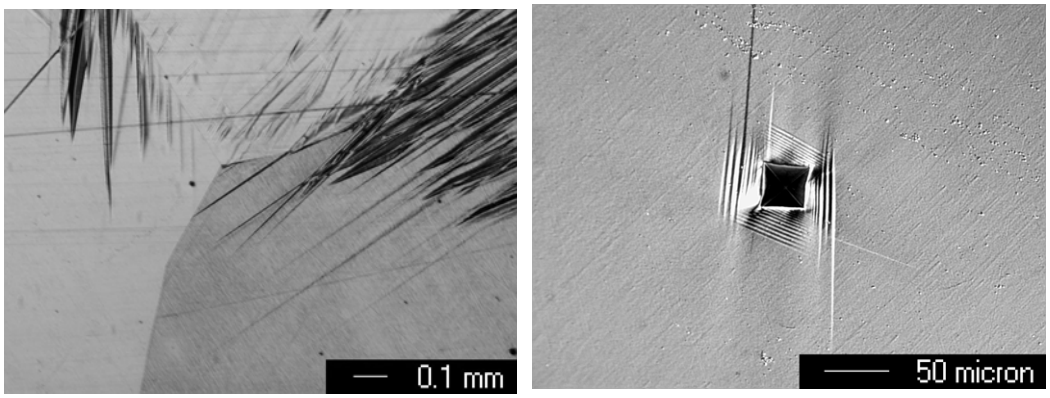

(a) (b)

Figure 4.1.2 Optical images after homogenization at 1350C for 24 hours.

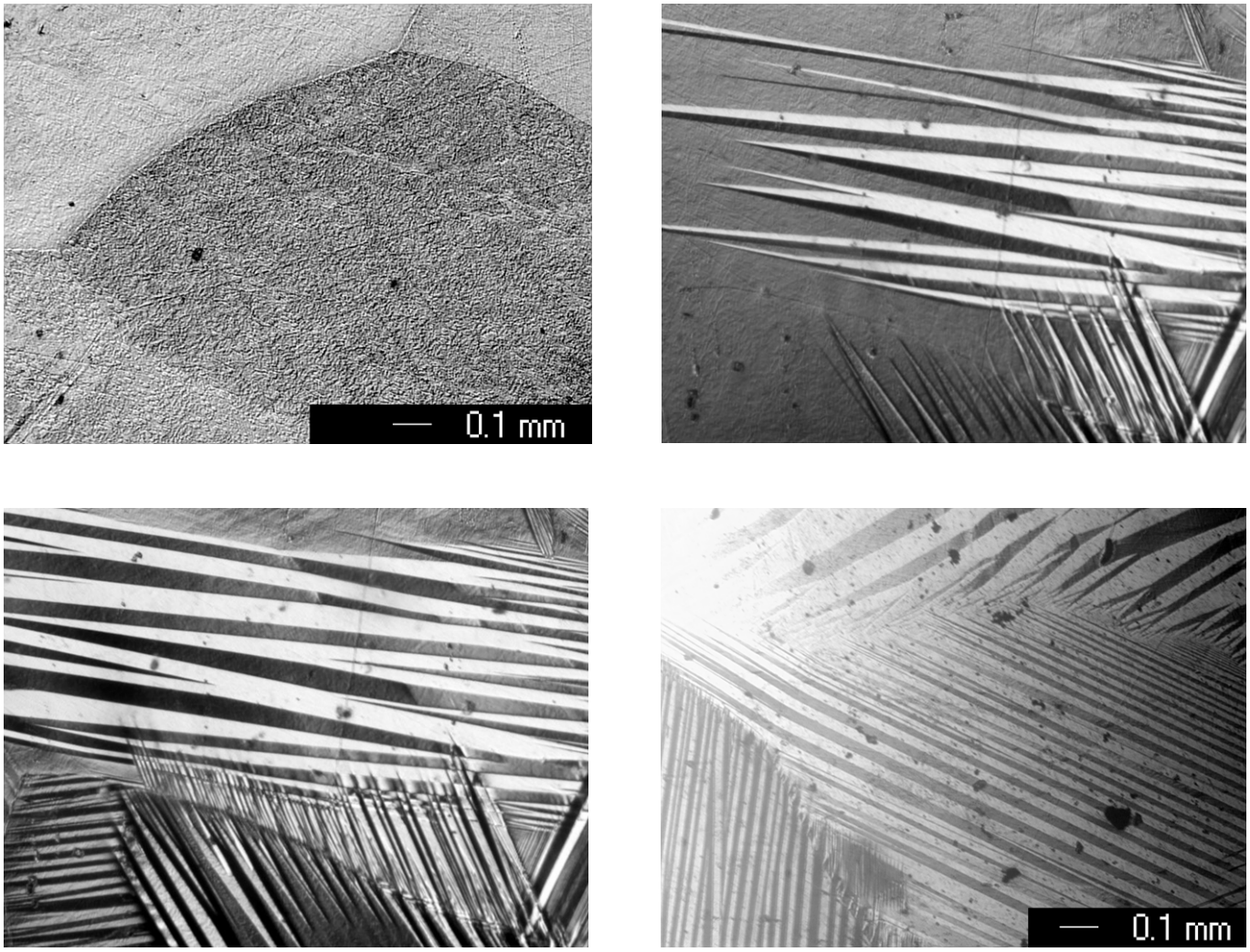

Figure 4.1.3 In-situ cooling experiment under OM reveals the thermoelastic martensitic transformation.

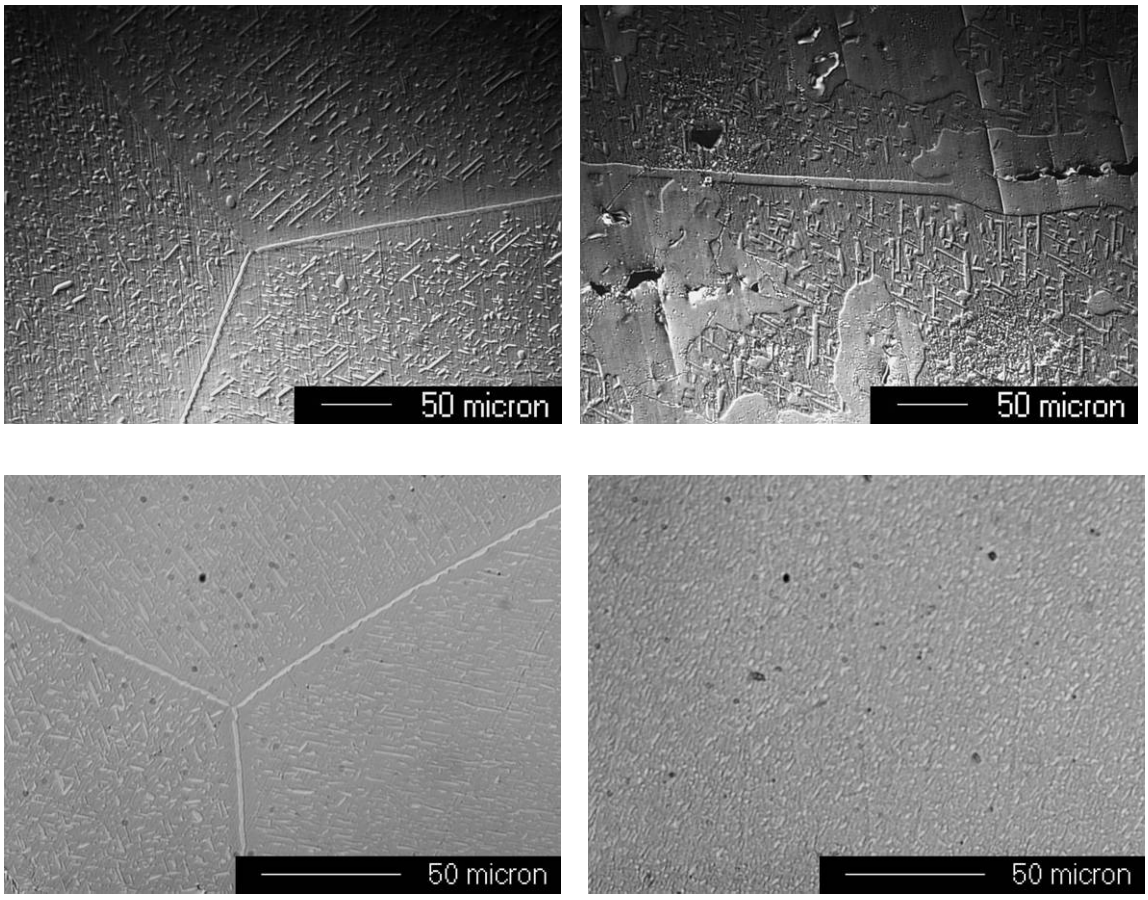

Figure 4.1.4. Effect of heat treatments on the microstructure a) 1100˚C for 10 hours, b) 1100˚C for 20 hours, c) 1000˚C for 10 hours, d) 900˚C for 10 hours.

Figure 4.1.5 shows the TEM image of internally twinned martensite phase with twin thickness of around 100 nm. Corresponding diffraction patterns are shown in Figure 4.1.4b and c where the former one is taken from inside of one twin and the latter includes two adjacent twins. In the figure M stands for matrix and T for twins where both of them are martensite and have $L1_0$ crystal structure. The twinning plane is determined to be (1-11).

Figure 4.1.6 shows the bright field image and corresponding diffraction patterns of different areas shown in a. The matrix is confirmed to be martensite. The matrix in the region A and B has a slight rotation, i.e. the diffraction patterns of the matrix in A and B do not coincide. Region D is considered as parent phase at first but diffraction pattern revealed that it is also martensite. The diffraction pattern in region D coincides with the twin pattern in region A, implying that the grain in the region D is indeed a twin of the region A. As a result, three types of martensite structures are available: very thin plate martensite, internally twinned martensite and martensite without internal twins.

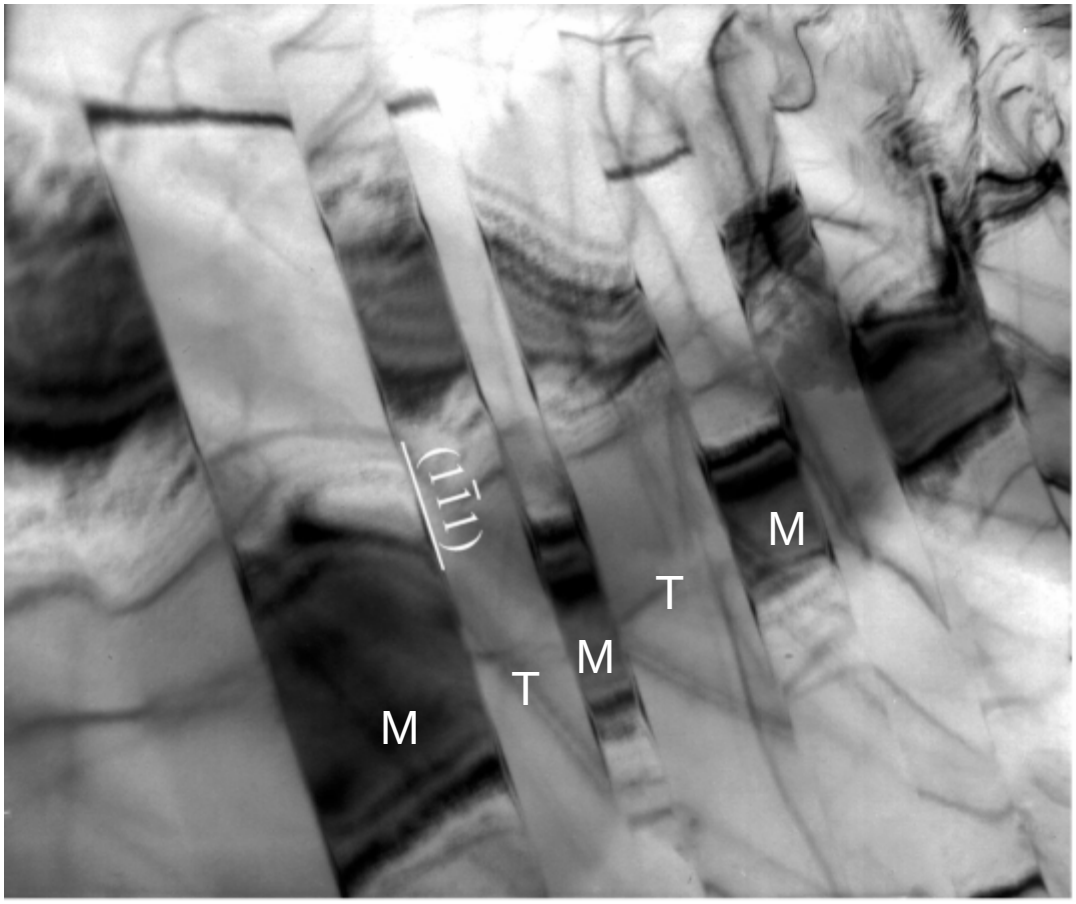

(a)

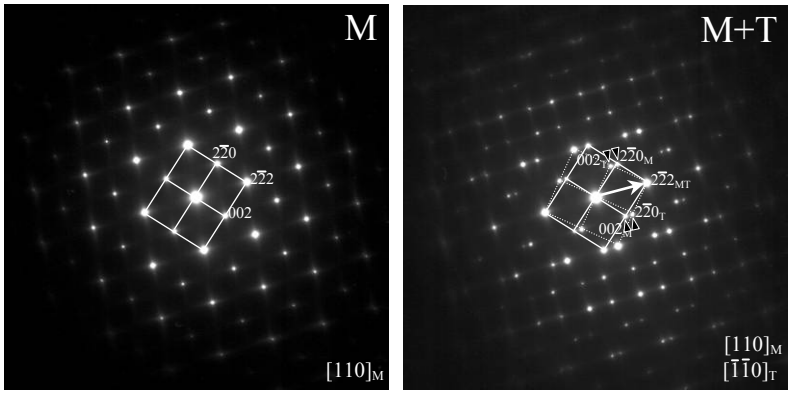

(b) (c)

Figure 4.1.5. a) Bright field TEM image of internally twinned martensite phase of CoNiAl, b and c) corresponding diffraction patterns.

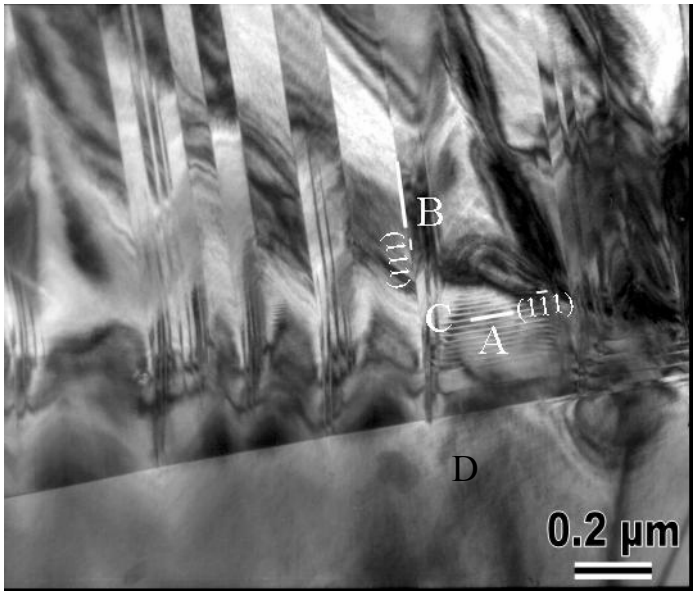

(a)

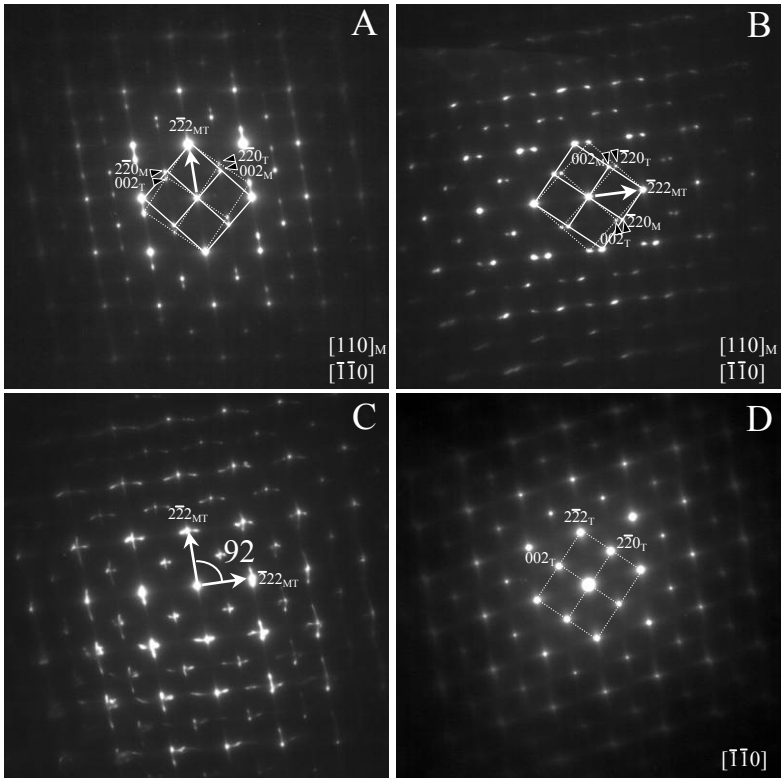

(b)

Figure 4.1.6. a) Bright field image of CoNiAl and b) corresponding diffraction patterns of different areas as shown in a.

4.2 Determination of Transformation Temperatures of CoNiAl Alloy

As explained in the introduction, there are several ways to determine the transformation temperatures. Figure 4.2.1 shows the transformation temperatures for CoNiAl obtained by DSC, thermal cycling under constant magnetic field (100 Oe) and susceptibility test. TTs obtained by these three methods are in good agreement and M_s and M_f temperatures were determined as -43 °C and -57 °C, respectively, while A_s and A_f were -43 °C and -26 °C, respectively. The DSC curve is different than the typical DSC curves for NiTi since there are several peaks instead of broad peaks. It is important to note that the martensitic structures of NiTi and CoNiAl are different. The grains and the martensite plates in CoNiAl are much larger than the ones in NiTi. A plate shaped martensitic phase could nucleate and transform till the end of the specimen .When the martensite plate hit the other end it will stop. Then, another one forms and follows the same path as the previous one. As a result all the peaks could be attributed to formation and growth of martensite plates. The reason for nucleation at different temperatures could be explained by the internal stress formed during quenching or composition variation.

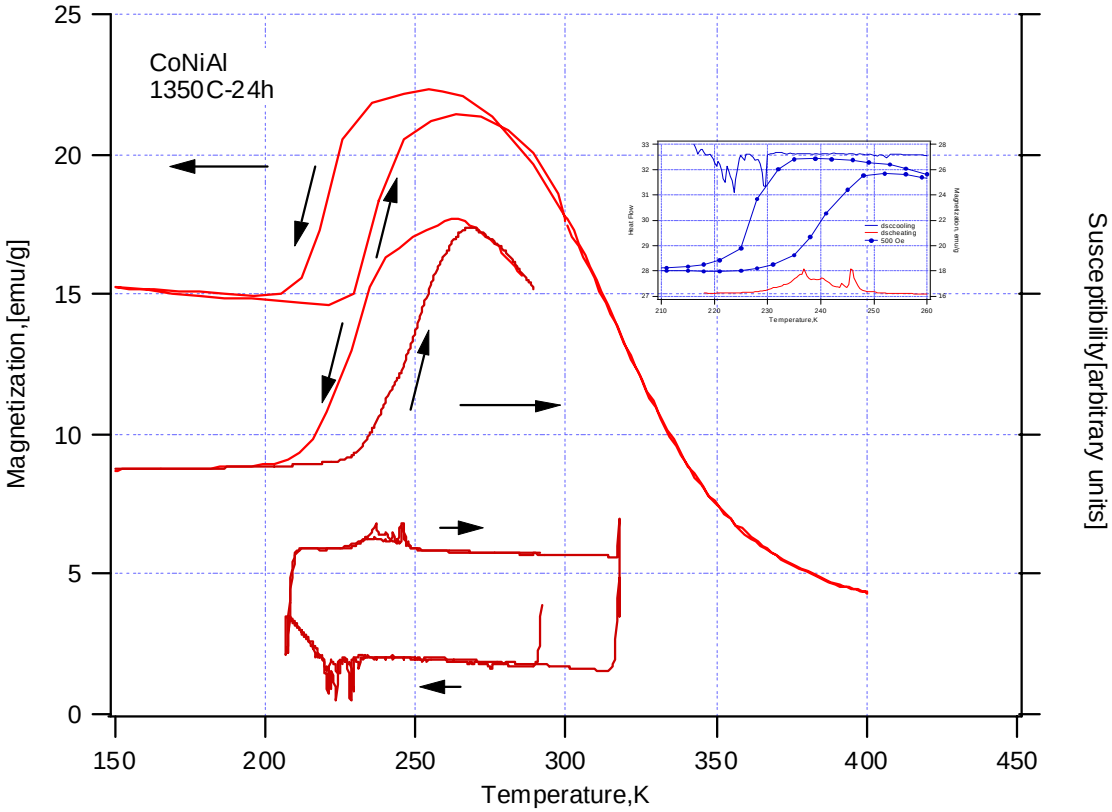

Figure 4.2.1. Determination of transformation temperatures by thermal cycling under constant magnetic field (100 Oe), DSC and susceptibility test. Enlarged DSC and thermal cycling under constant magnetic field is added in order to show the agreement on transformation temperatures.

4.3 Thermo-mechanical Response of CoNiAl

Figure 4.3.1 shows the incremental testing of CoNiAl at room temperature. The recoverable strains are superimposed on the compressive stress-strain curves with symbols in the Figure 4.3.1. The critical stress for the nucleation of stress-induced martensitic transformation is about 200 MPa while the maximum pseudoelastic strain is about 4%. The narrow stress hysteresis upon unloading is similar to the one observed in CuNiAl as opposed to the typical wide hysteresis for NiTi based SMAs. The response is initially elastic followed by transformation of parent (B2) phase to martensite phase ($L1_0$). The material is deformed further at the end of the plateau region, the response is virtually elastic with martensite deforming in an elastic manner. The second elastic loading is followed by another low strain hardening region which could be either yielding of martensite or another phase transformation stage, or both. The stress level for the onset of dislocation slip is quite high (~1100 MPa) showing the high resistance of the matrix against dislocation slip which is desired for MFIS.

After nucleation of martensite upon loading, the stress for phase propagation is decreased by 70 MPa and kept constant up to 3% transformation strain whereas during unloading the stress needed for nucleation is 40 MPa lower than the stress required for the propagation of back transformation front. The stress hysteresis between the plateau regions is about 20-25 MPa which is very low when compared to NiTi. Low stress hysteresis provides great advantages in actuator and heat engine applications. High strength for slip, low stress hysteresis, high pseudoelastic strain at room temperature can make CoNiAl a new ferromagnetic shape memory alloy that also can be used as a conventional SMA.

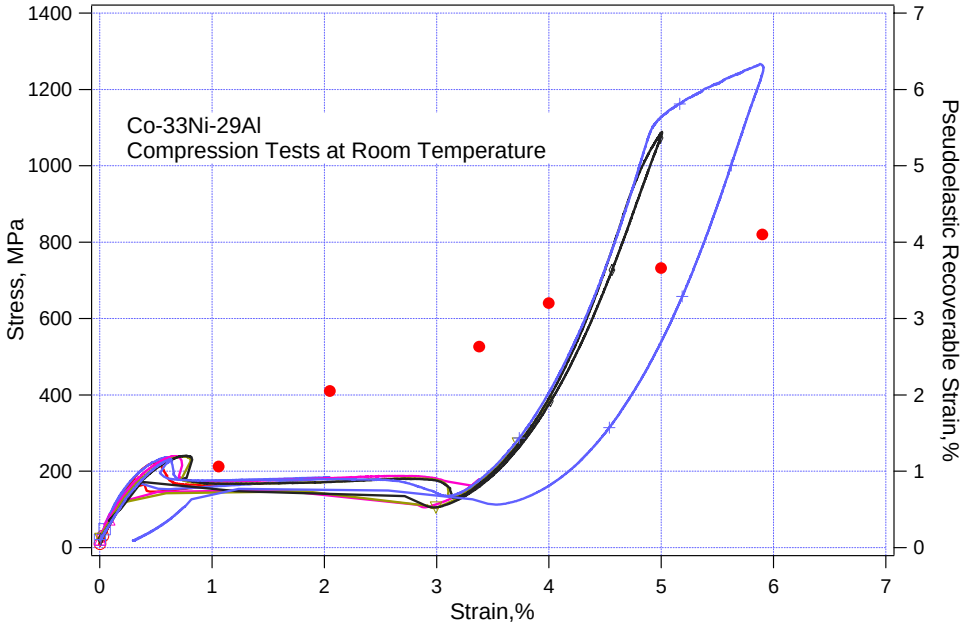

Figure 4.3.1. Compressive stress-strain response and recoverable strains of CoNiAl as obtained in an incremental strain test.

The stress drop at the beginning of the deformation is the indication of a significant difference between the nucleation stress of martensite and the stress required for phase front motion. At the end of the plateau region, it is expected that the transformation would end and elastic deformation of martensite would start. It is speculated that the second stress drop may be because of the formation of another phase front. The formation of a new phase front can be either because of the nucleation of a new martensite variant away from the previous one or because of a new phase transformation. The latter is more plausible and some direct and indirect evidences will be presented below. During unloading, the exact loading curve is followed and a jump occurs followed by a plateau-like strain and final elastic unloading. Another possible reasoning for the stress drops would be the following. The martensite plates with wedge shape form and grow till the end of the specimen's edges. When they hit the edge they will expand. The stress for nucleation is higher than its propagation since the wedge nose creates stress concentration which lowers the external stress needed for propagation. The

second stress drop can be attributed to the fact that when the nose hits the edge of the sample it expands and lowers the applied stress.

Under the application of stress, it is virtually impossible to distinguish, based only on the compressive stress-strain curve, a two/or more stage transformation. A similar behavior was observed in NiTiCu single crystals under compression in which only one stress plateau existed although the transformation was a two stage one (B2→B19→B19') as demonstrated by thermal cycling under stress and TEM [19,95]. If the individual curves in Figure 4.3.1 are compared with each other in detail, it is possible to see some significant differences as shown in Figure 4.3.2. Upon unloading at 2%, there is no stress drop which means that back transformation starts immediately after unloading starts. The stress hysteresis is extremely narrow. During loading to 4%, a second stress drop occurs at around 3% strain, which is attributed to a new phase transformation. The phase transformation continues after the second stress drop as the recoverable strains increases with increasing strain (Figure 4.3.1). Upon unloading at 4% strain, a stress jump occurs for the start of back transformation as opposed to the 2% unloading case. Note that there is a significant difference between the hysteresis loops of the 2% and 4% cases which can also be attributed to a two stage martensitic transformation. In NiMnGa [72-74] and Cu-based SMAs [71], multiple martensitic phases can form during deformation as well as in NiAl alloys [75,97]. However, the phases that form and the sequence of the nucleation of the phases are orientation and temperature dependent [71]. The change in hysteresis after second stress drop could also be explained by considering the formation of wedge shape martensite plates. The hysteresis in the plateau region is small since the wedge shape martensite plates are available and they could easily back transform if the externally applied stress decreased, but after they had reached to the edge of the sample, the other nucleation is necessary which results in lower stress for reverse transformation. Then the stress increase during plateau region is due to fast shrinkage of the martensite plates.

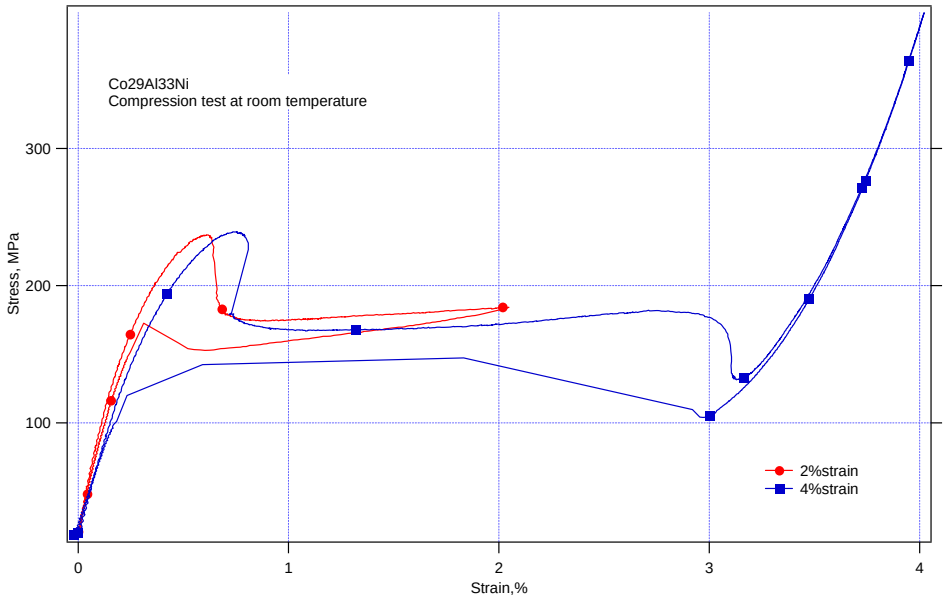

Figure 4.3.2 The details of compressive stress-strain response of CoNiAl as obtained in incremental strain test at the 2 and 4% strain levels.

The stress-strain curves of 5% and 6% straining after second stress drop looks like pseudoelastic behavior since loading and unloading curves follow the same path. This would be another evidence for two stage martensitic transformation. The small irrecoverable strain after 6% straining is due to the residual martensite as shown by the TEM image in Figure 4.3.3 and OM images in Figure 4.3.4. The sample is almost dislocation free. However, this residual martensite seems different from the stress or thermally induced martensite usually observed in typical SMAs such as NiTi and CuNiAl. The habit plane is clear in the figure, however, internal twins are not continuous and are somewhat wavy. The reason for the waviness is not clear at this point but it is believed that elastic, magnetic, and magnetoelastic energies control the structure of these boundaries [99].

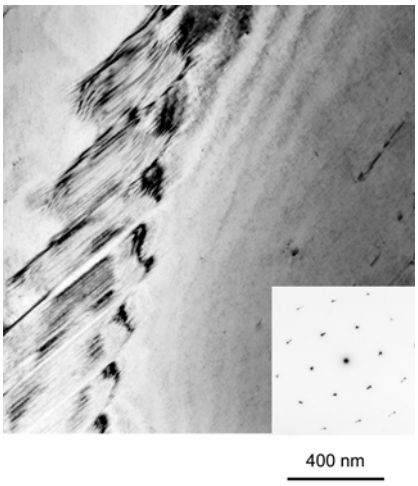

Figure 4.3.3 TEM image after the compression test shown in Figure 4.3.1.

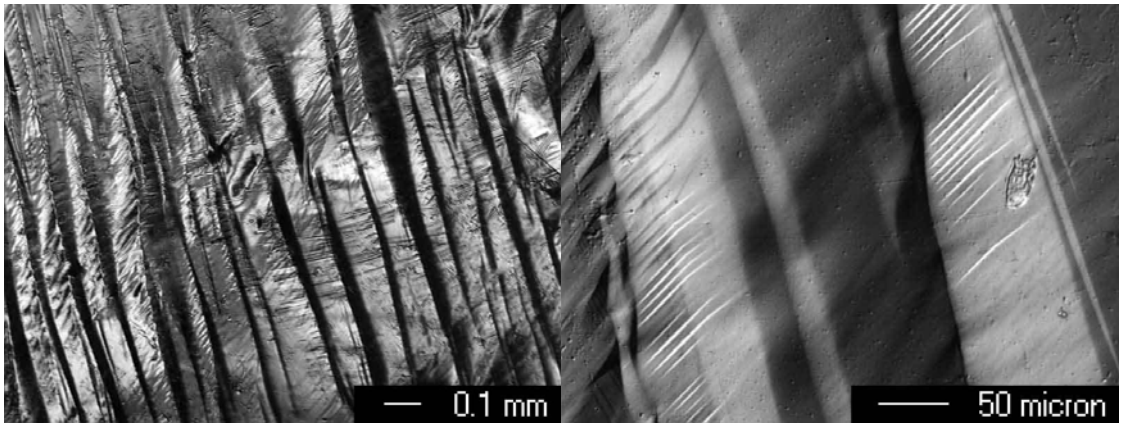

Figure 4.3.4.Optical microscopy images after the compression test shown in Figure 4.3.1.

The second important shape memory characteristic is the range of pseudoelastic temperature window which is the temperature range where perfect pseudoelasticity with no unrecoverable strain is observed. Figure 4.3.5 shows the effect of test temperature on the compression response.

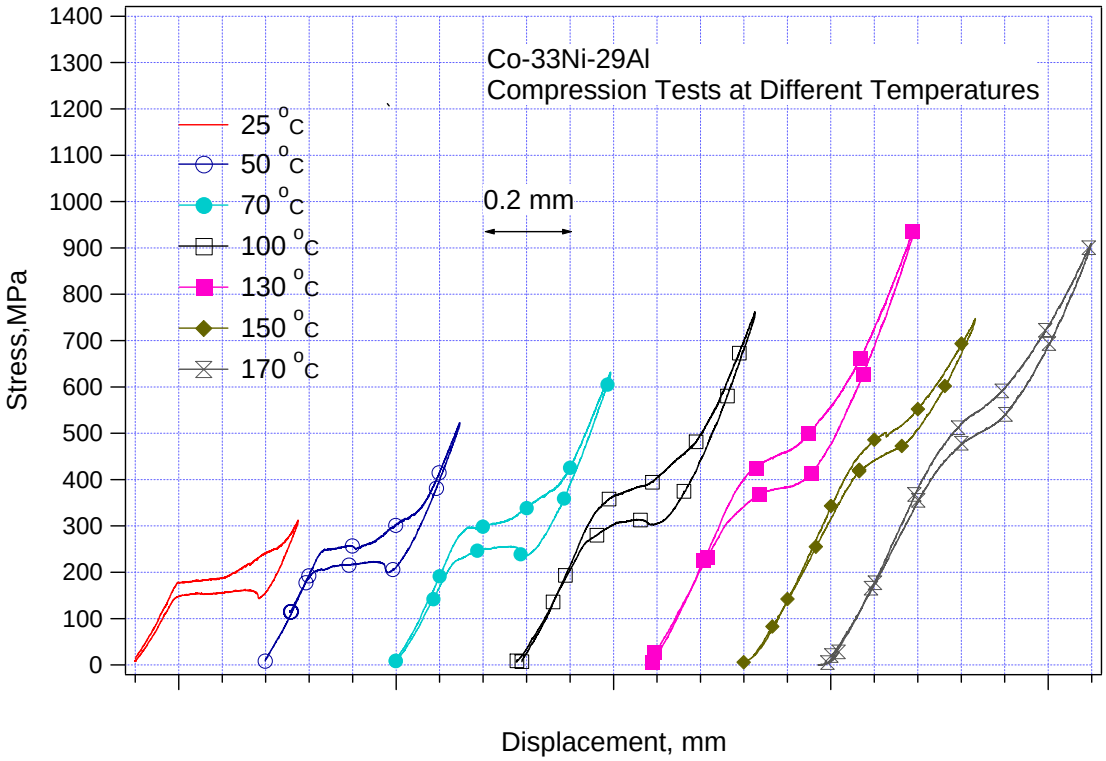

Figure 4.3.5. Compressive stress vs. displacement response of CoNiAl at different temperatures.

A perfect pseudoelastic behavior with a large pseudoelastic temperature window (>150˚C) is obtained at all temperatures. The figure is stress vs. displacement since it was not possible to use the miniature extensometer above 120 °C. The strain measurement at room temperature resulted in 4% strain. There is no stress drop during loading although there is still a stress jump during unloading for the back transformation. The difference between the shapes of the initial part of the stress-strain responses of different samples (Figures 4.3.1 and 4.3.5) is attributed to the different texture of the individual samples due to the large grain size. Moreover, two stage transformation is evident on the curves up to 130°C. Above 130°C, it is no longer possible to distinguish the two stages or one of the stages vanishes. The stress hysteresis increases from 30 MPa

at room temperature to 80 MPa at 130 ˚C. Then it decreases to 50 MPa at 150°C and 170°C.

The results in Figure 4.3.5 were used to construct the critical stress for martensitic transformation vs. temperature curve as shown in Figure 4.3.6. The values for both forward (M_s) and backward (A_s) transformation are included in the figure. It is evident that the trend satisfies the Clausius-Clapeyron (Cs-Cl) relation. The Cs-Cl slope is 2.47 MPa/K for loading. Through extrapolation of this data, the M_s temperature is obtained as –50 ˚C under zero load which is in between the M_s and M_f temperatures obtained from the DSC results. The Cs-Cl slope is significantly lower than what is observed in NiTi. This confirms that the pseudoelastic window for CoNiAl is significantly larger than in NiTi alloys even if they would have the same critical stress for slip. This can make CoNiAl a candidate material for high temperature SMA applications as well.

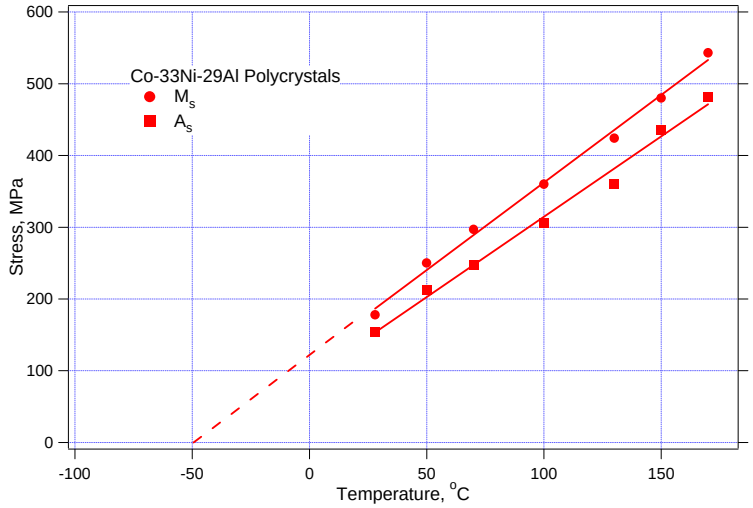

Figure 4.3.6. The critical stress for the onset of martensitic transformation as a function of temperature.

Another evidence for the two stage martensitic transformation is provided by the thermal cycling experiments conducted under external stress. Figure 4.3.7 presents the strain vs. temperature response of the present material at different stress levels (50, 100 and 200 MPa). Some of the observations are: (a) the transformation occurs in two stages, (b) the transformation temperatures are stress dependent, but the onset of lower temperature transformation is more temperature sensitive than the onset of higher temperature transformation, (c) the back transformation occurs in only one stage, (d) the transformation strain is about 4% which is in agreement with the compression experiments at room temperature, (e) transformation strain decreases with increased stress and (f) temperature hysteresis increases with increasing stress. Note that 200 MPa constant stress leads to almost one step forward transformation elucidating why the two stage deformation at room temperature compression experiments was not evident.

In order to investigate the second forward transformation on the back transformation a systematic experiment was conducted. The cooling process was interrupted during the second thermal cycle between the first and second steps of forward transformation and then heated. The result is shown in Figure 4.3.8. As it could be seen there is no jump during back transformation after the first step which means that the second step is the main driving force for the one step back transformation during heating. These results also support the two stage martensitic transformation on CoNiAl alloy.

Up to now ~4% pseudoelastic and shape memory strain is obtained. However, it is important to show that this behavior is consistent and repeatable after many cycles since most of the application such as actuators involves cyclic deformation. NiTi has a very good fatigue resistance while the other intermetallic alloys (CuZnAl, CuAlNi) has poor fatigue properties especially in polycrystalline form where they suffer from grain boundary fracture. Figure 4.3.9 shows the cyclic response of CoAlNi for 3023 cycles. Some cycles were selected to illustrate the response with cycles. The response almost saturates after 50 cycles and permanent strain of 0.86% remains after 3023 cycles. Stress hysteresis decrease from 15 MPa to 8 MPa. The initial cycle effects are expected and attributed to the defect and dislocation formation at initial cycles. After certain cycles the defects accumulates and don't allow further defect formation where the cyclic response saturates.

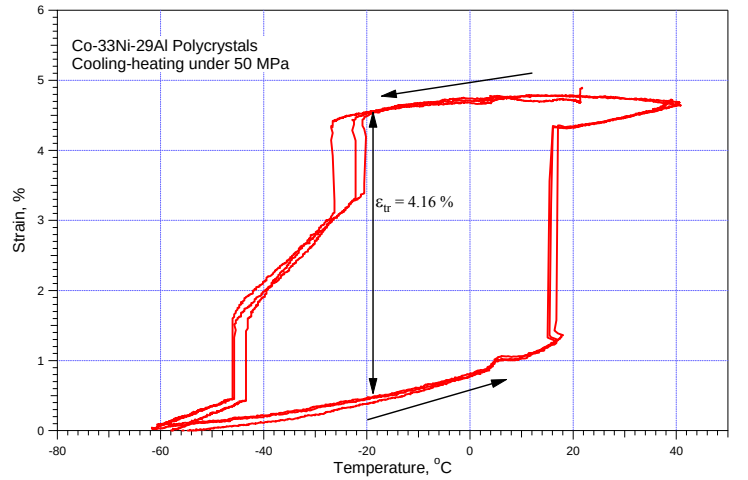

a)

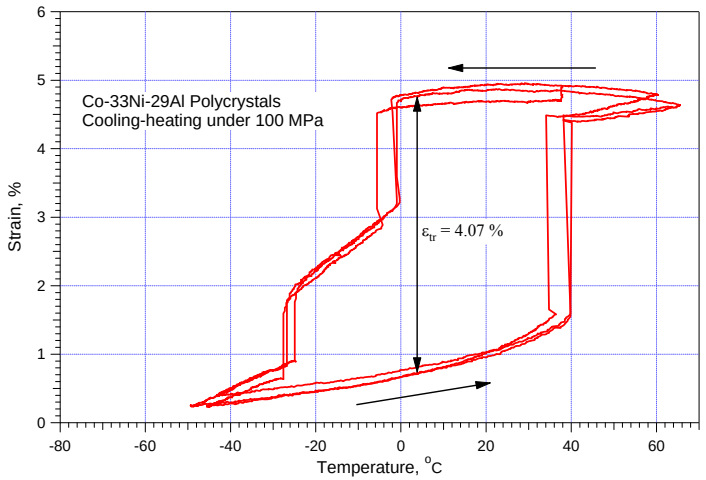

b)

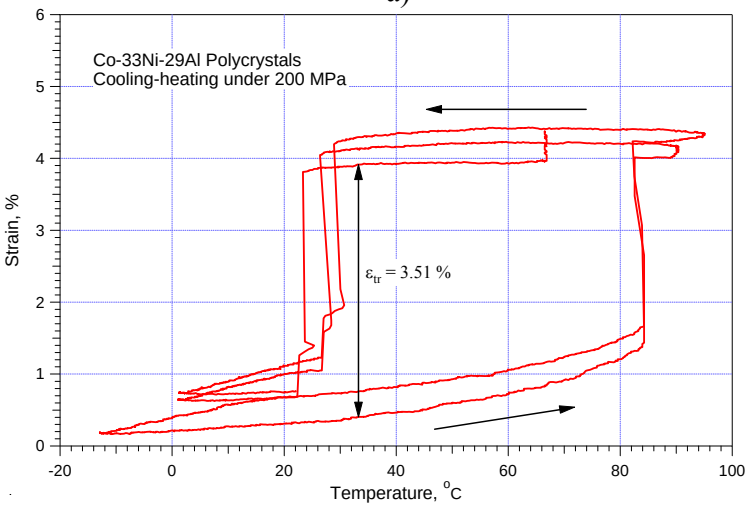

c)

Figure 4.3.7 Compressive strain vs. temperature response of CoNiAl under constant stress, a) under 50 MPa and b) under 100 MPa, and c) under 200 MPa.

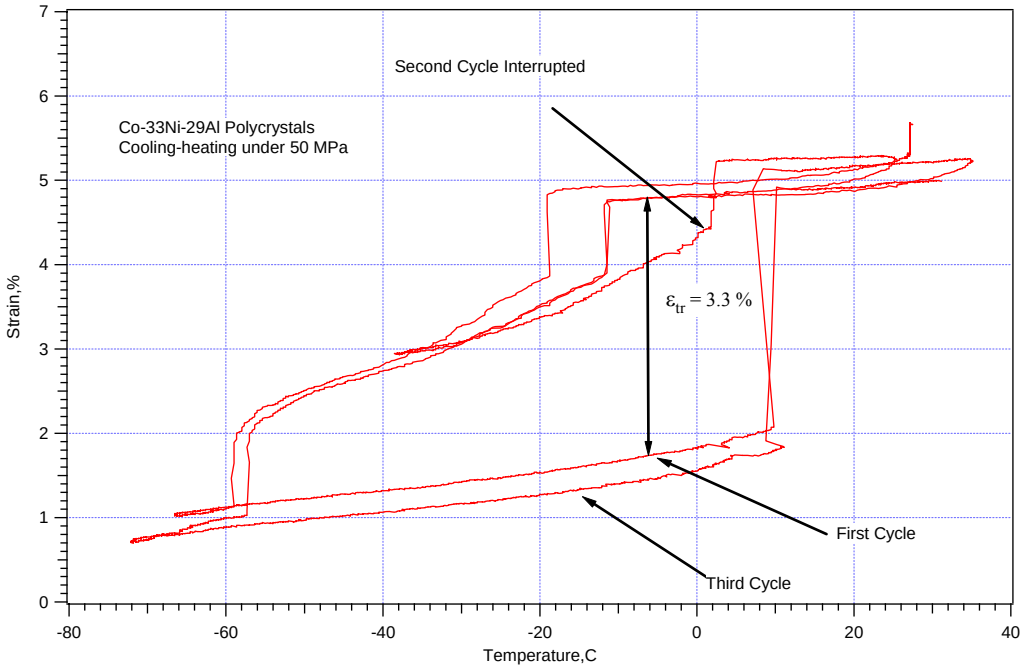

Figure 4.3.8 Compressive strain vs. temperature response of CoNiAl under constant stress.

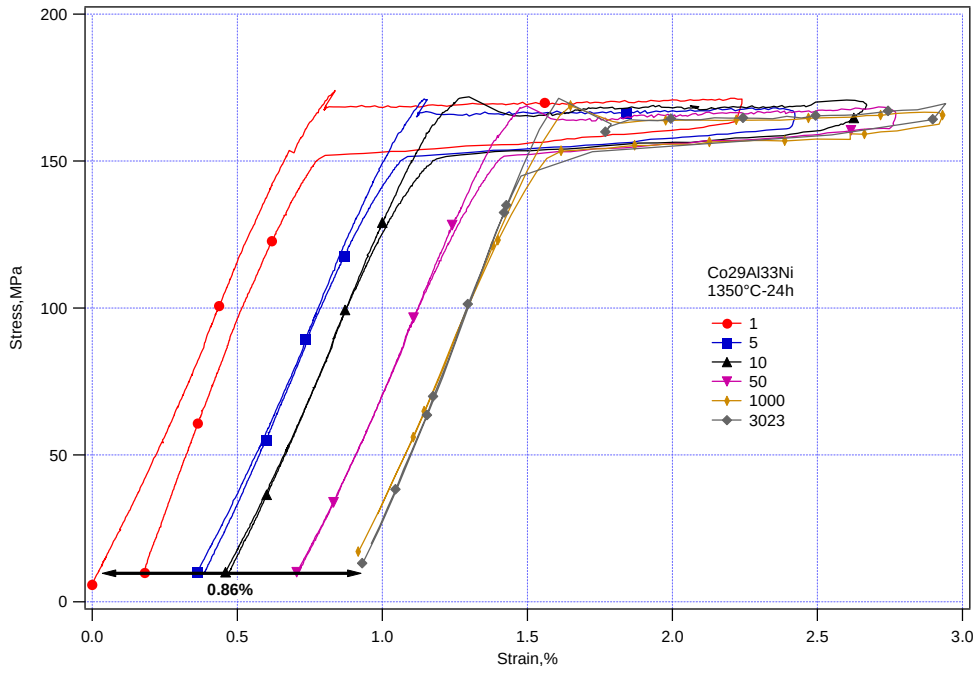

Figure 4.3.9 Cyclic compression response of CoNiAl.

CHAPTER V

CONCLUSIONS

In this work, Ti – 49.8 at.% Ni alloy samples were processed using equal channel angular extrusion at room temperature (in martensitic state), at 50 °C (in the martensitic state but only slightly below the A_s temperature) and at 150 °C (above A_f, in the austenitic state). The following conclusions have been reached after X-ray analysis, calorimetry, transmission electron microscopy and thermo-mechanical cycling of NiTi.

1. Regardless of the deformation temperature and the initial deforming phase, the final microstructure of the deformed samples are consisted of mostly heavily deformed martensite.
2. Although the austenite was the starting phase in the sample deformed at 150°C, the sample experienced stress induced formation of martensite and dislocation slip in the martensite resulting in a deformed martensite structure.
3. The B2 phase was observed on the fracture surface of the sample ECAE processed at room temperature. This is attributed to adiabatic deformation heating and thus localized macro shear banding in the austenitic state.
4. The deformation at room temperature led to martensite stabilization. The martensite stabilization caused an increase in the first martensite to austenite transformation temperature. However, in successive heating-cooling cycles, this effect vanished.
5. Although the M_s temperatures did not change, the A_{s2} temperatures decreased significantly after all deformation conditions. This is attributed to the relative ease of storing elastic energy during the austenite to martensite transformation with the help of the internal stress field caused by the deformed structure. The deformed samples annealed up to 500 °C experienced recovery and above 500 °C recrystallization started.
6. The severe marforming at room temperature followed by low temperature annealing resulted in the most favorable microstructure for post processing deformation under

compression which in turn led to higher strength levels, and high pseudoelastic strains as compared to the solutionized material and the samples deformed at 50 °C and 150 °C.

7. The different deformation mechanisms at different deformation temperatures (martensite reorientation, stress induced martensite, strain induced B2 phase and martensite slip), different amount of plastic deformation and the different resulting textures ([001] fiber or [111] fiber) upon deformation are believed to be responsible for high strength and pseudoelastic strain..
8. To eliminate localized catastrophic macro shear band formation, lower processing temperatures, and higher ECAE angles than 90° for smaller overall strain have to be used to hinder the formation of the B2 phase.

In the present work, conventional shape memory characteristics of ferromagnetic Co-33Ni-29Al alloy were also investigated. Following results are concluded after calorimetry, optical microscopy, transmission electron microscopy and thermo-mechanical cycling of CoNiAl.

1. After homogenization at 1350˚C for 24 hours, CoNiAl demonstrates up to 4% pseudoelastic strain with a narrow stress hysteresis of 20-25 MPa at room temperature. An extended plateau region was observed with the martensite nucleation stress being significantly larger than the propagation stress. This is an indication of the low twin boundary energy which is a necessary condition for magnetic field induced strains.
2. Perfect pseudoelasticity up to 170˚C was shown. A pseudoelastic temperature window of more than 150˚C is obtained which is significantly larger than in NiTi alloys making CoNiAl a candidate for high-temperature SMA applications.
3. The slope of the Clausius-Clapeyron curve obtained for the stress-induced martensitic transformation is in the 2-3MPa / ˚C range.
4. A two stage phase transformation was revealed

5. The stress required for the onset of dislocation slip is as high as 1100 MPa leading to a 900 MPa stress differential between stress-induced martensitic transformation and dislocation motion. This is also a necessary condition for obtaining large magnetic field induced strains.
6. Cyclic deformation behavior was investigated and saturation of mechanical response after 50^{th} cycle, decrease in stress hysteresis and increase in unrecoverable strain with increased number of cycles were revealed.
7. Formation of second phase (γ) along the grain boundaries and inside the grains was observed in samples after various heat treatments. Formation of second phase along the grain boundary increases the ductility of the material by preventing incompatibility between grains during deformation.
8. Martenistic phase was identified as $L1_0$ using TEM diffraction pattern analysis and twinning plane was determined as (1-11).

REFERENCES

1. H. Funakubo, Shape Memory Alloys, Gordon & Breach Publishing Group, Amsterdam, 1987, p.1.
2. K. Otsuka, C.M. Wayman, Shape Memory Materials, Cambridge University Press, Cambridge, 1998, p. 1.
3. Y. Murakami, K. Otsuka, Mater. Sci. Eng. A. 189 (1994) 241.
4. Y. Liu, Y. Liu, J.V. Humbeeck, Acta Mater. 47 (1999) 199.
5. J.A. Shaw, S. Kyriakides, J. Mech. Phys. Solids, 43 (1995) 1243.
6. H. Sehitoglu, I. Karaman, R. Anderson, X. Zhang, K. Gall, H.J. Maier, Y. Chumlyakov, Acta. Mater. 48 (2000) 3311.
7. www.ad.tut.fi/aci/courses/76527/Seminars2000/SMA.pdf (Accessed: 10.02.2003)
8. I. Mihalcz, Per. Pol. Mech. Eng 45 (2001) 75.
9. W.M. Wayman and J.D. Harrison, JOM-J Min Met. Mat. S, 41 (1989) 26.
10. T. Duerig, A. Pelton and D. Stockel, Mat. Sci. Eng. A. 273 (1999) 149.
11. J.V. Humbeeck, Mater. Sci. Eng. A. 273-275 (1999) 134.
12. M.Nishida, C.M. Wayman, T. Honma, Metall. Trans. A. 17 (1986) 1505.
13. K. Otsuka and X.B. Ren, Intermettallics. 7 (1999) 511.
14. Y. Kudoh, M. Tokonami, S. Miyazaki, K. Otsuka, Acta. Metall.33 (1985) 2049.
15. K. Otsuka, X. Ren, Mater. Sci. and Eng. A. 273 (1999) 89.
16. T.H. Nam, T. Saburi T, Y. Nakata, K.X. Shimizu, Met Trans. 31 (1990) 1050.
17. X. Ren, K. Otsuka, Scripta Mater. 38 (1998) 1669.
18. S. Miyazaki, K. Otsuka, ISIJ International. 29 (1989) 389.
19. H. Sehitoglu, I. Karaman, X. Zhang, A. Viswanath, Y. Chumlyakov, H.J. Maier, Acta. Mater. 49 (2001) 3621.
20. S. Miyazaki, K. Otsuka, C. M. Wayman, Acta Metallurgica. 137 (1989) 1873.
21. H.C Lin., S.K. Wu, Acta Metall. Mater. 42 (1994) 1623.
22. K. Gall, H. Sehitoglu, Y.I. Chumlykov, I.V. Kireeva, H.J. Maier, J Eng. Mater-T. ASME. 121 (1999) 19.

23. K. Enami, S. Menno, Met Trans. 2 (1971) 1487.
24. D. Wurzel, Mater. Sci. Eng. A. 273-275 (1999) 634.
25. Y. Liu, Mater. Sci. Eng. A. 273-275 (1999) 668.
26. Y. Liu and D. Favier, Acta Mater. 48 (2000) 3489.
27. H. Nakayama, K. Tsuchiya, Z.G. Liu, M. Umemoto, K. Morii and T. Shimizu, Mater. Trans. JIM. 42 (2001) 1987.
28. Y. Liu and S.P. Galvin, Acta Mater. 45 (1997) 4431.
29. H. Nakayama, K. Tsuchiya and M. Umemoto, Scripta Mater. 44 (2001) 1781.
30. Y.F. Zheng, B.M. Huang, J.X. Zhang, J. X. Zhoa, Met. Sci. and Engr. A. 279 (2000) 25.
31. M. Nishida, K. Yamauchi K, I. Itai, H. Ohgi, A. Chiba, Acta Metall. Mater. 43 (1995) 1229.
32. M. Nishida, C.M. Wayman, A. Chiba, Metallogrophy. 21 (1988) 275.
33. R.C. Olson, H.A. Cohen, Scripta Metall. 9 (1975) 1247.
34. L. M. Schetky, Robotics Age. 14 (1984) 13.
35. C. M. Wayman: R.W. Cahn and O. Haasen (eds) Phase Transformations, Physical Metallurgy, Amsterdam, Elsevier, 1996, p.21.
36. B.J. deBlonk and D.C. Lagoudas, Smart Mater. Struc. 7 (1998) 771.
37. B. Strnadel, S. Ohashi, H. Otsuka, S. Miyazaki, T. Ishihara, Mater. Sci. Eng. A 203 (1995) 187.
38. Y. Liu, Z.L. Xie, J.V. Humbeeck, L. Delaney, Acta Mater. 47 (1999) 645.
39. K. Gall, H. Sehitoglu, Y.I. Chumlyakov, V. Kireeva, Acta Mater. 47 (1999) 1203.
40. H. Sehitoglu, J. Jun, X. Zhang, I. Karaman, Y. Chumlyakov, H. J. Maier, K. Gall, Acta Mater. 49 (2001) 3609.
41. X. Xu, N.N. Thadhani, Scr. Mat. 44 (2001) 2477.
42. D. Wu, W. C. Crone, J. Prepezko, SEM Annual Conference Procedings, Milwaukee, 2002.
43. T. Saburi, M.Yoshida, S. Nenno, Scr. Matell. 50 (1984) 363.
44. R.Z. Valiev, R.K. Islamgaliev and I.V. Alexandrov, Prog. Mater. Sci. 45 (2000) 103.

45. V.M. Segal: Met. Sci. and Engr. A. 271 (1999) 322.
46. V.M. Segal: Met. Sci. and Engr. A. 197 (1995) 157.
47. D.W. Bier, M. S. Thesis, Texas A&M University, 1997.
48. L.R. Cornwell, K.T. Hartwig, R.E. Goforth and S.L. Semiatin, Mater. Charac. 38 (1997) 119.
49. J. Robertson, J.-T. Im, I. Karaman, K.T. Hartwig and I.E. Anderson, J. of Non-Crystalline Solids. 317 (2003) 144.
50. J. Koike, D.M. Parkin, N. Nastasi, J. Mater. Res. 5 (1990) 1414.
51. J. Koike, D.M. Parkin, N. Nastasi, Philosophical Magazine Letters. 62 (1990) 257.
52. E.V. Tatyanin, N.F. Borovikov, V.G. Kurdyumov, V.L. Indenborn, Phys. Sol. State. 39 (1997) 1097.
53. .V. Sergueeva, C. Song, R.Z. Valiev, A.K. Mukherjee, Mat. Sci. and Eng. A. in press.
54. K. Ullakko, J.K. Huang, C. Kantner, V.V. Kokorin and R.C. O'Handley, Appl. Phys. Lett. 69 (1996) 1966.
55. J. Murray, M. Marioni, P. G. Tello, S. M. Allen and R. C. O'Handley, J. Magn. Magn. Mater. 226 (2001) 945.
56. R. Tickle, R.D. James, J. Magn. Magn. Mater. 195 (1999) 627.
57. S. Muto, R. Oshima, and F.E. Fujita, Scripta Metall. 21 (1987) 465.
58. R.D. James, M. Wuttig, Phil. Mag. A. 77 (1998) 1273.
59. T. Kakeshita, T. Takeuchi, T. Fukuda, T. Saburi, R. Oshima, S. Muto, and K. Kishio, Mater. T. JIM 41 (2000) 882.
60. K. Oikawa, T. Ota, Y. Sutou, T. Ohmori, R. Kainuma, and K. Ishida, Mater. Trans. JIM. 43 (2002) 2360.
61. K. Oikawa, T. Ota, T. Ohmori, Y. Tanaka, H. Morito, A. Fujita, R. Kainuma, K. Fukamichi, and K. Ishida, Appl. Phys. Lett. 81 (2002) 5201.
62. T. Kakeshita T, K. Ullakko, MRS Bull. 27 (2002) 105.
63. A. Vassiliev, J Magn. Magn Mater. 242 (2002) 66.
64. M. Wuttig, J. Li and C. Craciunescu, Scripta Mater. 44 (2001) 2393.

65. K. Oikawa, T. Ota, F. Gejima, T. Ohmori, R. Kainuma, and K. Ishida, Mater Trans. 42 (2001) 2472.
66. K. Oikawa, L. Wulff, T. Iijima, F. Gejima, T. Ohmori, A. Fujita, K. Fukamichi, R. Kainuma, and K. Ishida, Appl. Phys. Lett. 79 (2001) 3290.
67. Y. Murakami, D. Shindo, K. Oikawa, R. Kainuma, and K. Ishida, Acta Mater. 50 (2002) 2173.
68. H. Morito, A. Fujita, K. Fukamichi, R. Kainuma, K. Ishida, and K. Oikawa, Appl. Phys. Lett. 81 (2002) 1657.
69. R. Kainuma, M. Ise, C.C. Jia, H. Ohtani, and K. Ishida, Intermetallics. 4 (1996) 151.
70. K. Ishida, R. Kainuma, N. Ueno, and T. Nishizawa, Metall. Trans. A. 22 (1991) 441.
71. K. Otsuka, H. Sakamato, and K. Shimizu, Acta Metall. 27 (1979) 585.
72. V.A. Chernenko, V.V. Kokorin, O.M. Babii, and I.K. Zasimchuk, Intermetallics. 6 (1998) 29.
73. V.V. Martynov, V.V. Kokorin, J. De Physique III. 2 (1992) 739.
74. V.A. Chernenko, V. L'vov, J. Pons, and E. Cesari, J. Appl. Phys. 93 (2003) 2394.
75. D. Schryvers,P. Boullay, P.L. Potapov, R.V. Kohn, J.M. Ball, Int. J. Solids Struct. 39 (2002) 3543.
76. J.C. Ewert, I. Bohm, R. Peter, and F. Haider, Acta Mater. 45 (1997) 2197.
77. H. Nakayama, K. Tsuchiya, Z.G. Liu, M. Umemoto, K. Morii and T. Shimizu, Mater. Trans. JIM. 42 (2001) 1987
78. M. Piao, K. Otsuka, S. Miyazaki and H. Horikawa, Mater. Trans. JIM 34 (1993) 919.
79. E. Hornbogen, V. Mertinger and D. Wurzel, Scripta Mater. 44 (2001) 171.
80. E. Hornbogen, J. Mater. Sci. 34 (1999) 599.
81. Y. Liu and G.S. Tan, Intermetallics. 8 (2000) 67.
82. F. Khelfaoui, G. Thollet and G. Guenin, Mater. Sci. Eng. A. 338 (2002) 305.
83. J. Khalil-Allafi, A. Dlouhy, G. Eggeler, Acta Mater. 50 (2002) 4255.
84. D. Favier, Y. Liu, P.G. McCormick, Scripta Metall. 28 (1993) 669.
85. L. Batillard, R. Gotthardt, J. de Physique IV. C8 (1995) 647.
86. F. Khelfaoui, G. Guenin, Mater. Sci. Eng. A. 335 (2003) 292.

87. H. Sitepu, W.W. Schmahl, J.K. Allafi, G. Eggeler, A. Dlouhy, D.M. Toebbens, M. Tovar, Scripta Mater. 46 (2002) 543.
88. H.C. Lin, S.K. Wu, T.S. Chou and H.P. Kao, Acta Metall. Mater. 39 (1991) 2069.
89. H.F. Lopez, Mat. Lett. 51 (2001) 144.
90. A.A. Bulbich and P. Toledano, Phys. Rev. Lett. 81 (1998) 838.
91. Y. I. Chumlykov, N.S. Surikova, A.D. Korotaev, Phys. of Metals and Metall. 82 (1996) 102.
92. K. Gall, T.J. Lim, D.L. McDowell, H. Sehitoglu and Y.I. Chumlyakov, Inter. J. Plas. 16 (2000) 1189.
93. D.R. Pank, M.V. Nathal, D.A. Koss, J. Mater. Res. 5 (1990) 942.
94. E.P. George, C.T. Liu, J.A. Horton, C.J. Sparks, M. Kao, H. Kunsman, T. King, Mat. Charac. 39 (1994) 665.
95. H. Sehitoglu, I. Karaman, X. Zhang, H. Kim, Y. Chumlyakov, H.J Maier and I. Kireeva, Metall. Mater. Trans. A. 32 (2001) 477.
96. V.A. Chernenko, V. L'vov, J. Pons, and E. Cesari, J. Appl. Phys. 93 (2003) 2394.
97. D. Schryvers, L.E. Tanner, Ultramicroscopy. 32 (1990) 241.
98. Y. Kishi, C. Craciunescu, M. Sato, T. Okazaki, Y. Furuya, and M. Wuttig, J. Magnestism Mag. Mater. 262 (2003) 1186.

VITA

Haluk Ersin Karaca, son of Muzaffer and Seyide Karaca and younger brother of Erdem Karaca, was born in Canakkale, Turkey in 1979. He graduated from Bogazici University, Department of Mechanical Engineering, in May 2001. In Fall 2001, he enrolled in Texas A&M University to pursue a graduate degree. He completed his research and received a Master of Science in Mechanical Engineering in December of 2003. Following graduation, Haluk continued his studies at Texas A&M University as a Doctor of Philosophy candidate in the same department. During his study, he was an author of two journal publications. His permanent adress is:

Hurriyet Mahallesi
Cami Sokak, No:22
16800
Orhangazi, Bursa, TURKEY